Empirical Modeling and Correlation of the Interactions between Blood and Artificial Surfaces.

by

Peter W. Wojciechowski, B.Sc.(Eng.), M.Eng.

A Thesis
Submitted to the School of Graduate Studies
in Partial Fulfillment of the Requirements
for the Degree
Doctor of Philosophy

McMaster University

November 1991

DOCTOR OF PHILOSOPHY (1991) McMASTER UNIVERSITY
(Chemical Engineering) Hamilton, Ontario, Canada

TITLE: Empirical Modeling and Correlation of the Interactions between Blood and Artificial Surfaces.

AUTHOR: Peter Witold Wojciechowski, B.Sc.(Eng.), Queen's University
M.Eng., McMaster University

SUPERVISOR: Professor J.L. Brash

NUMBER OF PAGES: x, 190

Abstract

Blood coagulation and protein adsorption were studied on a series of model surfaces. Silanes were used to covalently attach chemical groups (including sulfonate, amine, polyethylene oxide (PEO), lysine, methyl, and octadecyl) to pure silica substrates. Surface chemical analysis by x-ray photoelectron spectroscopy (XPS) was used to quantify the elemental composition of these surfaces. All silane layers were estimated to be monolayers or less with thickness in the range 0.2 nm (for methyl groups) to 2.0 nm (for PEO).

Contact angles were measured to help quantify the interaction between the model surfaces and pure solvents (water, glycerol, dimethyl sulfoxide (DMSO)). The data were fit to established interfacial tension (interfacial free energy) models but none was found to be adequate. A new empirical model, not related to surface energetics, was developed and demonstrated to be capable of fitting the data more precisely. Small deviations from the empirical model (± 2° to 8°) for DMSO and water contact angles were attributed to the possible influence of surface charge.

Protein adsorption kinetics on the model surfaces was measured using ^{125}I-labeled fibrinogen and albumin as single proteins under static conditions. A simulation of transport and reaction in this experimental system was written and used to fit data to proposed models for protein adsorption. A simple bilayer mechanism was found to fit the kinetic data better than a number of multistate monolayer models for adsorption. The adsorption of fibrinogen from plasma was also measured in order to investigate a possible relationship between the Vroman effect and surface activated blood coagulation.

A surface activated blood coagulation assay based on the partial thromboplastin time test was used to characterize the blood compatibility of model surfaces prepared on glass test tubes. The kinetics of cleavage of a fluorogenic substrate for thrombin was measured in real time on surfaces which were assumed to be closely comparable to those prepared on pure silica. Clotting times ranging between 2 and 11 minutes were measured.

A correlation analysis was performed using surface chemistry, contact angle, protein adsorption, and blood coagulation data. Clotting times were found to be empirically related to surface chemistry, but not to fibrinogen adsorption or the Vroman effect. The Vroman effect for fibrinogen was found to be predictable in most cases given only single component

fibrinogen adsorption data. Fibrinogen adsorption from buffer was found to increase with sulfur (sulfonate) content and decrease with nitrogen (amino) content, but contrary to suggestions in the literature was not a strong function of wettability.

A multivariate approach to studying the interactions between blood, proteins and model surfaces proved to be a practical approach to a complex problem. It was demonstrated that univariate relationships are often inadequate in their ability to explain the interfacial behavior of blood and its elements, and in fact may lead to erroneous conclusions.

Table of Contents

Table of Figures

Table of Tables

Acknowledgements

The author would like to thank the many people who contributed to the completion of this work. Dr. Brash supported me throughout the project and was always available to give input and encouragement. Pauline ten Hove was helpful and friendly during our discussions and performed a large portion of the protein adsorption studies upon which the modeling and correlation studies were based. Jon van Buskirk and Gary Skarja contributed a great deal to the preparation and characterization of the surfaces in the extended survey of model materials as part of their fourth year thesis projects. Union Carbide supplied some of the silanes for the model surfaces. The staff at the XPS facilities in Toronto (Rana Sohdi) and Seattle (Deborah Leach-Scampavia, Dave Castner and Buddy Ratner) were very cooperative. The Seattle facility provided their service free of charge. Mike Sefton and Gord Rollason at the University of Toronto made available their knowledge, facilities and materials for doing thrombin generation assays. Many of the staff and students in the Chemical Engineering Department at McMaster have at one point or another made important contributions to this work by giving technical advice and by simply making my four years there a pleasant experience. Special thanks to Paul Gloor, my personal software guru and miscellaneous problem solver. Finally I would like to thank my wife Ausra for performing the enormous task of typing this thesis and to whom I can now promise more time.

1 Introduction and Literature Review

In the early 1980s it appeared that biomedical engineering had achieved the goal of a workable total artificial human heart. Although the Jarvik VII heart met most of the stringent mechanical requirements it had a fatal flaw. The material that contacted the blood, Biomer, although in many ways the best available material, did not have the necessary biocompatibility. Blood coming into contact with Biomer, a segmented polyurethane (Lelah and Cooper, 1986) would "recognize" it as a foreign surface and form thrombi. In human patients anticoagulants were administered chronically to inhibit clotting and thrombosis but this practice subsequently created many more problems. Despite the use of anticoagulants the patients suffered frequent strokes, believed to result from embolization of thrombi formed on the material surface. The success of the artificial heart was severely limited by its lack of blood compatibility (Ward et al, 1987). Perhaps more importantly the same problems affect millions of patients who require treatments using blood oxygenators, vascular grafts, prosthetic heart valves and artificial kidneys every year.

Recent efforts have led to a much greater appreciation of the number and complexity of processes involved in blood coagulation on foreign surfaces (Leonard et al, 1987). The resulting research has drawn from experience in a number of fields including engineering, materials science and hematology (Andrade, 1985a,b; Salzman and Merrill, 1982; Sawyer, 1965). Despite the many years of research into blood-surface interactions, we seem no closer to producing a material that is as compatible with blood as the endothelium which lines the entire circulatory system (Spaet, 1987). Perhaps one way to increase understanding of this complex problem is via systematic study of the surface properties affecting reactions with blood. It has been repeatedly shown that blood is more compatible with some surfaces than with others, suggesting that compatibility must be correlated in some way with surface properties such as water contact angle, roughness, surface chemistry, charge or other as yet undefined characteristics (Andrade, 1985a). No single macroscopic or microscopic property has yielded a simple correlation with blood compatibility. There are clearly many surface properties which simultaneously contribute to material interactions with blood. In the same way, blood compatibility cannot be assessed, much less quantified by a single test, and correlating short term *in vitro* tests with animal implant studies has proven to be difficult (Didisheim et al, 1984; Wilson et al, 1987). The validity of animal models for testing devices intended for use in humans is itself a contentious issue.

Blood interactions are not necessarily directly correlated with surface properties *per se* since intervening events can rapidly alter the surface that reacts with blood. The first event on a surface coming into contact with blood is the deposition of plasma proteins (Vroman, 1987b). This rapidly adsorbed layer of protein mediates the longer term response between blood and surface, thus making the study of protein adsorption a cornerstone to the understanding of blood compatibility (Vroman, 1987b). The work described in this thesis has as one of its key elements, a study of plasma protein adsorption to synthetic surfaces.

Single component protein adsorption has proven to be a complicated system in itself (Brash and Horbett, 1987), so that the prospect of predicting multicomponent adsorption from blood plasma, with perhaps as many as two hundred competing proteins is somewhat daunting. An established knowledge base in the field of coagulation has justified a focus on those proteins known to be important in initiating fibrin formation on surfaces (Bouma and Griffin, 1986) and those which are most abundant in blood plasma (Andrade and Hlady, 1987).

While protein adsorption appears to be a key event in blood-material interactions it is also crucial in a wide variety of other problems (Andrade, 1985b; Andrade and Hlady, 1987). The food industry is concerned with the fouling of its process equipment by protein biofilms (Arnebrant and Nylander, 1986). Biotechnologists have studied the techniques of enzyme immobilization to maximize reactive properties while maintaining strong surface binding. Adsorption tends to bring about significant conformational changes in enzymes, thus adversely affecting their precisely shaped active sites. Genetically engineered cells may be designed to produce proteins which must be separated by chromatography in which adsorption plays a key role. Contact lenses are limited by protein deposition from tear fluid (Holly, 1984). The fouling of ship hulls by barnacles, which causes a significant increase in drag, is mediated by an adsorbed protein layer. The interaction of biomaterials with proteins in bodily fluids is only one of many areas in biotechnology, medicine and environmental engineering in which protein adsorption has been studied. Fundamental investigations of protein adsorption at solid-liquid and solid-vapor interfaces (Norde, 1986; MacRitchie, 1978) continue to be important and may someday provide answers for a wide range of practical problems.

One method for testing our understanding of the processes involved in protein adsorption has been the development and testing of mechanistic models to be fit to experimental data (Lok et al, 1983; Beissinger and Leonard, 1982, 1981; Cuypers et al, 1987). The complexity of protein adsorption has limited researchers to semi-empirical models often involving parameters with no direct physical significance but necessary for an adequate fit to the data. There is in general, disagreement as to which processes are occurring at the protein solution-solid interface. A combination of modeling and planned experimentation (Box et al, 1978) is needed to discriminate between models and determine which are the best for describing events at the interface.

Blood compatibility is a problem which encompasses concepts from a variety of scientific disciplines. It cannot be argued at this point that the influence of surface chemistry, surface energetics or protein adsorption dominates blood-material interactions and so every effort must be made to understand the importance of each. At the very least, analyses relevant to them should be reported so that others may be better able to draw their own conclusions from blood compatibility studies.

1.1 Protein Adsorption

1.1.1 Introduction to Protein Adsorption

At almost any interface involving a biological system the phenomenon of protein adsorption is important (Andrade, 1985b). The initial migration of protein molecules to the interface is typically very rapid and thus the original surface does not remain for long in direct contact with the biological system (Price and Rudee, 1987). In a multicomponent solution of proteins the adsorbed layer will vary markedly in composition as a function of the surface (Horbett and Brash, 1987). A long term goal in this field is to learn enough about the relevant properties of proteins and surfaces to be able to predict their interaction.

1.1.2 Proteins

Proteins are macromolecules (MW up to 1000kD) consisting of one or several polypeptide chains. The sequence of amino acids (Schulz and Schirmer, 1979; Creighton, 1984) determines the protein's "primary structure". The sequence of amino acid side groups along the chain leads to secondary structures such as α-helices and β-sheets. The polypeptides

are generally folded into a globular "tertiary structure" which minimizes the free energy of interaction between the protein and the (usually aqueous) medium in which it exists. In its natural surroundings a protein is in its "native state" in which hydrophobic groups tend to be on the inside of the globular structure and hydrophilic groups on the outside. External patches of hydrophobicity along with charged amino acid side groups (R-groups) and overall solubility contribute to the surface activity of the individual protein. Proteins are, in general, strongly attracted to any interface due to their high molecular weight and amphiphilic nature (see Fig. 1.1). Hydrophobic surfaces have been hypothesized to adsorb the most protein since their interfacial tension is high and thus present a large driving force for adsorption (Bagnall and Arundel, 1982).

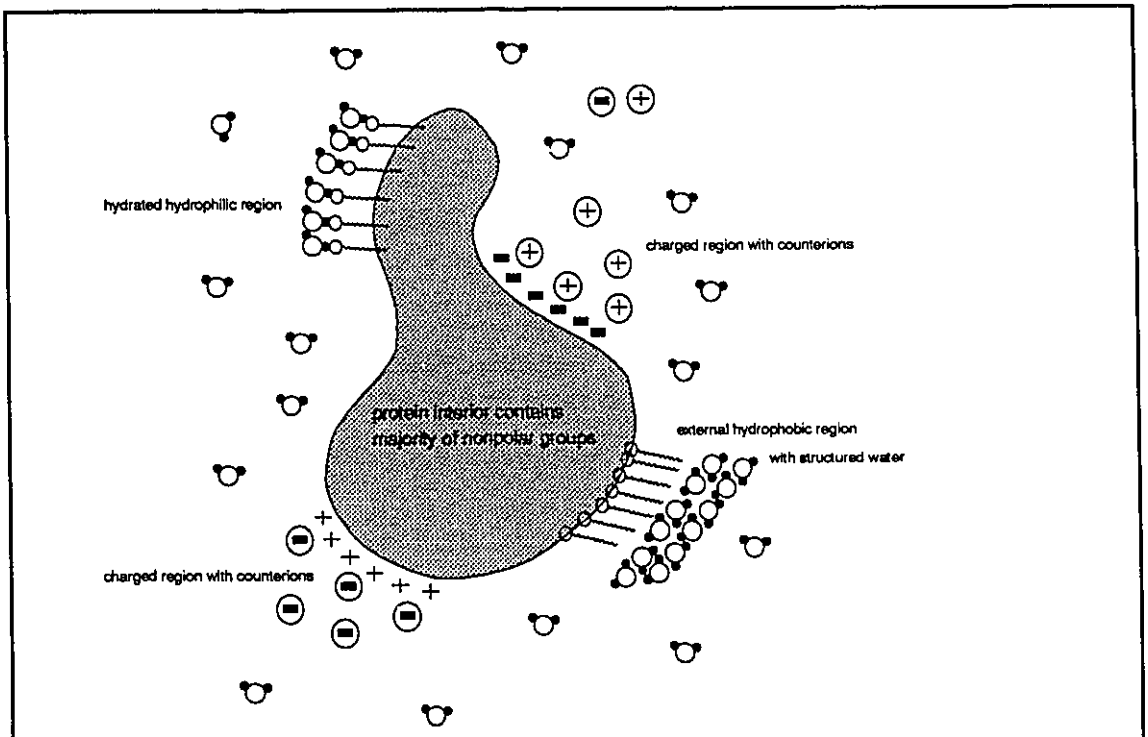

Figure 1.1: An illustration of the amphiphilic nature of proteins and the different modes by which they may attach to surfaces. Adapted from Andrade (1985b).

The adsorption of fibrinogen and albumin to biomaterials has been given special consideration when evaluating blood compatibility. They are both abundant components of blood plasma with albumin present at an average level of about 42 mg/mL (well over half the total protein content of plasma) and fibrinogen at about 3.0 mg/mL. Adsorbed albumin has been observed to reduce blood coagulation and platelet activation on surfaces while adsorbed fibrinogen apparently has the opposite effect in most cases (Lyman et al, 1975). Human fibrinogen (Hfb) has most commonly been described as a trinodular rod about 45 nm long and 5 nm in diameter (Laki, 1968; Doolittle, 1981; Brynda et al, 1987) although different shapes have also been observed depending on the sample preparation methods (Laki, 1968; Nygren and Stenberg, 1988). Its molecular weight has been estimated to be 340,000 daltons (Laki, 1968). Human serum albumin (HSA) has a less rigid tertiary structure but has been estimated to be oblong with dimensions 14 nm by 4 nm and a molecular weight of 69,000 daltons (Soderquist and Walton, 1980). If the molecular dimensions indicated above are used, the monolayer coverages of side-on or end-on adsorbed proteins may be estimated. For albumin, assuming grid packing, the estimates are 0.7μg/cm^2 for end-on and 0.2μg/cm^2 for side-on. For fibrinogen the estimates are 2.3μg/cm^2 for end-on and 0.25μg/cm^2 for a monolayer adsorbed side-on.

1.1.3 Protein Adsorption Fundamentals

Two analogies are frequently used in the description of protein adsorption, *viz* the adsorption of long chain polymers and small rigid molecules, representing the extreme ends of the adsorption "spectrum". Small, rigid molecules follow the thermodynamically reversible behavior described by the Langmuir isotherm (Adamson, 1990). The adsorption of linear flexible polymers (Eirich, 1977) is not as completely understood but observed behavior indicates irreversible adsorption in some cases and hysteresis in all others. Protein adsorption (Vroman and Adams, 1987; MacRitchie, 1987) is an intermediate case but has many more similarities with the flexible polymer model than the Langmuirian one.

A review paper by Eirich (1977) discusses some of the most notable features of long chain flexible polymer adsorption. Such polymers are almost exclusively adsorbed as monolayers. Multiple layers may occur via covalent bonding, ionic or dipole interactions, ion exchange, hydrophobic bonding or chelation, but frequently the adsorbed layer thickness increases merely by rearrangement of the monolayer. A good solvent allows the "loops"

and "tails" of an adsorbed long chain molecule to extend out into the liquid phase. At high concentrations of dissolved polymer the adsorbed species may detach at several sites to facilitate the deposition of a new molecule. Thus, molecules can appear to attach themselves to a completely filled surface by this "rearrangement" process (Pefferkorn et al, 1985). The adsorbed monolayer thickness will increase as fewer contacts result in longer loops and tails. These molecules are much more readily desorbed than those adsorbed from a low concentration solution. The latter may "spread" to cover the surface as completely as possible and thus are more irreversibly adsorbed.

Two major types of binding for polymers are discussed by Eirich. Ionic bonding occurs at specific sites on the surface and very likely involves counter-ion incorporation. This requires the presence of charged groups on both the surface and the substrate. The other mode of binding, which is more important, involves Van der Waals interactions which are nonspecific. The Langmuir theory of adsorption postulates specific sites and thus is not strictly applicable to nonspecific binding mechanisms. Despite this fact, the isotherms observed when Van der Waals interactions are involved frequently have Langmuirian characteristics including a linear initial portion with a slowly developing plateau at high concentrations. The observed Langmuir-like isotherms are not fully understood but it is felt that intermolecular interactions or solvent competition on the surface causes the finite slope at low concentrations while rearrangement of the monolayer results in an increase in adsorption over the high concentration range.

Protein adsorption differs from the long chain polymer case in several ways (Gendreau et al, 1982). The variety of chemical groups on the surface of proteins in solution allows for many more different modes of binding than for chemically simple long chain synthetic polymers (see Fig.1.2). Although proteins are found in aqueous environments, hydrophobic patches may still exist on the exposed surface allowing rapid adsorption to hydrophobic surfaces. Subsequently the adsorbed protein may unfold or "denature" to expose its internal hydrophobic groups to the surface (McMillin and Walton, 1974; Schaaf and Dejardin, 1988; Walton and Koltisko, 1982; Bohnert and Horbett, 1986). Because of their well-defined, usually asymmetric shape, the orientation of proteins on a surface becomes an important issue. A long rod shaped molecule such as fibrinogen (Brynda et al, 1987; Nygren and Stenberg, 1988) will cover different areas depending on whether it is adsorbed in an "end-on" or "side-on" orientation.

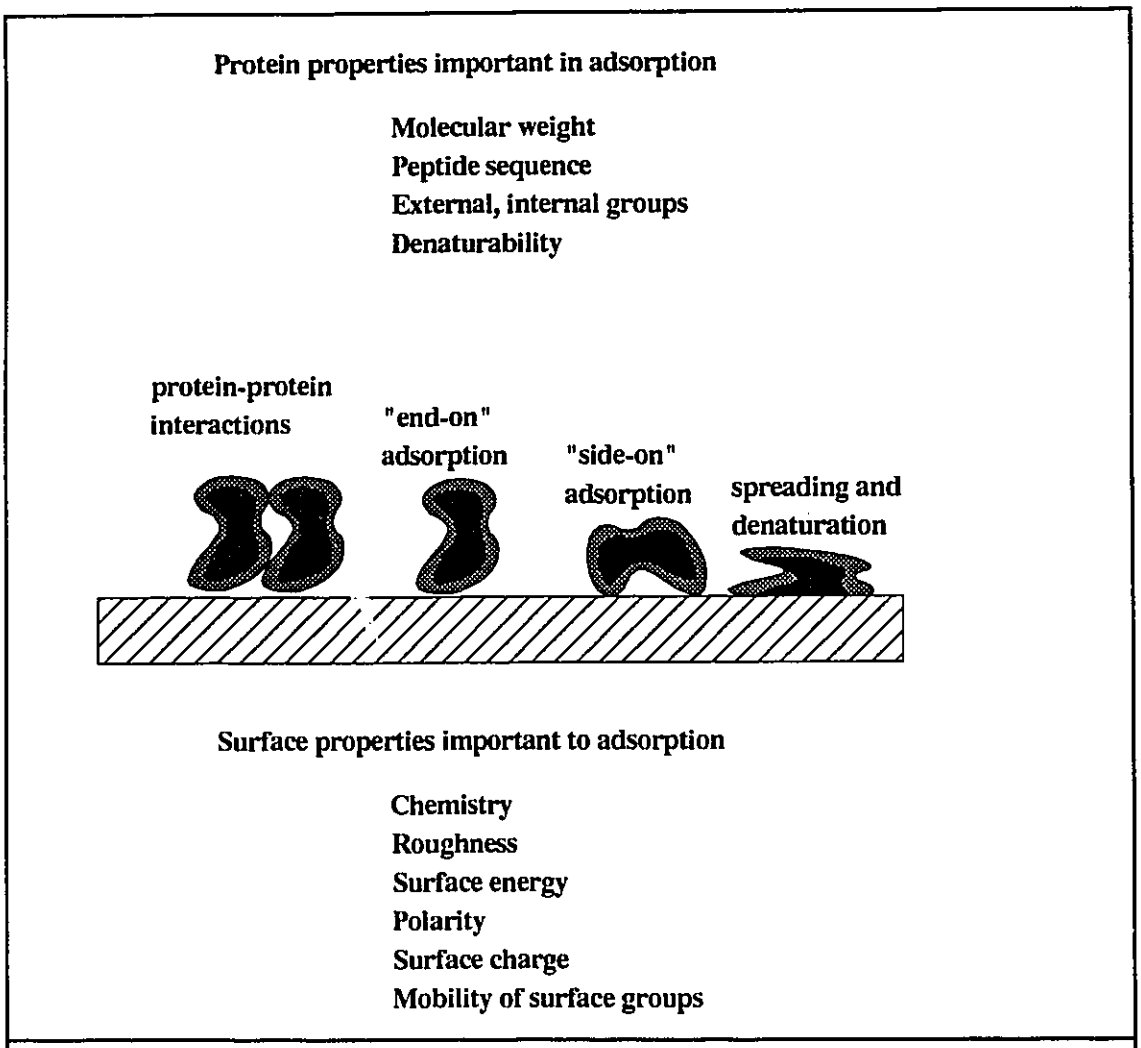

Figure 1.2: Examples of possible protein-surface interactions.

Clearly proteins are not small, spherical, rigid molecules capable of adsorbing reversibly to individual sites (Burghardt and Axelrod, 1981). Nonetheless their adsorption isotherms appear to fit the Langmuir model quite well in many cases (Moreno et al, 1987). Proteins often deviate from the Langmuir model by showing extensive hysteresis when attempts are made to "descend" the isotherm (Jennissen, 1985). Some of the observed

hysteresis is due to time dependent conformational changes of the protein on the surface (Lyklema, 1984; Moreno et al, 1987; Beissinger and Leonard, 1981 and 1982; Soderquist and Walton, 1980).

Proteins are extremely sensitive to changes in their environment (Norde and Lyklema, 1978; Privalov, 1979). The solvent, temperature, pH and concentration are some of the factors which have large effects. Beyond certain narrow limits of pH, temperature or other environmental conditions, proteins may actually lose their tertiary structure resulting in particularly strong adsorption or precipitation of the protein from solution. Experimental studies of protein adsorption thus require closely controlled conditions.

1.1.4 Thermodynamics of Protein Adsorption

Protein adsorption to foreign surfaces is ubiquitous and nearly always spontaneous under normal conditions of temperature, pressure and solvent type. This would imply that the change in Gibbs free energy, dG, is negative. dG has an enthalpy and an entropy component as shown in its defining relationship:

$$dG = dH - TdS \qquad [1.1]$$

Studies by Norde and Lyklema (Norde and Lyklema, 1979), showed that for albumin adsorption on negatively charged polystyrene dH could be positive or negative depending on the pH. Since the adsorption occurred spontaneously under all conditions of pH it was concluded that the process was entropically driven and any enthalpic contributions were small. It was found for pH near the isoelectric point that protein adsorption became endothermic suggesting that entropically-driven hydrophobic interactions had become dominant. The increase in entropy associated with hydrophobic interactions occurs as a result of the disruption of structured water at the interacting hydrophobic regions of the protein and the surface. Exothermic adsorption can occur as a result of electrostatic, covalent or hydrogen bonding while a positive value of dH may be due to unfolding of the tertiary and secondary structure.

Lyklema pointed out these six main contributions to the enthalpy and entropy of protein adsorption (Lyklema, 1984):

1. "Hydrophobic dehydration" or disruption of structured water molecules causes an increase in entropy.
2. "Overall electrostatic interaction" affects the enthalpic contribution and depends on the charge sign of the protein and the surface.
3. "Structural alterations" yields positive values for dH and dS.
4. "Ion incorporation" has varied effects on dH and dS. They are both negative if ions are merely used in the interlayer between the surface and a like-charged protein.
5. "Van der Waals interactions" contribute only slightly to the enthalpy term.
6. "Specific binding" depends on the properties of the surface and the protein and is a result of many simultaneous interactions between the two.

   Thermodynamic parameters depend on all aspects of the system but in particular on the structure of the protein itself.

If protein adsorption can be understood from a thermodynamic viewpoint the ability to predict protein adsorption will depend on appropriate thermodynamic characterizations of the protein, surface and solvent. Even if this theory cannot be used to predict adsorption quantitatively, the results of microcalorimetry experiments contribute to the understanding and elucidation of protein adsorption mechanisms. Arguments will be presented in the following section to suggest that thermodynamic modeling of protein adsorption is not generally appropriate and that kinetic models may be more useful.

1.1.5 A Review of Some Concepts in Protein Adsorption Mechanisms

Some of the more frequently encountered hypotheses regarding protein adsorption mechanisms need to be reviewed to put into perspective the complexity of events that should be considered in any attempt to create mathematical models. Protein adsorption probably requires more than one or two mechanisms to adequately describe the wide range of behavior observed. For a review of protein adsorption modeling in significantly more detail the reader is referred to the text of Andrade (1985b) and the articles by Lundstrom (1985) and Andrade and Hlady (1986). The following discussion exposes the breadth of opinion and variety of observations that have been made.

Protein adsorption data are typically collected in the form of kinetics or isotherms. The results often closely resemble those expected for a reversible Langmuirian mechanism despite the fact that none of the assumptions for such a mechanism is valid for macromolecular adsorption. The data for a single component system may be well fit by a Langmuir model as shown by Moreno et al (1987) but the meaning of the parameters obtained is questionable. Moreno et al (1987) also showed that single protein models could not be used to predict binary system behavior, so a thermodynamic model with additional parameters was developed for this case.

The validity of models based on the assumption of thermodynamic equilibrium is challenged by sequential adsorption studies (Beissinger and Leonard, 1981 and 1982; Ivarsson and Lundstrom, 1986). These studies, along with many others, show protein adsorption to be a highly "path dependent" process which cannot be predicted using an equation of state. Desorption of protein from surfaces into a protein-free buffer indicates that there is an irreversibly bound fraction which cannot be desorbed in a reasonable time frame (Chan and Brash, 1981). The isotherm therefore demonstrates "hysteresis" because the adsorbed amount is not a unique function of the "equilibrium" protein solution concentration. The concept of hysteresis as it pertains to protein adsorption has been developed in detail by Jennissen (1985). He showed that the hysteretical behavior of gas adsorbing in narrow pores is analogous to protein adsorption. However there are mechanisms specific to protein adsorption which may be able to account for hysteresis. All of these are related directly to the violated assumptions of the Langmuir model.

Most proposed mechanisms for protein behavior at an interface allow for multiple surface states. Proteins are not generally spherical and thus may be expected to take on a variety of orientations on the surface. For example, in a simple two state case the possible orientations may be referred to as "side on" or "end on" (Lundstrom, 1985; Brynda et al, 1986). As the residence time of the protein on the surface increases, its lack of rigidity allows it to increase the number of surface contacts resulting in stronger binding and possibly an increased area per molecule (MacRitchie, 1978; Bohnert and Horbett, 1986; Schaaf and Dejardin, 1988). The states which a protein molecule may attain on a surface are numerous but an adequate model may require only a few generalized states to predict a wide range of

behavior. Beissinger and Leonard (1981 and 1982) for example used two states to model adsorption and desorption of plasma proteins, while Lundstrom (1985) used a two state model for the adsorption of various proteins to hydrophobic silica.

The organization of protein molecules on a surface may also change with time and thus affect overall adsorption behavior. Randomly adsorbed molecules cannot be expected to achieve a perfect hexagonally close-packed monolayer as has been shown in Monte Carlo simulations of random sequential adsorption (RSA) (Giaever and Keese, 1987; Schaaf and Talbot, 1989; Schaaf et al, 1988). In fact the maximum coverage expected for RSA has been shown to be about 54.7% of the total surface. Surface diffusion of proteins has been observed (Burghardt and Axelrod, 1981) and may allow more efficient packing on the surface subsequent to the initial RSA. The evolution of an efficiently packed monolayer may also be driven by cooperative processes which encourage protein-protein interactions as reported by Nygren (1988a). Adsorbed molecules have been shown to exchange with the bulk solution to a limited extent (Chan and Brash, 1981) but it is unclear whether the exchange is due to desorption and replacement or to an actual displacement of the surface bound molecules by those in solution (Andrade, 1985b page 64). In either case the turnover promotes the filling of the surface by more compact molecules with a shorter average residence time. Not only do the processes discussed above result in a larger number of molecules per surface area but also in a stronger adsorption due to the cooperative binding. All of these surface rearrangement phenomena may contribute to the hysteresis or path dependent nature of real protein adsorption data.

Once a monolayer has been formed there is some question whether additional adsorption leading to multilayer formation may occur. It is the belief of some (Eirich, 1977) that under most circumstances, nonspecific macromolecular adsorption leads to only a monolayer. It is possible that surface rearrangements may be able to explain the ability of some surfaces to continue adsorbing even after they are completely covered. Young et al on the other hand have observed what they believe to be multilayer adsorption of albumin on silicone rubber (Young et al, 1988a,b).

The processes which govern protein adsorption are clearly numerous and many if not all of the mechanisms described above contribute to the behavior seen in any given protein/surface system. It is questionable whether the adsorption of molecules as heterogeneous as proteins can be described adequately with a few parameters and a general model form.

However, if an appropriate model form is found in a specific case, the fitted parameters may yield important insights into the surface properties which have the greatest impact on protein adsorption.

1.1.6 Measuring Protein Adsorption

Ex situ measurements of the adsorption of radiolabeled proteins is the best currently available quantitative technique for obtaining accurate, absolute data. Other methods have major shortcomings. Labeled antibody binding to the adsorbed protein is subject to the effects of nonspecific binding and hidden binding sites due to orientation of the adsorbed protein. Solution depletion, an *in situ* method, is relatively inaccurate and error is strongly influenced by the ratio of protein in solution to adsorbed protein. Other *in situ* techniques such as ellipsometry, FTIR-ATR (Fourier transform infrared attenuated total reflectance) spectroscopy, TIRF (total internal reflection fluorescence), TIRIF (total internal reflection intrinsic fluorescence), and SERS (surface enhanced Raman spectroscopy) are capable of obtaining real time data related to adsorbed quantities and molecular conformation. However, calibration and quantification is more difficult with these methods due to the confounding effects of protein in solution near the surface and conformational changes in the adsorbed protein. The estimates of adsorbed quantity are less precise and the type of adsorbing surface is generally limited by the optical or electrical requirements of the individual techniques. The volume edited by Andrade (1985b) contains descriptions of the most frequently used methods for measuring the adsorption of proteins.

An *in situ*, real time method for measuring adsorption has been developed in our laboratory (R. Cornelius, 1988). The technique involves the adsorption of labeled protein onto glass beads in a well-stirred flow cell. The interpretation of data is more complicated, but protein adsorption determined in this system reflects the total quantity of irreversibly and reversibly bound protein. To date the technique has been applied to the study of only one surface, soda-lime glass beads. In the future silanes could be employed to provide a variety of surface chemistries for evaluation. Any attempt to fit kinetic adsorption models to such data will require a well-calibrated and well modeled physical system.

1.1.7 The Vroman Effect

Much research has been devoted to the study of single protein systems in order that the knowledge gained may be applied to the multicomponent systems encountered in nature and in systems of practical interest. Blood plasma for example, contains approximately two hundred proteins of varying properties and concentrations. Each protein has its own specific biological function. The adsorption behavior of some of the most abundant plasma constituents has been studied in single, binary and ternary protein solutions (Beissinger and Leonard, 1982; Soderquist and Walton, 1980; Brash and Samak, 1978; Merritt et al, 1988). In systems involving albumin, IgG and fibrinogen, which are among the most abundant plasma proteins, the surface composition was found to influence strongly the composition of the adsorbed protein layer. In most cases it was concluded that fibrinogen was adsorbed preferentially from binary and ternary protein solutions on surfaces which promote thrombus formation, especially glass. However, attempts to measure adsorption of fibrinogen from blood plasma produced a surprising result first reported by Vroman and Adams (1969). After times of a few minutes or longer fibrinogen was not present on glass following exposure to plasma while albumin and IgG with their presumably lower affinities were detected in substantial quantities (Horbett, 1984; Brash and ten Hove, 1984; Wojciechowski et al, 1986). A binary or ternary system is thus apparently not an appropriate model for plasma. Later it was shown that high molecular weight kininogen, HMWK (the significance of which is discussed in section 1.3), a trace protein, specifically displaces fibrinogen from the surface during the first few seconds of contact with plasma (Brash et al, 1988). These events constitute what is now known as the "Vroman Effect".

The Vroman effect was also studied by Elwing and coworkers (1987a) who found that HMWK displacement of fibrinogen occurred on hydrophilic surfaces, but HMWK was not adsorbed from plasma onto hydrophobic surfaces. It is possible that the displacement of fibrinogen in this case is due to other plasma components. The work of Breemhaar et al (1984) suggests the involvement of lipoproteins.

Clearly there are significant interactions in blood plasma that cannot be accounted for by individual protein-surface affinities determined from single protein experiments. Specific displacements take place to determine the steady-state interfacial composition in a poorly understood process that is a strong function of surface properties. These phenomena may be observable events in the processes that control thrombosis on an artificial surface.

1.2 Blood Coagulation and Thrombus Formation

When blood and a foreign surface come into contact the first important event to take place is the adsorption of proteins from blood plasma (Brash, 1987). Before the cellular blood components become involved, there is a competition for available surface among the proteins which ultimately determines the interfacial protein composition. The final composition depends on the nature of the underlying solid surface and presumably has an influence on the rate of activation of the intrinsic coagulation pathway. The solid surface acts as a catalyst, facilitating the reactions which eventually cause fibrinogen to polymerize. In regions of low blood flow rate, the fibrin clot is more likely to remain attached to the surface and grow, entrapping red blood cells and other cellular components to form a thrombus (Williams, 1987). Depending on the composition of the adsorbed protein layer, platelet adhesion, aggregation and release may also occur and contribute to thrombus formation. In a vascular prosthesis or other vascular implant, a thrombus may continue to grow causing occlusion of the flow path or, if the flow is strong enough it could break off to form life-threatening "emboli" in downstream locations. In order to better appreciate the significance of blood interaction studies, such as carried out in this project, a more detailed discussion of the enzymatic pathways for blood coagulation and the role of foreign surfaces in these pathways, is given in this section.

1.2.1 Coagulation Pathways

Blood coagulation occurs as a "cascade" of sequential enzyme-substrate reactions which may be initiated via two mechanisms (see Figure 1.3) (Hirsh and Brain, 1983; van Dam-Mieras and Muller, 1986). If a blood vessel wall is ruptured, the damaged endothelial tissue releases thromboplastin in small quantities and in the presence of calcium, factor VII is activated. This constitutes the "extrinsic" coagulation pathway. The "intrinsic" (surface activated) pathway, on the other hand, is a slower but more important mechanism, in relation to blood-material interactions. The zymogen (enzyme precursor) factor XII is activated to the enzyme factor XIIa either by a negatively charged surface or through a set of feedback reactions involving small quantities of the activated forms of prekallikrein and high molecular weight kininogen (HMWK) in the presence of a surface. Although a distinction is made between the two pathways for explanation purposes, in reality considerable interaction occurs between them. In the case of vessel wall damage for example, exposed collagen

(a structural protein) may play the role of a negatively charged, foreign surface and participate in the activation of factor XII. In the presence of platelet phospholipids and calcium the common pathway for coagulation beginning with activation of Factor X, leads to the polymerization of fibrinogen by thrombin to form a fibrin clot.

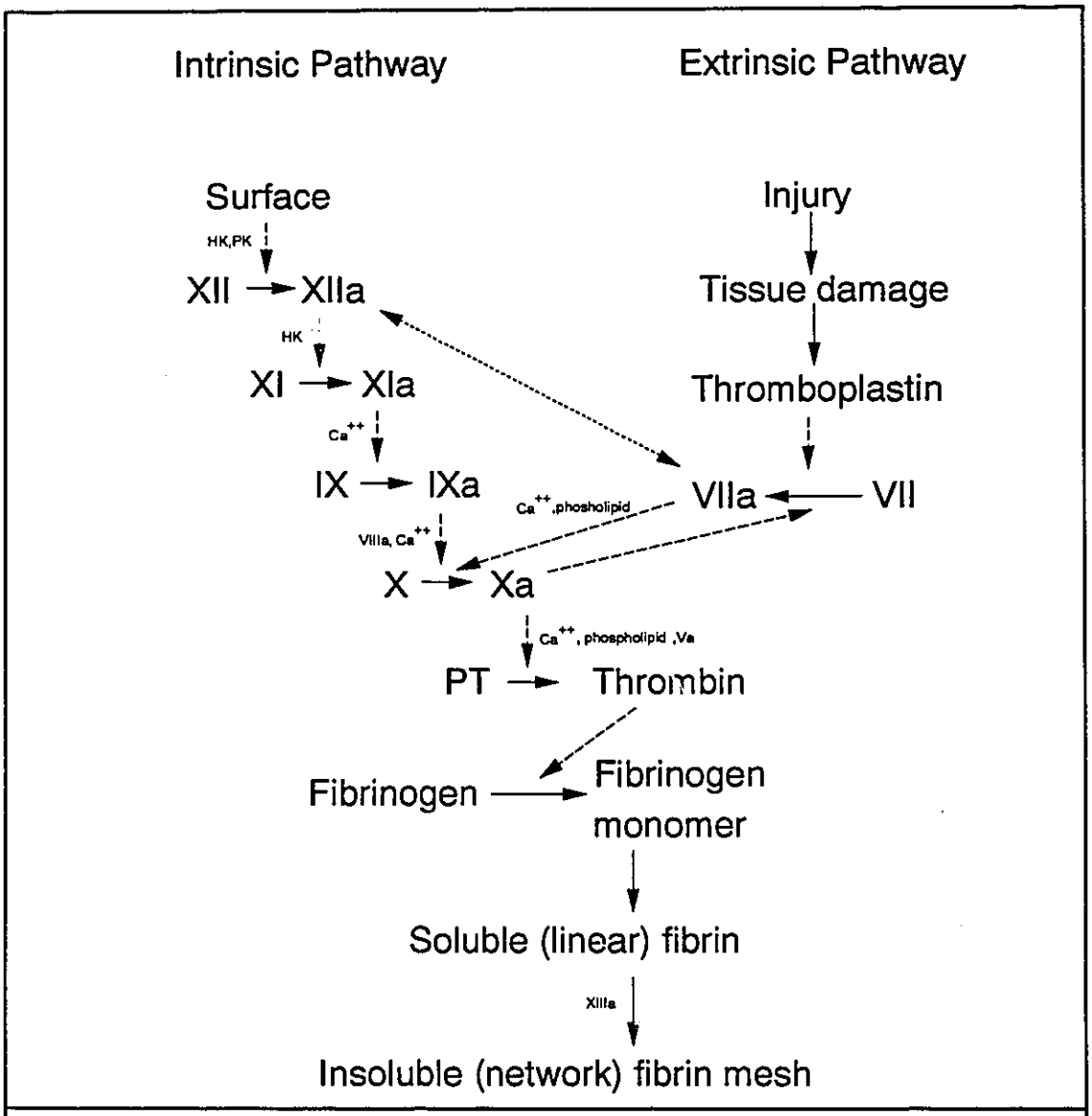

Figure 1.3: The main enzymatic pathways leading to fibrin formation.

Although the activation of factor XII is depicted in figure 1.3 as a simple surface catalyzed reaction the complete mechanism of this first step is far more complicated and needs to be described in greater detail.

1.2.2 Activation of Factor XII by a Surface: The Contact Phase of Coagulation.

Although it has been shown in the past that a negatively charged surface can activate factor XII, more recent evidence suggests that this reaction is very slow in the absence of kallikrein (Silverberg and Diehl, 1987), the activated form of prekallikrein. Figure 1.4 (Ogston and Bennett, 1978; Bouma and Griffin, 1986; Scott et al, 1985) depicts an hypothesized mechanism by which the intrinsic coagulation pathway is initiated. Factor XII may be activated to a surface-bound αXIIa form or the much less active βXIIa which exists as a free fragment in solution. The reactions which lead to the mutual activation of factor XII and prekallikrein (PK) have been named the "reciprocal proteolytic pathway". Factor XII (normally present in plasma at a level of 40 μg/mL) may be activated by factors XIIa, XIa, or kallikrein (KAL) in the presence of HMWK (70-90 μg/mL) (high molecular weight kininogen). HMWK exists in plasma as bimolecular complexes with prekallikrein (50 μg/mL) and factor XI (6 μg/mL) and is required for full surface activation of these zymogens (Silverberg and Diehl, 1987). HMWK has a large positively charged region (rich in histidine and lysine) which makes it ideally suited for the role of transporting and attaching the cofactors, PK and XI to negatively charged surfaces (Colman et al, 1987; Bouma and Griffin, 1986).

It is important to note that a patient with a deficiency in any of the factors XII, pre-kallikrein or HMWK is asymptomatic. Only *in vitro* tests show prolongation of the clotting times. The cyclic reactions which make up the reciprocal proteolytic pathway have no distinct beginning, leaving open the possibility that other enzymes or autoactivation may be required to initiate the cascade. It remains a challenge for those in coagulation research to explain how contact activation can continue to result in factor IX cleavage even in the absence of several of the four contact phase zymogens (Berrettini et al, 1987).

Patients with a deficiency in factor XI do experience abnormal bleeding. If factor XI could be activated in the absence of HMWK, PK and factor XII it might help to explain how patients deficient in these factors appear to be asymptomatic, and how *in vitro* tests

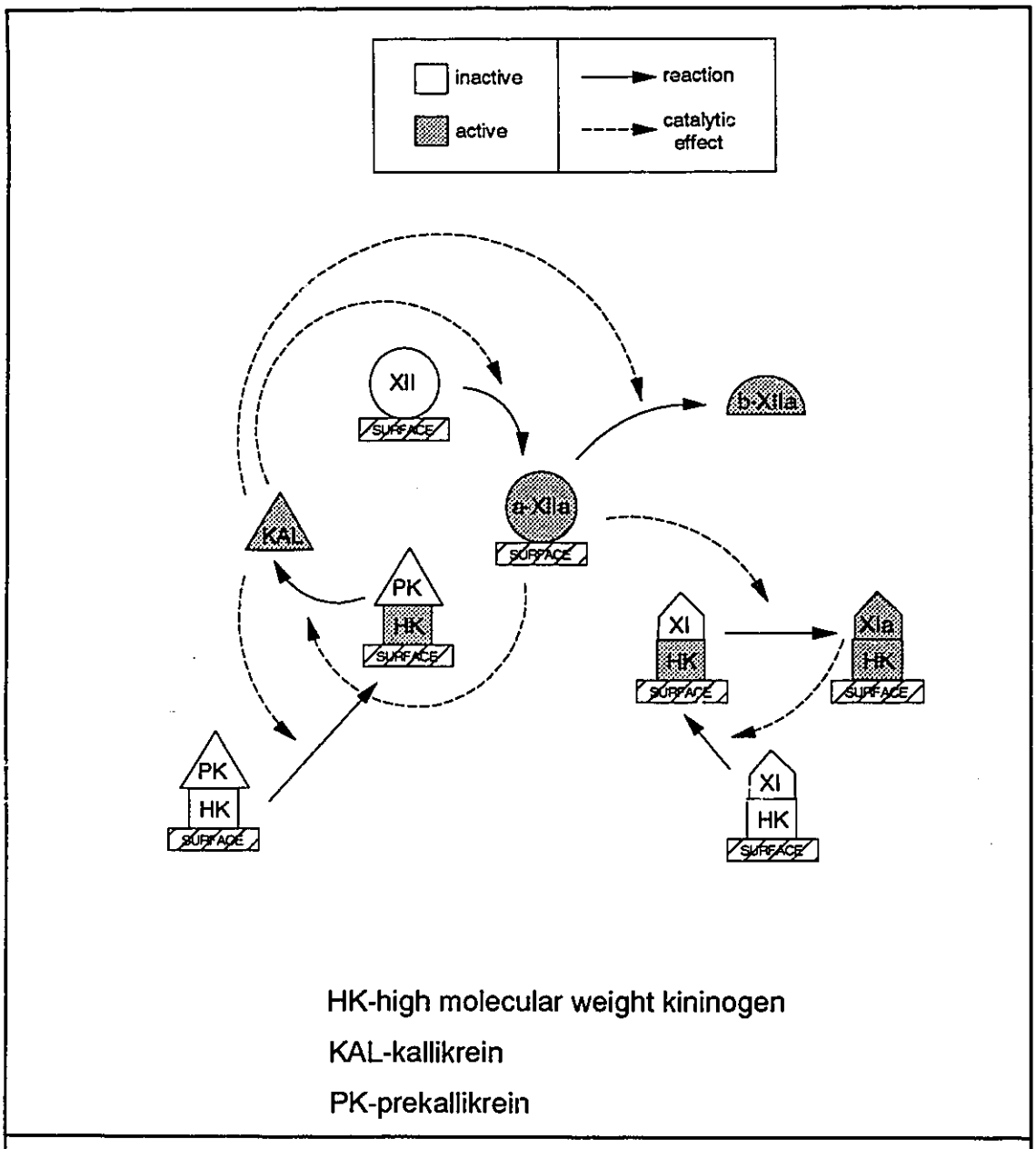

Figure 1.4: The contact phase of coagulation.

using their plasmas show only a prolongation, and not an absence of clotting. Recent evidence reported by Naito and Fujikawa (1991) suggests that factor XI can be autoactivated or activated by thrombin in the presence of a negatively charged surface. They observed that purified factor XI was autoactivated only by dextran sulfate, and activation by thrombin was possible in the presence of dextran sulfate and to a lesser extent of sulfatide and heparin. If a slight activation of factor XI is possible on surfaces in general it may be enough to begin the cycle of reactions that make up the reciprocal proteolytic pathway.

Positively charged surfaces have also been implicated in the indirect activation of the intrinsic pathway. Pederson et al (1989) reported that factor VII was autoactivated in the presence of polylysine. Factor VIIa can activate factor XII to XIIa (and vice versa, see Fig. 1.3). Understanding of the behavior of the contact phase proteins at solid surfaces is incomplete and for this reason among others, it is not yet possible to develop a model capable of predicting, even qualitatively, the short term blood compatibility of biomaterials.

1.3 Blood Contacting Materials

1.3.1 Blood Compatibility: An Important Concern in Biomaterials Science

The definition of "biomaterials" encompasses all artificial devices which may be used to replace bone, soft tissue or a functioning organ of the body either in acute or chronic, external or internal applications. The design of such materials may involve many considerations including toxicity, chemical stability, mechanical properties, and biocompatibility (Bruck, 1980). Blood compatibility is a particular aspect of biocompatibility. Biomaterials that contact blood face a wide range of potential problems including infection, complement activation and calcium deposition. As already referred to, the most difficult problem has been the prevention of thrombus formation induced by the surface of the material. It may be argued that blood compatibility is the single most important problem in biomaterial science since the annual U.S.A. production of artificial kidneys (6.5 million) and blood oxygenators (310,000) outnumber, by far, the production orthopedic prostheses (235,000) (Galletti, 1984). Researchers in this field are faced with the challenge of finding a mechanically appropriate material which resists thrombus formation.

The only material intended to come into contact with blood is the vascular endothelium, a single tight layer of specialized cells which lines the entire circulatory system. Some researchers have attempted to culture layers of endothelial cells onto vascular grafts to render them thromboresistant (Ryan, 1987). To this point only short term benefits have been obtained by the implantation of endothelialized grafts produced by cell "seeding" or "sodding" (Burkel et al, 1987; Williams et al, 1987). Recently some success in attaching viable endothelial cells specifically to glass via a cell binding peptide has been achieved *in vitro* (Massia and Hubbell, 1991). The same peptide (Arg-Glu-Asp-Val) rejects the attachment of unwanted cells including fibroblasts, smooth muscle cells and platelets. If this technology can be applied *in vivo*, other synthetic biomaterials may not be needed for long term blood-contacting implants. Many practical problems have yet to be addressed including the stability of the cell layer in flow. Research on synthetic surfaces must continue however, in order to improve materials for acute and extra corporeal applications such as blood storage containers and membranes for blood dialysis and oxygenation.

1.3.2 Blood Contacting Materials

In the seventeenth century, William Hewson observed that blood remained fluid inside an isolated segment of peripheral vein but clotted quickly when poured out into a bowl (Salzman and Merrill, 1982). Later work by Lister (Lister, 1863) seemed to indicate that the clotting time for blood outside the body was prolonged in non-wettable materials. Until quite recently it was felt that the solution to the blood compatibility problem was to find an inert or nonwettable surface. At the present time the concept of total inertness has been all but abandoned.

Heart valve leaflets and vascular segments obtained from human and animal donors have been tanned (to stabilize the collagen matrix as well as to destroy antigenicity) in order to prepare them for implantation (Dardik, 1978). The fixed materials have only fair compatibility properties and can degrade over time. The endothelial lining is disintegrated by the tanning process and exposed collagen can trigger the activation of factor XII and the intrinsic pathway.

Some metals (e.g. alloys of titanium, chromium, cobalt, molybdenum, nickel) have the required strength and corrosion resistance to be used in heart valves but careful design is required to prevent regions of stagnant flow where thrombus formation can occur. In

order to make a more passive surface, coatings of LTI (low temperature isotropic) carbon have been deposited on metals and other surfaces (Andrade, 1985a). This provides a homogeneous, unreactive surface with a low interfacial free energy which resists clotting.

Polymers have been the most widely studied class of potential biomaterials due to their fair compatibility and good mechanical properties (Andrade, 1985a; Horbett et al, 1986; Chuang, 1984; Dong et al, 1987). Initial attempts to minimize interactions with blood focused on finding inert materials with a low surface free energy and led to the development of medical grade silicone rubbers (SR) and the proposal to use polytetrafluoroethylene (PTFE) and similar materials. These hydrophobic materials and others including polyethylene (PE) and polypropylene (PP) are mechanically appropriate for many applications, but are not ideally compatible with blood. In contrast to these materials, hydrophilic and water swellable polymers (hydrogels) such as poly(hydroxyethyl methacrylate) (pHEMA), have also been studied in contact with blood in the hope that a virtual water-water interface will be formed. Attempts have also been made to find the best combination of hydrophilicity and hydrophobicity since both interactions appear to be necessary for compatibility (Horbett, 1981; Horbett and Weathersby, 1981).

The complexity of issues in blood compatibility has required polymers whose mechanical properties are generally good and whose chemistry is easily modifiable. Segmented polyetherurethanes (SPUs) have been among the most successful and important biomaterials for these reasons. SPUs are thermoplastic elastomers due to the microphase separation of physically incompatible segments of the macromoleclules. This feature gives them their processability and good elastomeric properties. The two incompatible regions of the polymer chains include the so-called "hard" aromatic segment and the "soft" polyether chains. The fact that the relatively inert polyether segments dominate the surface of a solid SPU specimen appears to be responsible for the biocompatibility of these materials (Lelah and Cooper, 1986). Attempts continue to be made to modify the chemistry of the more thrombogenic hard segments of SPUs in the hope that they be made even more compatible (Santerre, 1990; Grasel and Cooper, 1989). Unfortunately, it is not possible to control independently both the blood compatibility and mechanical properties of SPUs. This is a problem for bulk polymer modification methods in general and suggests that the future of blood compatible materials may lie in the ability to control surface chemistry independent of the bulk.

1.4 Surface Characterization of Biomaterials

The reaction between blood and an artificial biomaterial is logically a strong function of the properties of the biomaterial surface. The challenge has been to find simple parameters describing the surface properties which may be directly correlated with *in vivo* or *in vitro* compatibility and performance. No single parameter has proven to be capable of predicting any aspect of blood compatibility. In fact, new methods for surface characterization and theory for interpreting data are proposed at virtually every biomaterials conference. The problems of characterizing synthetic biomaterial surfaces in a quantitative and relevant manner are at least as important (and poorly understood) as developing meaningful assays for estimating blood compatibility.

1.4.1 Physicochemical Methods

A knowledge of surface chemistry is fundamental to the characterization of biomaterials in that from it one should in principle be able to predict other properties including wettability, surface charge, solvent penetration, protein adsorption and even blood compatibility. In the past when sophisticated tools were not available it was often assumed that the surface chemistry of a given material was similar to that of the bulk. Vroman (1965) was early among those who suspected that contamination made such assumptions invalid. More recently Ratner (1985) has been a strong proponent of surface chemical analysis and in the process has made X-ray photoelectron spectroscopy (XPS) virtually a "required" analytical technique in biomaterials science. Auger spectroscopy and secondary ion mass spectrometry (SIMS) are related techniques that have not been used as widely as XPS (Andrade, 1985a).

XPS or electron spectroscopy for chemical analysis (ESCA) is capable of giving quantitative information about the elemental composition and chemical structure of a solid surface to a depth of 20 to 200 Å. A flat sample is placed in a vacuum chamber (10^{-7} to 10^{-10} torr) and bombarded by a monochromatized X-ray source. Due to the bombardment by X-ray photons the material emits photoelectrons with kinetic energies related to their binding energies, and by measuring the spectrum of energies produced information about the chemical structure of the material may be deduced. Photoelectrons have a limited mean free path (MFP) through solid matter and thus only those from about the first hundred angstroms of the bulk material will escape to be detected. This fact is used to advantage in

elucidating the compositional profile of the surface layer. The sample may be placed at an angle away from the perpendicular relative to the detector. This is known as the take-off angle (θ_{XPS}). Only electrons emitted from a depth of cosine(θ_{XPS}) times the MFP or less are detected. The angle dependent data may be used qualitatively to show enrichment of specific chemical groups near the outer surface. Software is available to estimate a continuous depth profile. Such depth profiles do not represent unique solutions to the angle dependent data and are recommended for qualitative interpretation as well.

Early studies seemed to indicate that water wettability was an important property for blood compatibility. Many techniques have since been developed to quantify this property including contact angle measurements of many kinds, and more recently interfacial free energy estimations. Contact angles have had an important role in the characterization of biomaterials for many years. It is estimated that the technique is sensitive to the properties of only the outer 5 to 10 Å of a solid surface (Barenberg et al, 1987). The experimental technique is simple and inexpensive. A liquid droplet is placed on a smooth flat surface and the angle between the solid-vapor (SV) interface and solid-liquid (SL) interface gives the contact angle $\theta_{L/S/A}$ of a liquid (L) on a solid (S) in air (A). Many examples of complete wetting ($\theta_{L/S/A}$=0) have been found, but the maximum observed water contact angles are 130° (approximately) on certain fluoropolymers. A wide range of wettability can be measured with good reproducibility and thus the technique has found an important niche in the characterization of biomaterial surfaces.

Theories based in thermodynamics, mechanics, and chemical physics have been used for the interpretation of contact angle data. The Young equation (equation 1.2) is a one dimensional force balance at the three phase contact line on the edge of a spreading liquid drop.

$$\gamma_{LA} \cos\theta_{L/S/A} = \gamma_{SA} - \gamma_{SL} \qquad [1.2]$$

$\theta_{L/S/A}$ and γ_{LA} may be measured independently and in fact, tabulated values of γ_{LA} are available for many pure liquids. γ_{LA} is the liquid surface tension which is only a weak function of the gaseous "A" phase. The liquid surface tension is equivalent to its surface free energy. For a solid surface which cannot freely rearrange under the influence of surface stresses, no such direct relationship between tension and free energy exists (Zangwill, 1988). Nonetheless,

equation 1.2 has been used to obtain estimates of the solid surface tension, γ_{SA} and the liquid-solid interfacial tension, γ_{SL}. It has been hypothesized that the interfacial free energy, γ_{SL} represents the driving force for interaction between the surface and blood, including protein adsorption and enzyme activation (Ruckenstein and Gourisankar, 1984; Bagnall and Arundel, 1982). Since equation 1.2 contains two unknowns, the value of γ_{SA} has never been directly available, but a number of theories and methods have been used to interpret the contact angle data. (See section 4.2.5).

Zisman (1950) found that plots of $\cos\theta_{L/S/A}$ against γ_{LA} (for a series of liquids on a given solid) produced a reasonably straight line. By extrapolating the linear data to $\cos\theta_{L/S/A}=1.0$, a critical surface tension, γ_C, characteristic of the surface was obtained. The method was limited to fairly hydrophobic surfaces and yielded no estimates of the thermodynamic parameter γ_{SA}. Fowkes (1964) addressed this issue by proposing that surface tension was a sum of surface tension components which, for most practical purposes, could be assumed to be dominated by so-called polar (γ^p) and dispersive (γ^d) forces. Fowkes' model calculated interfacial tension between immiscible phases by a microscopic interaction equation (see section 4.2.5.3). Neumann (1974) argued that the contact angle is a macroscopic phenomenon with different behavior on a microscopic level. He proposed a purely macroscopic interaction model based on an empirical thermodynamic correlation, which directly related the three surface tension values in the Young equation. The model has not been widely accepted despite Neumann's valid criticism of the use of microscopic models to interpret macroscopic contact angles. No single theory has emerged as definitive, but the Fowkes model has been the most frequently employed in the biomaterials field.

The focus of the present study was on the use of XPS and contact angles to characterize a series of model surfaces, but there are many other properties which are either less important or more difficult to determine. Surface charge (Lyklema, 1987), for example, has been proposed as playing a key role in blood compatibility. Blood vessel walls are believed to have a net negative charge (Hirsh and Brain, 1983) which has been assumed to help maintain blood fluidity but, paradoxically, the negatively charged surfaces of kaolin and glass have been implicated in the direct activation of factor XII and the intrinsic coagulation pathway (Hirsh and Brain, 1983; Ogston and Bennett, 1978). The roughness or porosity of a surface affects its wettability, area available for interaction, and adhesion properties, making it an

important property to measure or control. The ability of a surface to absorb solvent, especially water, can profoundly influence blood compatibility as well as attempts to characterize the surface by adsorption or contact angle methods. The chemical and mechanical stability of a surface must be sufficient to ensure that short term tests are representative of long term function. The mobility of molecular chains at a surface has been hypothesized to reduce protein adsorption (Andrade, 1985b) and thus may reduce contact activation (Nakao et al, 1986) but measuring such a property directly is not possible.

To this point only macroscopic surface properties have been discussed, but in recent years microscopic properties of surfaces have been of increasing interest. The chemical heterogeneity of real surfaces has an important influence on interactions with blood and its elements. It is also implicated in the phenomenon of contact angle hysteresis. XPS does not have the resolution to map the detailed chemical composition of a smooth surface. New scanning probe microscopy methods, especially atomic force microscopy (AFM), are being used to elucidate surface features of smooth surfaces on an atomic scale. The same tools have recently been used to look at individual proteins adsorbed from solution onto mica, but the 1 to 10 nN tracking force of the probe appears to change the shape of the adsorbed molecule (Andrade et al, 1991). This is less of a problem if dried protein is used but observations of dried proteins have questionable relevance to real systems in which fully hydrated proteins are adsorbed from aqueous solution (Marchant et al, 1991). AFM will be more useful when the tracking force of the scanning probe can be reduced to the point where adsorbed molecules are not affected by it. The technique will be limited to dilute protein solutions and thus to the sparsely covered surface that is already easily modeled. New methods will be required to observed the nature of proteins adsorbed from concentrated, multicomponent solutions such as blood plasma.

1.4.2 Blood Compatibility Testing

Blood compatibility testing for artificial blood-contacting materials requires studies ranging in complexity from *in vitro* protein adsorption studies (Horbett, 1987) to clinical trials with human patients (Wenzel et al, 1984). Biomaterials development relies heavily on tests at the *in vitro* end of the spectrum with some limited use of *in vivo* and *ex vivo* animal studies (Wilson et al, 1987). The criteria for evaluating the results of these tests tend to be based on the comparison of measured responses on test and reference materials.

Usually, one looks for a reduction in the response of blood elements to an artificial surface by adhesion, adsorption, or activation. Unfortunately according to various authors (Wilson and Cooper, 1986; Didisheim et al, 1984), none of the simple tests has proven to be capable of accurately predicting the *in vivo* performance of implants. On the other hand, the same authors state that *in vitro* studies have been shown to be useful for predicting short term contact with blood, *in vitro* or *ex vivo*. Thus materials for dialysis membranes, blood oxygenators, and catheters can be tested *in vitro* to predict their behavior in clinical applications.

The scope of *in vitro* surface-induced thrombosis tests includes those for clotting factor activation (Vroman, 1987), platelet activation (Joist, 1987), and whole blood clotting times (Chandler, 1958). Evaluation of these tests may be done visually with or without the aid of a microscope, by other optical methods including light transmittance, by rheological methods (Lemm, 1991), and via immunoassays and assays involving radiolabeling of blood components.

Park et al (1990) have proposed a method for quantifying the information obtained on spread platelets observed under a light microscope. Lindon (Lindon et al, 1989) evaluated platelet-surface interaction by total adhesion, aggregation, β-thromboglobulin release, and SEM. Platelet factors 3 and 4 may be detected after they are released using a chromogenic substrate and immunoassay respectively (Pelzer, 1984). It has recently been reported that platelets show enhanced adhesion in the presence of light, which casts doubt on many of the *in situ* microscopy studies that have been done (Haycox et al, 1991a,b). Platelet-surface interactions must continue to be evaluated in any assessment of blood-contacting biomaterials but their obviously complicated behavior is avoided in assays of the intrinsic coagulation system using platelet-free plasma.

Many enzymes in the coagulation cascade described in section 1.3 are the targets of assays for the clinical evaluation of bleeding disorders. Some of these tests have been applied to the study of blood compatibility including the recalcification time (RT), partial thromboplastin time (PTT), thrombin time (TT) and prothrombin time (PT). The RT test involves the incubation of citrate anticoagulated plasma with a test material. The plasma is reconstituted with calcium and the time to clot formation can be measured by a number of methods. The presence of traces of platelet phospholipids in platelet poor plasma (PPP) or even platelet free plasma (PFP) can lead to large variability in the results of RT tests.

The PTT test overcomes this problem to some extent by the addition of a known quantity of rabbit brain cephalin (RBC) or other platelet membrane substitute. The results of PTT tests tend to be more reproducible than RT tests but the presence of RBC may confound the interpretation of results which are assumed to be surface-specific. The TT test is a test of the common pathway (fibrinogen to fibrin conversion in particular) and is thus insensitive to the suppression of certain reactions in the intrinsic portion of the coagulation pathway. Heparin-like surfaces are expected to indirectly inhibit thrombin by binding antithrombin III and thus the TT test is a valid assay for these "actively" anticoagulant surfaces. The TT test is not a good general method of evaluating the blood compatibility of biomaterials.

The standard PTT test (Nye et al, 1962) is typically conducted by visually detecting the onset of coagulation in a test tube. Since this methodology is subject to significant observer bias, a more quantitative method was developed by Sefton (Rollason and Sefton, 1991) which measures thrombin generation directly. The cleavage of a substrate for thrombin resulted in the release of a fluorophore at a rate proportional to the concentration of thrombin present. The kinetic data were fit to a first-order autocatalytic model for thrombin generation. The technique was very sensitive to the presence of even small quantities of thrombin. One disadvantage of this method is that thrombin generation comes late in the coagulation cascade and is far removed from reactions at the plasma-surface interface. An assay based on a chromogenic substrate for kallikrein has been employed by Bots et al (1986) to compare activation of the contact system by polyethers with glass and silicone rubber as the positive and negative standards. The kallikrein generation results were strongly correlated with PTT tests on the same materials. This suggests that PTT and related tests can be good indicators of the rate at which a surface activates the contact system.

1.5 Past and Present Hypotheses Concerning Blood-Compatible Materials

Various rationales for designing synthetic blood compatible surfaces have been proposed ranging from inertness (Clark et al, 1970) to specific bioactivity (Andrade et al, 1987). While endothelialized surfaces (Burkel et al, 1987) may in the future become available for implantable vascular grafts, synthetic blood compatible materials will probably continue to have a larger share of the total biomaterials market. The materials for short term applications such as blood bags, oxygenators, and artificial kidneys have changed little over the years

especially with respect to the properties of their blood contacting surface. Only recently has the design of surfaces for such applications been seriously considered. In practice the effect of flow on blood compatibility is important (Goldsmith and Turitto, 1986) but only the effect of surface properties will be considered here.

In 1970, Clark et al summarized the current state of knowledge regarding blood compatible surfaces. Then, as today, the preparation and characterization of surfaces was complicated by the presence of additives, cleaners, and adsorbed vapor species. Conclusions were often contradictory and results were difficult to reproduce, but a consensus regarding the importance of certain surface properties began to develop. Surveys of a variety of materials suggested that hydrophobic surfaces caused the least damage to blood elements. Ross et al (1961) came to a different conclusion, namely that compatibility was a stronger function of surface chemistry than of wettability or charge. Most researchers agreed that a negative surface charge, similar to that on the endothelium was necessary for blood compatibility. In fact, by analogy with endothelium, Lyman (1965) suggested that hydrophilic surfaces could also be blood compatible. While negatively charged surfaces, including immobilized heparin (Gott et al, 1961), showed promise, positively charged surfaces with adsorbed heparin were also successful in short term *in vitro* systems (Merrill et al, 1966). Clark et al cited the importance of nonspecific protein adsorption, water structure at interfaces, and the changes in tertiary structure of adsorbed protein, as important considerations in the design of blood contacting surfaces.

Much more is now known about individual aspects including protein adsorption, surface chemistry, and blood coagulation, but the relationships among them continue to be difficult to discern. The goal of developing a surface which is totally unreactive toward blood has been largely abandoned in favour of materials designed to have specific desirable bioreactivity. Some of these new technologies (Andrade et al, 1987) involve controlled protein adsorption, covalent attachment of anticoagulants, and surface mobility.

The control of protein adsorption has been of interest due in part to the results of studies of platelet activation on adsorbed protein layers (Lyman et al, 1975). Albumin has been found to passivate surfaces while adsorbed fibrinogen and fibronectin promote platelet adhesion, spreading, and activation. Park et al (1991) have found that platelet activation is complete if the fibrinogen surface concentration on dimethyldichlorosilane glass is greater than 0.02 $\mu g/cm^2$; only 2-15% coverage. Lindon et al (1987) have found that protein con-

formation is more important than adsorbed quantity in determining the extent of platelet activation. The contrasting compatibilities of albumin and fibrinogen have led to the precoating of surfaces with albumin (Chang, 1974). Surfaces have also been developed which are expected to adsorb albumin preferentially from blood plasma (Pitt and Cooper, 1988; Munro et al, 1983). Albumin precoating of surfaces has been successful for short term applications like dialysis but desorption and disintegration of the albumin layer in the long term make the technique impractical for vascular implants.

The covalent attachment of anticoagulants to polymers has been largely focused on heparin (Cottonaro et al, 1982; Heyman et al, 1985) although antiplatelet agents (diatazole, dipyridamole, apyrase, prostacyclin), fibrinolytic agents (urokinase, plasmin), and heparin-like materials have also received considerable attention (Sefton et al, 1987). Hirudin, a highly specific thrombin inhibitor derived from the leech, has been attached to agarose and polystyrene (Ku et al, 1991), though no definite data on blood interactions are as yet available.

The control of surface-induced coagulation almost certainly lies in the control of factors XII, XI, prekallikrein and HMWK. Heparin is an anticoagulant frequently used to control thrombosis in part through its actions on some of these clotting factors. It is a highly sulfated mucopolysaccharide with a fairly broad molecular weight distribution (10 to 30 kD) (Platé and Valuev, 1986) and elemental composition. Through its interaction with ATIII, heparin inhibits the actions of five clotting factors: XII, XI, IXa, Xa and thrombin. Its ability to inhibit activated clotting factors directly has made the attachment of heparin to surfaces either covalently or ionically the subject of much research (Platé and Valuev, 1986; Jozefowicz and Jozefonvicz, 1985; Heyman et al, 1985). In general the molecules have been bound either too strongly to maintain their activity or too weakly to prevent desorption back into the blood.

The incorporation of sulfonate groups directly into polymers to produce heparin-like surfaces is an area of active current research (Santerre, 1990; Grasel and Cooper, 1989; Migonney et al, 1988; Douzon et al, 1987). Many heparin-like materials incorporate sulfonate groups (SO_3^-) as well as carboxyl, sulfonamide, and amine groups, all of which occur naturally in heparin. Recent studies have shown reduced platelet adhesion and activation (Grasel and Cooper, 1989) on sulfonated polyurethane anionomers despite increased fibrinogen adsorption. Paradoxically, similar polymers showed slower blood coagulation (by a thrombin time assay, Santerre, 1990) despite the widely accepted "rule of thumb" that

negatively charged surfaces rapidly activate the intrinsic coagulation pathway. Santerre and Brash (1991) may have found a connection to the intrinsic pathway in that they observed the "Vroman effect" (see section 1.1.6) was inhibited by the presence of sulfonate groups. Heparin-like materials (Jozefowicz and Josefonwicz, 1986) are more easily synthesized and may give greater long term stability than heparin-grafted materials.

Natural blood contacting surfaces and polyurethane biomaterials contain a significant amount of nitrogen in various forms. Nitrogen is present in peptide bonds and many amino acid side groups. Ten per cent of the nitrogen in heparin occurs as free amine groups (Platé and Valuev, 1986). An alkyl amine side group distinguishes lysine from other amino acids and may determine its affinity for plasminogen, the precursor to the fibrinolytic enzyme, plasmin. At physiological pH, the amine groups are largely protonated and carry a positive charge. Positively charged surfaces may avoid the activation of factor XII.

Fibrinolytic surfaces are distinct from anticoagulant surfaces in that they promote the dissolution of a thrombus already formed on the surface. If thrombolytic activity is sufficiently rapid, clot formation may cease to be a significant problem (Brash and Thibodeau, 1986; Brash et al, 1985). Woodhouse et al (1991) have proposed the bulk modification of a segmented polyurethane with lysine which has a strong affinity for plasminogen. For such a material, the prevalence of plasminogen near the surface would provide the potential for fibrinolysis via conversion of plasminogen to plasmin. A more directly fibrinolytic surface was developed by Sugitachi et al (1978) by attaching urokinase (UK, a plasminogen activator) to nylon. Whole blood clotting times were increased from 10 to 30 minutes on these materials, presumably because UK was able to convert plasminogen to plasmin. To help maximize plasmin activity, the antiplasmin inhibitor, nitrophthalic acid, was also immobilized. Streptokinase (SK) may also be useful in designing fibrinolytic surfaces, but the existence of SK antibodies in human plasma and SK's indirect cofactor role (Collen and Lijnen, 1986) make it less promising than UK.

While much of the current interest in the field has been focused on preparing actively compatible surfaces some consideration has also been given to the rational design of passive surfaces. A theoretical criterion for creating passive surfaces was proposed by Ruckenstein (Ruckenstein and Gourisankar, 1984) based on minimizing the interfacial free energy (see also Bagnall and Arundel, 1982), and therefore the driving force for interaction between phases. The minimum interfacial free energy criterion led to the concept of "mobile surfaces"

to reduce cellular adhesion and protein adsorption. Surface mobility is imparted by the grafting of flexible poly(ethylene oxide) (PEO) to synthetic materials. Nagaoka (Andrade et al, 1987) has shown that hydrophilic copolymers grafted with large PEO chains (of chain length 50 or more) minimize adsorption and adhesion of blood elements. It is hypothesized that a combination of PEO chain motion and hydration gives these surfaces their relative inertness.

It seems likely that surface modification (Hoffman, 1987) will continue to become more important than bulk modification (Sefton et al, 1987) in the development of blood compatible materials. Chemical methods involving silanes (Elwing et al, 1987b), radiation grafting, and plasma treatments (Pitt, 1989) have been employed to produce the reactive groups necessary to attach actively and passively compatible molecules to substrate materials. It will become increasingly expected that surfaces be fully characterized with respect to all important properties including chemistry, wettability, protein adsorption and whatever other parameters may be found to be important. Only with this multivariate information will it be possible to test and defend the hypothesis that blood compatibility is improved as a direct result of modified surface chemistry (as opposed to indirect effects of changed protein adsorption behavior or increased wettability).

The practical disadvantages of bulk polymeric modification for the purpose of producing model biomaterial surfaces are numerous. Modification of segmented polyurethanes (SPUs) may not be reflected directly in the surface composition of solid specimens due to microphase separation (Lelah and Cooper, 1986). The molecular structure of SPUs allows some rearrangement of the surface groups in response to their environment. This can result in a different physicochemical surface composition, for example in contact with polar and nonpolar solvents. To compare contact angles for two cases in which the surface compositions are different would be inappropriate despite the fact that the bulk material in question is the same in both cases. The swellability of SPUs (Santerre, 1990) and other hydrophilic polymers makes them less appropriate for protein adsorption studies. Adsorption and compatibility data can be complicated by the absorption of solvent, ions, and even protein itself.

1.6 Objectives

This project was intended to provide a unified study of the relationships among the properties and processes which govern the blood compatibility of artificial surfaces. The problem is an enormously complex one and as a result the work was necessarily limited in its scope. Three general areas of interest were identified: surface characterization, protein adsorption and blood compatibility. While studies in any one of these three areas could produce useful scientific contributions it was of greater interest to synthesize all the available data in an informative way. Frequently such data are obtained when characterizing biomaterials but the comparability of the data is suspect since the variety of environments under which tests are performed can significantly modify the surfaces under scrutiny. For some biomaterials, chiefly hydrophobic polymers, this assumption can be justified, but in general for wettable and swellable materials the same claim cannot be made. As a result the range of surface chemistries for which such studies have been made and compared, has been limited. In order to study directly the effect of different surface chemistries on protein adsorption and blood compatibility a series of model surfaces had to be developed. The goal of the experimental design was to collect enough data to find a quantitative, multivariable relationship that could be used to predict blood compatibility and/or protein adsorption given independently determined surface properties alone. In the past qualitative, univariate relationships have been proposed linking blood compatibility to surface charge, wettability, water content, albumin adsorption and many other individual surface properties. Clearly this univariate approach has been overly simplistic and in some cases misleading in its attribution of cause and effect.

A study with the aforementioned objectives was dependent upon the design and characterization of a series of model surfaces. Silanized silica was adopted as the model. Silica (clear fused quartz) is readily available in many forms with a very smooth and relatively impenetrable surface. It has the advantage over glass that its chemistry is simple, nominally containing only silicon and oxygen, thus making surface chemical analyses easier to interpret. The surface of silica may be modified by covalently attaching silanes, available commercially in a wide variety of chemical forms. The chemistry of the modified silica was quantified using x-ray photoelectron spectroscopy (XPS) to determine the amount of carbon and other new elements, and the thickness of the layer of silane deposited upon the pure silica (SiO_2) substrate during the preparation process.

Surface energetics were probed using contact angles and the nonreacting, impenetrable silanized surfaces were expected to be ideal physical models with which to perform these studies. A large experimental design involving a selection of pure liquids was employed in order to test some of the theoretical models available for the interpretation of contact angle data. Models were tested for their internal consistency, and compared with each other before choosing the best or most useful model for characterizing the surface energies of the modified silicas. XPS and contact angle studies are among the most widely used methods for the characterization of smooth biomaterial surfaces but their relevance is not fully understood. By comparing these data to data relevant to blood compatibility, old hypotheses regarding surface properties and compatibility were tested in a quantitative manner.

Protein adsorption studies were a cornerstone in the design of this research project since the processes involved have been hypothesized to be an important bridge between the surface chemistry of artificial surfaces and their blood compatibility. The adsorption process from whole blood is a complicated one in which certain key phenomena have been identified as potentially important to the biochemical process of blood coagulation. It was the goal of this study to investigate two relationships with respect to multicomponent protein adsorption from blood plasma. The first objective was to correlate the adsorption behavior of a single protein (fibrinogen) in solution, to its adsorption from plasma. In order to understand the mechanisms which govern single component adsorption better, experimental data were fit to a number of published and newly proposed models. While many protein adsorption models have been proposed, their adequacy in fitting real data has rarely if ever been tested. The second objective related to protein adsorption was to determine its relationship to surface-activated blood coagulation. Therefore protein adsorption served as a "middle ground" from which to study the indirect effect of surface chemistry on blood compatibility.

It was hoped that this project could lead to a number of contributions to the biomaterials science field including: 1. The use of well characterized model surfaces for fundamental studies of blood- and protein-surface interactions. 2. The use of multivariate techniques to analyze the relationships (especially well-established rules of thumb) between surface properties and their activation of blood coagulation. 3. A critical evaluation of theories for the estimation of solid surface tension based on contact angle data. 4. A simulation of protein adsorption in a static system. 5. A search for the kinetic model which best fits experimental

data for fibrinogen and albumin adsorption in a static, one-component system. 6. The establishment of a relationship between the "Vroman effect" (competitive protein adsorption from blood plasma) and intrinsic coagulation and/or single component protein adsorption. 7. The establishment of a relationship between surface properties and protein adsorption kinetics.

2 Methods and Experimental Design

2.1 Silane Surface Preparation

2.1.1 Surface Selection for Experimental Design

The relatively "static" nature of silanized silica surfaces contrasts with the dynamic nature of many polymeric surfaces and makes them better models for the study of interfacial behavior (see Section 1.6). A variety of studies on the preparation and characterization of silanized materials have been collected in a volume edited by Leyden (1986). A silica substrate is unlikely to be useful in biomedical implants requiring flexibility but it is useful for fundamental surface studies since it is available in many geometric forms, it is smooth and it is easily modified using silanes having a wide range of chemical functionality.

2.1.2 Initial Surface Preparation

Having selected functionalized silica as the basis for development of model biomaterial surfaces, consideration was given to the desired surface chemistry and substrate form.

In consultation with the National ESCA Center in Seattle it was determined that surface chemical analysis by XPS required flat samples measuring 8x8x1 mm and tubing which was 10mm in length by 4mm o.d. by 0.5mm wall thickness.

Contact angle studies required flat, smooth samples (75x10x1 mm) with a range of wettability from hydrophilic to hydrophobic. The possibility for polar, nonpolar, electron donor, and acceptor interactions was also considered desirable.

For protein adsorption studies, quartz tubing (200x3x0.5 mm) was used for functionalization by silanes. Materials providing possibilities for specific (chemical, biochemical) and nonspecific (physical) binding were desired.

Silanized test tubes (12x75 mm) with a range of clotting responses were required for clotting assays. Clear test tubes were preferred for these studies since this would allow the on-line collection of real time data for kinetic evaluation. The off-line experiments required for opaque or partially light transmitting tubes are time consuming and reduce the amount of data available for quantitative interpretation.

Silica substrates were purchased from Heraeus Amersil (Buford, GA, USA) in different forms. The flat plate (3" x 1" x 1 mm) was clear fused quartz (crystalline SiO_2) with a purity of greater than 99% (CFQ T08 Commercial plate). Tubing (36" x 4 mm o.d. x 0.5 mm wall thickness) was described as flaw-free, lamp grade, clear fused quartz (CFQ T08 HLX Tubing). Test tube substrates were not readily available and custom manufacture was prohibitively expensive. Disposable glass culture tubes (12x75 mm, Maple Leaf Brand, MacMillan Bathurst, Canada, cat. No. 60825-404) were substituted for pure quartz. The surface hydroxyl groups of glass have a similar reactivity to those of pure quartz, but the bulk chemistry of glass is more complex. It was expected that the surface properties of the silanized glass would be closely comparable to those of silanized silica.

Pure silanes were obtained from two sources. Union Carbide donated pure samples of γ-aminopropyl triethoxysilane (cat. No. A-1100), abbreviated name "NH2"; γ-glycidoxypropyl trimethoxysilane (A-187), "Ep"; γ-mercaptopropyl trimethoxysilane (A-189), "SH"; and γ-ureidopropyl triethoxysilane (A-1160), "Ur". Other silanes were purchased from Huls America (Piscataway, NJ, USA) including dimethyl-n-octadecylchlorosilane (cat. No. D5636), "C18"; hexamethyldisilazane (H7300), "CH3"; and 2-(4-Chlorosulfonylphenyl) ethyl trichlorosilane (C3355, as a 50% solution in CH_2Cl_2), "SO3". These seven silanes were used along with a pure silica control (abbreviated to "Qz") to produce the initial eight model surfaces used in this study (see Figure 2.1.1).

Those silanes that are monofunctional with respect to their reactivity with silanol groups (C18, CH3) can in principle form only monolayers. All the other silanes used are trifunctional, and for them the possibility of multilayering was a concern (see Figure 2.1.3 and the related text later in this section). Conditions were therefore designed to reduce the presence of water by performing the reactions under dry nitrogen, so as to promote the reaction of silane molecules with the surface and not with each other. The method described below was adapted from one used by Phillips and Hercules (1986) for borosilicate glass substrates.

The reaction apparatus is depicted schematically in Figure 2.1.2. Flat and tubing substrates were loaded into a 500 mL cylindrical separatory funnel. The culture tubes were loaded into a 300 mL wide mouth amber bottle. All substrates were rinsed once in distilled water, washed with a dilute solution of soap (Liquinox, Alconox Inc., New York, NY) followed by three more rinses in distilled water. (XPS studies of the surface chemistry did

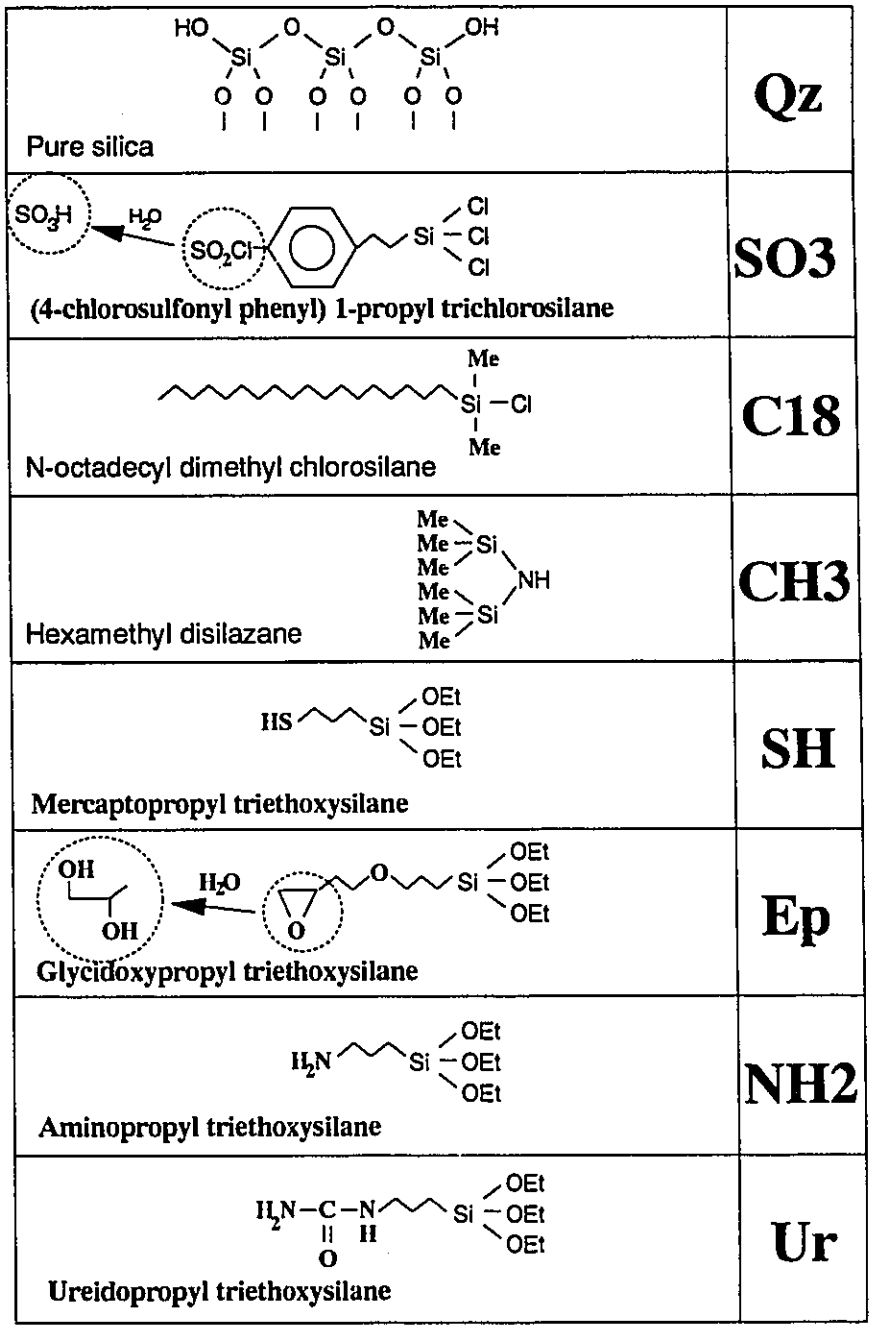

Figure 2.1.1: The original eight model surfaces based on silane functionalized silica.

not reveal the presence of residual soap on the pure silica substrate treated in this way.) The materials were then soaked in a 1 M NaOH solution for only 5 minutes (longer exposure would involve the risk of hydrolyzing the silica) to help remove impurities. After a single distilled water rinse, the silica was soaked in a 1:1 mixture of HNO_3 and deionized water for one hour at room temperature. This procedure was intended to clean the surface and more importantly to increase the number of silanol groups available for reaction at the surface (Phillips and Hercules, 1986). Si-O-Si siloxane bonds are hydrophobic and unreactive but may be "opened up" by treatment with acid to form the more reactive, hydrophilic silanol groups. The HNO_3 was then drained off and the materials were rinsed three times in deionized water. Excess water was drained off as much as possible and the substrate materials were placed in a vacuum oven at 60°C for two to three hours. Excessive heat was avoided to prevent the condensation of surface silanol groups to form siloxane bonds.

The separatory funnel containing the clean, dry, silica substrates was set up in a fume hood and kept under a steady flow of dry nitrogen in preparation for reaction with silane. 700 mL of a 1% v/v silane solution in toluene was prepared in a 1 L round bottom flask and kept under dry nitrogen. The silane solution was transferred under nitrogen to the vessel containing the silica substrates. For those silanes having three groups capable of reacting with the substrate (SO3, SH, NH2, Ur, Ep) the reaction time was limited to 10 minutes in order to reduce the opportunities for multilayering (see Fig. 2.1.3). Monofunctional silanes (CH3, C18), on the other hand, were allowed to react for one hour. All reactions were performed at room temperature (approximately 23°C). Culture tubes could not be kept under nitrogen but were reacted in air with the same toluene solutions as their silica counterparts. There was some concern that by exposing the reacting system to air the availability of water would increase the tendency to form silane multilayers or at least change the reaction conditions. Later in this study six additional surfaces were prepared such that all substrates were reacted in toluene under air (see section 2.1.3). Subsequent surface chemical analyses did not indicate a significant increase (or decrease) in the amount of silane attached to the surface in these cases.

After draining away the unreacted silane solution, the materials were rinsed once with toluene. Then a 1% v/v hexamethyldisilazane (HMDS) solution in toluene was introduced in order to block any unreacted silanol groups at the surface. This blocking reaction was allowed to proceed for one hour at room temperature. The HMDS solution was then drained

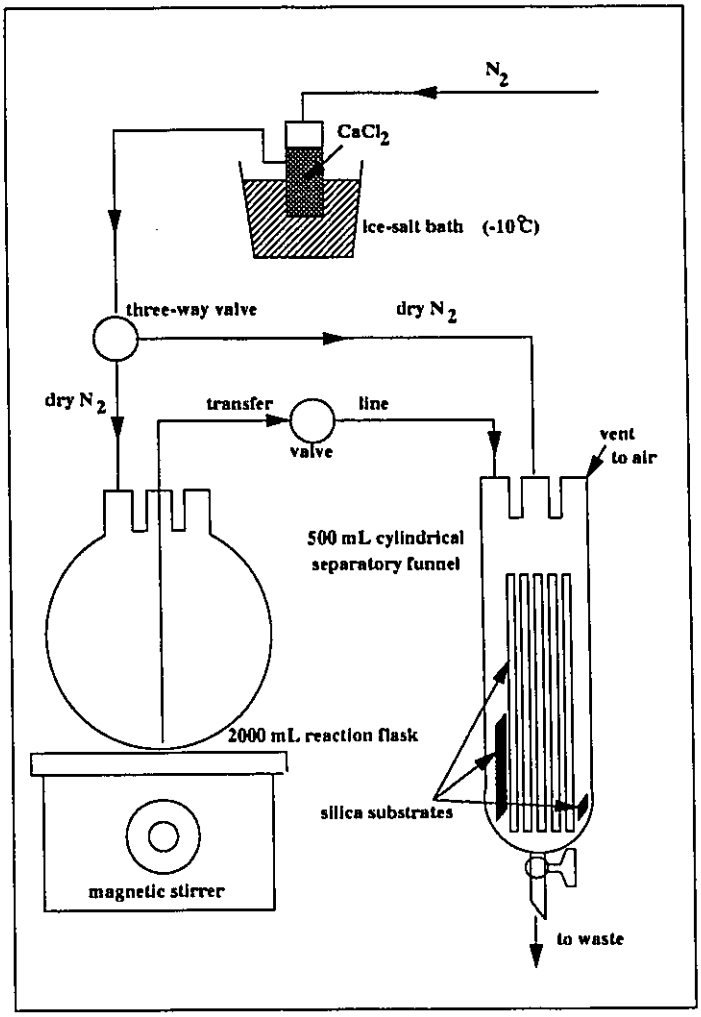

Figure 2.1.2: Apparatus for silanization.

off and the surfaces were rinsed twice with toluene and once with acetone. Materials were dried overnight in a 60°C vacuum oven and stored in closed containers until they were needed for subsequent testing. The reaction vessels were soaked overnight in 1 M NaOH in order to remove any loosely bound silanes prior to the next surface preparation procedure.

Control silica surfaces were cleaned in the same way as all others prior to silanization, including treatment with NaOH and HNO_3 solutions.

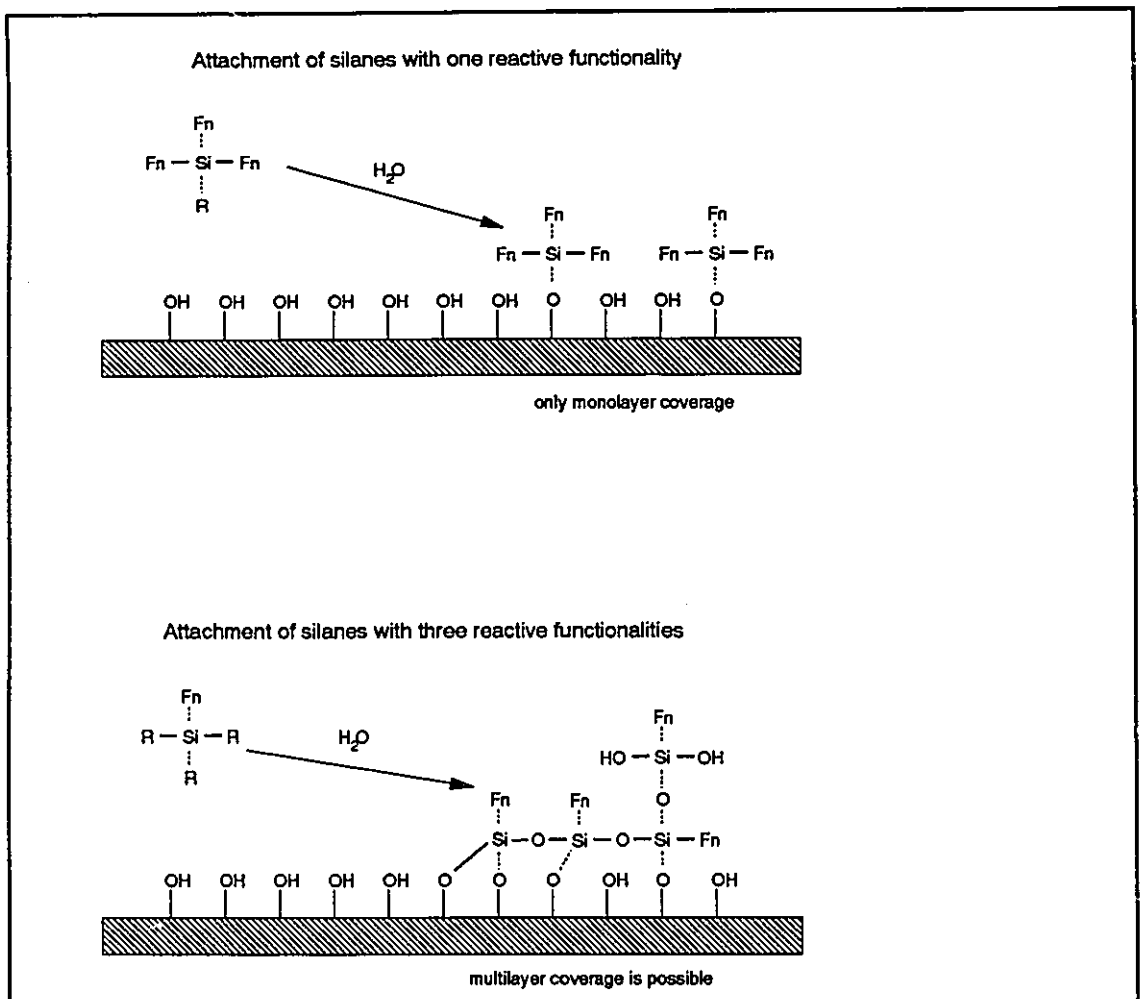

Figure 2.1.3: Silane reactions with silica. The different types of surface coverage possible with one and three reactive groups. Fn represents a nonreactive functionality while R (typically an alkoxy or halogen) can react with silanol groups.

The preparation of sulfonated silica (SO3) required an extra step to convert the sulfonylchloride group (SO_2Cl) to sulfonic acid group (SO_3H). This was accomplished by adding water in the form of an aqueous phosphate buffer of pH 7.0. The buffer was used to reduce the possibility of damaging the silane monolayer by dramatic local changes in pH. The sulfonic acid group was of interest to the study of blood compatibility because of its use in the synthesis of heparin-like biomaterials (see section 1.5).

The octadecyl silane (C18) was of interest due, in part, to its contrasting properties with SO3. In addition the long chain hydrocarbon was expected to yield a hydrophobic and nonpolar surface with a reputed high affinity for albumin (see section 1.5), a passivating protein. Therefore, C18 was expected to interact with plasma in a nonspecific (physical) manner as well as in a specific (chemical or biochemical) manner.

Hexamethyldisilazane (CH3) is typically used as a blocking reagent for unreacted silanol groups but in this study it was used to produce a nonpolar, hydrophobic surface consisting of a monolayer of trimethysilyl groups. The protein interactions on CH3 were to be compared with those on C18 to help distinguish between any specific and/or nonspecific interactions with plasma and with albumin in particular.

The amino silane (NH2) was of considerable interest due to both its physical and chemical properties. The basic nature of NH2 was expected to contrast with the acidic behavior of other surfaces in this study.

The ureido silane (Ur) contains two nitrogens in the form of a urea group. Urea linkages occur in polyetherurethane ureas (PUUs) and their possible role has been largely overlooked. The model Ur surfaces would provide an opportunity to examine the effect of urea groups independently. The net positive charge of Ur at neutral pH makes it useful for comparison with that for the similarly charged NH2 surface.

The mercapto silane (SH) was chosen for its potential interaction with similar SH side groups of cysteine. Sulfhydryl groups are capable of forming disulfide bridges which give proteins their secondary and tertiary structure and allow cysteine to exist as a dimer (cystine). It was also of interest to compare the behavior of SH to that of SO3, the other sulfur containing surface in this study.

2.1.3 Extension of Surface Database

After the originally designed model surfaces had been fully characterized the study was expanded to include six new silanized surfaces based on the chemistry of the SO3 and NH2 model surfaces. The new materials were intended to provide a larger database so that hypotheses advanced based on data for the original eight surfaces could be further investigated. A modified surface preparation protocol was established based on experience from earlier surface chemical analyses. XPS data showed that monolayer or submonolayer

coverage of silane occurred and that multilayering was unlikely, especially for the alkoxy silanes (SH, NH2, Ur, Ep). In subsequent surface preparations, there was thus little concern about the introduction of excessive amounts of water via the toluene or from the air. The revised silanization protocol was performed under air at 23°C. A 1% v/v silane solution in toluene was introduced to clean dry silica substrates, and allowed to react for one hour rather than the ten minutes originally specified. The solution was then drained, and samples were rinsed and dried as before. One new sulfonate ("SO3b") and one new amino ("NH2b") surface were prepared in this manner with the expectation that higher surface coverage could be achieved than in the previous ten minute treatments.

In addition, attempts were made to place mixtures of SO3 and NH2 on silica surfaces. Solutions 1% v/v of 2-(4-chlorosulfonylphenyl) ethyl trichlorosilane and 1% v/v γ-aminopropyl triethoxysilane in toluene were mixed and reacted with the silica substrate for five minutes. A large quantity of precipitate was formed in this mixture, but no extraneous solids were visible on the surfaces after rinsing. This model surface is referred to as "SO3+NH2" and was prepared as a surface having both negative and positive charges. A similar surface was prepared by the sequential surface reaction of sulfonate and amino silanes in order to avoid the undesirable solution reaction observed when the two silanes were mixed. The sulfonated silane was reacted for only 5 minutes and rinsed away. The surface was then reacted with water to convert the highly reactive sulfonyl chloride to sulfonic acid. The surface was then vacuum dried and a 1% v/v solution of amino silane in toluene was allowed to react with the remaining surface silanols for one hour. The resulting sequentially prepared surface was referred to as "SO3>NH2".

Two additional surfaces were initially prepared in the same way as SO3b. The sulfonyl chloride group is versatile in its ability to bind new functionalities and may in the future be used to attach a variety of amino acids or polypeptide sequences. Free SO_2Cl groups were not converted to SO_3H but rather were reacted overnight with either polyethylene glycol (PEG 1025, BDH, Poole, England) or L-lysine (Sigma, St.Louis) to give two new surfaces referred to respectively as PEG and LYS. It was expected that PEG would react via a terminal OH group and lysine via an amine group. In the latter case, it is not known whether the α-amine or ε-amine group reacted preferentially or whether these groups reacted with equal probabality. Polyethylene glycol (also referred to as polyethylene oxide, PEO, in the biomaterials literature) has been of increasing interest in the biomaterials field due to its

surface mobility, hydrophilicity, and bioinertness (Andrade et al, 1987; Ikada, 1984). Some polymers grafted with much longer PEO chains have been shown to be "protein resistant" (Andrade and Hlady, 1986). In the current study the main effect of the small PEO groups was expected to be to render the surface very hydrophilic. Lysine is an amino acid whose ability to bind plasminogen is well known (Woodhouse et al, 1991).

All of the surfaces prepared for this study are listed in Table 2.1.1. The selection of this series of materials was designed to give a wide range of chemical, physical, and biological properties.

Table 2.1.1: A brief description of the model surfaces.

Abbreviated Name	Description	Expected Charge	Biological Relevance	Biomaterials Interest
Qz	pure clean quartz	-		No
SO3	sulfonate	-	Yes	Yes
C18	octadecyl	0	Yes	Yes
CH3	trimethyl silyl	0		Yes
NH2	amino	+	Yes	Yes
Ur	ureido	+	Yes	Yes
SH	sulfhydryl (or mercapto)	?	Yes	No
Ep	Epoxy ring	?		No
SO3b	sulfonate #2	-	Yes	Yes
NH2b	amino #2	+	Yes	Yes
Qzb	clean quartz #2	-		No
SO3 + NH2	SO3 and NH2 mixture	±	Yes	Yes
SO3 > NH2	SO3 and NH2 sequence	±	Yes	Yes
Lys	Lysine on -SO_2-	±	Yes	Yes
PEG	PEO graft on -SO_2-	?		Yes

2.2 X-ray Photoelectron Spectroscopy (XPS) of the Model Surfaces

The XPS technique is an application of the photoelectric effect which provides information about the elemental composition and chemical bonding in a solid surface to a maximum depth of about 20 nm. For a more complete description of the principles involved

and some additional references the reader is referred to section 1.4.1.

The model surface design consisting of silane monolayers on pure silica was expected to show a well-defined depth profile of chemical composition for the 2 to 20 nanometer layer closest to the surface. Those silanes containing sulfur and nitrogen were expected to be especially useful for quantifying the extent and thickness of surface coverage.

XPS studies were performed in two locations. Preliminary studies were done at the National ESCA and Surface Analysis Center for Biomedical Problems at the University of Washington in Seattle. A more complete survey of the surfaces was done at the University of Toronto XPS facility.

The following experimental procedure was employed by the group in Seattle (Leach-Scampavia et al, 1990). Twelve samples were analyzed including a set of four Qz controls, (two tubing samples and two flat plate samples) four SO3 samples and four C18 samples.

Elemental composition of the surface was determined on the flat plate samples using a Surface Science Instruments (SSI) X-Probe ESCA instrument. Tubing was analyzed at a single takeoff angle to obtain data to compare with those for the flat samples. An aluminum $K_{\alpha 1,2}$ monochromatized X-ray source was used to stimulate photoelectron emission. The energy of the emitted electrons was measured at pass energies ranging from 25 eV to 150 eV. An electron flood gun set at 5 eV was used to minimize surface charging of the samples. Typical pressures in the analysis chamber during spectral acquisition were 10^{-9} torr.

Data analysis software was used to calculate the elemental compositions. The binding energy scale was standardized by setting the CH_x peak maximum in the C-1s spectrum to 285.0 eV.

A survey scan (0 to 1000 eV) of each plate sample was done at a photoelectron takeoff angle of 0° relative to a vector normal to the surface (sometimes called a 'detector angle' of 90° relative to the surface plane) to determine which elements were present. High resolution spectra were acquired at takeoff angles of 0, 55, and 80°. Only those elements detected in the survey scan were scanned for at all three takeoff angles. The deepest sampling depth was at a takeoff angle of 0°, and the smallest sampling depth was at a takeoff angle of 80°. A 12° aperture was placed over the analyzer lens for the variable angle data acquisition.

The spectra for tubing samples were taken at a nominal photoelectron takeoff angle of approximately 55° to determine the elemental surface composition. Due to the curved nature of the tubing samples, a wider range of takeoff angles was accepted by the analyzer lens. Therefore the data obtained on tubing samples were not strictly comparable to those for the flat plate samples, but the results were quantitatively very similar (see section 3.1.1).

At the University of Toronto all eight surfaces were analyzed at two detector angles (90 and 30°). The procedure was similar to that used in Seattle with a few notable exceptions. A non-monochromatized magnesium K_{α}, 1253.64 eV source was used to stimulate photoemission. Software was provided to subtract the X-ray satellites and to normalize the energy spectrum to a constant transmission. Additional software calculated the atomic% of each element present in the samples using empirically determined sensitivity factors.

2.3 Contact Angle Measurements

A broad range of polarity, charge, and hydrophilicity was expected for the model surfaces used in this study. Such a range of surface physical properties was required for the evaluation of various energetic theories for the interpretation of contact angle data. The surfaces were expected to minimize interactions with test liquids such as absorption, or chemical reaction which could alter their surface properties in each new environment. Contact angles were measured using a Ramé-Hart goniometer (Mountain Lakes, NJ, model #100-00 115). The syringe and needle tips were disassembled, washed, rinsed, and dried prior to the use of each liquid.

2.3.1 Sample Cleaning and Storage

The first measurements of contact angles were for advancing water droplets on silanized silica microscope slides that had been stored in air in clean, amber glass bottles. Subsequent contact angle measurements were performed over a period of two months during which the cleaning and storage method varied slightly. The samples had to be rinsed and vacuum dried after tests using different liquids in order to remove residual solvent. At first the samples were rinsed in acetone and stored dry. Later, the samples were rinsed and stored in acetone and thoroughly dried just prior to testing. Advancing water contact angles were repeated to determine the effect of storage and aging over the two month period of experimentation. Most of the eight surfaces did not significantly change their interaction with

water during this period. Only the pure silica and sulfonated silica surfaces seemed to undergo any change, namely a slight increase in contact angle. The effect was, however, small and these two surfaces continued to be among the most wettable of those investigated throughout the study.

2.3.2 Contact Angle Measurement

The pure liquids employed for this study were: purified water (18 MΩ/cm) obtained using a Milli-Q Water system (Millipore, Bedford MA); n-octane; toluene; dimethylsulfoxide; glycerol; ethylene glycol; and aniline. For all contact angle measurements, a day's supply of liquid was taken up into a teflon and glass precision syringe (Gilmont Instruments, cat. #GS-1200, obtained through Ramé-Hart) from new bottles without further purification. The vapor phase for the sessile drop experiments was room temperature air.

Contact angles were measured for pure liquid sessile droplets of less than 3 mm in diameter. Advancing contact angles were created by increasing droplet volume until the three phase line was observed to move. In cases where the contact angle was high, the needle tip was kept in contact with the liquid in order to balance gravitational forces and maintain a spherical drop shape. Reading of the angle was most precise in the range 20 to 80° where the error was approximately ± 2°. Outside this range, especially for low angles, the reading error was as much as ± 4°. Ten measurements were made for each liquid/solid system in order to reduce the effect of both reading and systematic error arising from spatial surface variations. Angles were measured on both sides of five droplets.

Receding angles were created by inserting the syringe needle tip into a large liquid droplet. The volume of the droplet was reduced until the contact line was observed to move and the liquid droplet detached from the needle.

The contact angles of octane droplets in water at the solid surface were also measured. Octane drops of about 2-3 mm diameter were formed at the slide surface in highly purified water contained in a clear, flat sided polystyrene container. Silanized slides were supported by a pair of stainless steel hexagonal nuts and allowed to equilibrate in the deionized water for approximately five minutes before measurements were begun. Measurements took about ten to twenty minutes to complete and over this time period no systematic decrease in contact angle (indicating absorption or continuing equilibration) was observed. The container and

nuts were washed in soapy water, rinsed thoroughly in deionized water, and dried in an oven (60°C) prior to experimentation. Captive air bubble experiments were performed in the same way as for captive octane droplets except that air was used instead of octane.

2.4 Protein Adsorption

Protein adsorption studies were designed to fulfil two requirements. Extensive studies of fibrinogen and albumin adsorption on C18 (a hydrophobic surface with an affinity for albumin (Munro et al, 1983)) and SO3 (an hydrophilic surface with an affinity for fibrinogen (Santerre et al, 1989)) were performed. These data were intended for use in kinetic modeling studies. Less extensive adsorption studies were performed using single component protein solutions and diluted blood plasma on all the model surfaces in order to yield comparative data to be correlated with surface chemical and physical properties and with plasma coagulation data.

2.4.1 Protein Labeling and Solution Preparation

Proteins were labeled with ^{125}I by the "Enzymobead" method, (Biorad, Richmond CA) a heterogeneous reaction based on the homogeneous chemistry developed by Marchalonis (1969). This technique, referred to as the "lactoperoxidase method" has been found to produce a higher specific activity under most circumstances (Yu and Brash, manuscript submitted) in comparison to the iodine monochloride procedure described first by McFarlane (1963). Higher specific activity is preferred for precise estimates of protein adsorption especially when surface coverage is low. Free iodide content was found to be similar (about 2%) for both methods in the case of fibrinogen labeling. The iodine monochloride method, however, yielded in the range of 7-8% free iodide for albumin labeling, while the lactoperoxidase method produced much lower levels (approx. 2%). The lactoperoxidase method was adopted as the standard technique for this study.

The materials used to prepare the labeled proteins are listed below.

Human fibrinogen (Hfb, Kabi, Stockholm, catalog #5302), 93.3% thrombin clottable. Traces of immunoglobulins, fibronectin and plasminogen (less than 0.2%) may be present in this material according to the manufacturer.

Human serum albumin (HSA, Hoechst-Behring, Marburg, France, catalog #ORHA 20/21), 99.1% pure. Traces of lipids (0.286%) and moisture (0.29%) are present in this material, which was also screened for trace metals, HIV antibodies and Hepatitis B. The presence of a small amount of lipids in the albumin may affect its adsorption properties, especially on nonpolar surfaces. No other plasma proteins were detected in the product by the manufacturer. SDS-PAGE studies in our laboratory suggested a small but significant percentage (5% or less) of the protein existed in concentrated solution as dimers and trimers. The manufacturer provided no information on dimer and trimer content.

Anion exchange resin, AG 1-X4 (Biorad., Richmond CA)

Na ^{125}I, 100 mCi/mL (Amersham, Arlington Heights IL)

Enzymobeads (Biorad, Richmond CA)

Phosphate buffer, pH 7.2 (9.45g Na_2HPO_4, 4.6g $NaH_2PO_4.H_2O$, to 500 mL final volume in deionized water, pH adjusted with NaOH).

Tris buffer, 0.05M, pH 7.35 (48.4g Tris (hydroxymethyl) amino methane, Biorad, Richmond, CA, in 1000mL final volume with deionized water yields "stock solution"; 840mL of stock solution combined with 700mL of 0.4N HCl and 460 mL deionized water; pH adjusted with HCl).

D-glucose (BDH), 2% aqueous solution, allowed to mutorotate overnight to 1% β-D-glucose.

In a glass test tube, the following materials were added in sequence: 100 μL of 0.2 M phosphate buffer, pH 7.2; 0.10 mL of a 10 mg/mL fibrinogen solution or 0.064 mL of a 1 mg/mL albumin solution in phosphate buffer (the protein had previously been dialyzed overnight at 4°C to remove salts); 50 μL of Enzymobeads (Biorad) suspended in phosphate buffer as per the manufacturer's instructions; 10 μL of Na^{125}I; and 50 μL 1% β-D-glucose solution.

The reaction was allowed to proceed at room temperature for 30 minutes resulting in the incorporation of ^{125}I into the phenol group of tyrosine residues of the protein to be labeled. The reaction sequence has been described in more detail by Yu and Brash (1991). Enzymobeads are polyacrylamide microspheres with covalently-linked lactoperoxidase and glucose oxidase. D-glucose reacts with the glucose oxidase to produce hydrogen peroxide (H_2O_2). H_2O_2 in turn, reacts with Na^{125}I to produce molecular $^{125}I_2$. Only radioactive iodine is present to react with the tyrosine residue thus ensuring a high specific activity. The stoichiometry of the reaction was designed to limit iodine substitution to an average of less

than one per protein molecule. In their review, Yu and Brash cite a number of papers which suggest that the biochemical activity of a number of proteins remains unaffected at this level of substitution. The labeling procedure used in this work was designed to have 2 moles of protein for every mole of radioactive iodine in order to favor single substitution.

After the 30 min., the reaction tube was centrifuged at 1000 g for 1 min. to stop the reaction. The unreacted ^{125}I was removed from the supernatant by passing it through a small (3 mL) anion exchange column. The column was rinsed with 7 mL buffer and the protein in the eluate typically had an activity of about 3×10^8 cpm/mg protein.

The labeled protein was added as a tracer to either unlabeled protein in buffer or to plasma. Labeled protein was present at a level of 1.14% of total protein for fibrinogen and 0.1% for albumin. "Stock" protein solutions had a total concentration of 1.0±0.05 mg/mL of the protein in question, whether in diluted plasma or in buffer. Protein concentrations in plasma were determined in the hematology laboratory of the McMaster University Medical Centre. Pure protein solution concentrations were determined by UV spectrophotometry at 280 nm. From stock solutions, dilutions were made for isotherm experiments to give concentrations of 1.0, 0.6, 0.3, 0.1, 0.03, 0.01, 0.006, 0.003, 0.001, and 0.0005 mg/mL and kinetic studies were done at 0.1, 0.03, and 0.003 mg/mL. These solutions were prepared immediately before the adsorption experiment. 30 mL quantities were kept in small glass beakers and covered. The surface to volume ratio was small enough that solution depletion was insignificant, even for the most dilute solutions. This was checked by solution count for each experiment. No bacteriostat was added to the protein solutions since the studies were of relatively short duration.

The experimental protocol for protein adsorption studies involved the following steps. The adsorbing surfaces were equilibrated overnight at room temperature with Tris buffer. At zero time of the adsorption experiment, 20 mL of a labeled protein solution was injected into the equilibrated tubing at the rate of about 2 mL per second. After a set adsorption time at room temperature, the protein solution was displaced from the tubing by 60 mL of Tris buffer injected at a rate of about 2-3 mL per second. Within a few minutes of this rinsing procedure, the tubing was drained and subsequently cut into six pieces. The end pieces of 2 cm length were discarded (to avoid anomalous end effects). The radioactivity of the four

middle pieces of 4 cm in length were individually counted to determine the amount of adsorbed protein on each. The position of each of the four pieces was also noted in order to observe any position dependence of protein adsorption.

2.4.2 Kinetic and Isotherm Adsorption Studies of Albumin and Fibrinogen on C18 and SO3

The *ex situ* method chosen for this study was the best quantitative and the best understood technique available. However, the method is not without its own problems which affect the interpretation of the data it produces. The *ex situ* nature of the method requires that the bulk protein solution be rinsed from the test material, but the effect of rinsing loosely-adsorbed protein is unknown. The original protocol developed in this laboratory (Brash and ten Hove, 1984; Wojciechowski, 1985) called for two rinses to be performed over a ten minute interval after the adsorption phase of the experiment was complete. The potential for significant desorption during this period was a concern. The most loosely adsorbed protein is probably removed during the first rinse. The ten minute interval between 30 mL rinses called for in the original protocol had the undesirable potential to desorb the more tightly bound molecules. The rinsing protocol for the present work was therefore changed to a single 60 mL rinse lasting at most two minutes to minimize the time available for the desorption of protein.

Single protein adsorption from Tris buffer (pH 7.4) was performed for fibrinogen and albumin on the C18 and SO3 surfaces. The experimental design for each protein-surface pair (of which there were a total of four) involved 60 data points, including nine pairs of replicates. All replicate experiments were performed on separate days to ensure an unbiased evaluation of the true magnitude of experimental error.

Half of the experiments were kinetic runs (at 0.003 mg/mL, 0.03 mg/mL, and 0.1 mg/mL) for adsorption times ranging from one minute to 20 hours at roughly logarithmic intervals. The other data consisted of three adsorption "isotherms" (for 2, 30, and 1200 minutes) at ten bulk protein concentrations spaced logarithmically in the range 0.0005 mg/mL to 1.0 mg/mL. The independent variables were varied logarithmically in order to better elucidate the transition from the fast adsorption processes that occur at low surface coverage to the much slower ones at long times and high surface coverage. The data were intended to shed some light on the question of whether there is a true adsorption plateau as

a function of either concentration or time. Protein adsorption mechanisms under these conditions are the least understood. The data were used to investigate the ability of recently proposed models for protein adsorption on solid surfaces to fit real behavior over a wide range of conditions.

Silanized silica tubing (2.5 mm I.D.) was ready for use any time after preparation was complete. Prepared tubes were stored in clean polypropylene graduated cylinders covered by Parafilm. The 20 cm long tubes were equilibrated overnight in isotonic Tris-HCl buffer, pH 7.35, prior to the adsorption experiments.

2.5 Coagulation Assay

There is no laboratory method currently available to predict the blood compatibility of biomaterials (see section 1.4.2 for a more complete review of testing methods). The overall question of blood compatibility is complex, involving intrinsic coagulation, the complement pathway, bacterial adhesion, toxicity, mechanical stability, and cellular interactions of many types. Even individually, these aspects of compatibility are difficult to characterize and predict given *in vitro* data. The intent of this study was to establish a simple, quantifiable technique which would give a specific, albeit limited, indication of blood compatibility. The intrinsic coagulation pathway, activated by the adsorption of the Hageman factor (XII) to a surface, was selected to be the criterion by which the compatibility of the model surfaces would be rated. Clinically, the intrinsic pathway for coagulation is evaluated by recalcification times (RT) or more reproducibly by the partial thromboplastin time (PTT).

The partial thromboplastin time (PTT) test has been used clinically to distinguish between normal and abnormal surface activated coagulation. *In vitro* tests to evaluate blood compatibility of biomaterials deal with the inverse problem to that normally encountered clinically. Whereas the PTT test characterizes plasma samples given a standard activating surface, biomaterial testing requires that plasma samples from the same source be brought into contact with different activating surfaces. The presence of other surfaces, such as metal hooks, or stir bars used in clinical tests must be avoided when evaluating materials. The air interface may also influence clotting times, but its presence is much more difficult to avoid. Proteins are surfactants and their increased concentration at an air interface may trigger the intrinsic pathway by mechanisms similar to those at a solid surface.

The *in vitro* test chosen to indicate the blood compatibility of surfaces was based on a procedure developed by Rollason and Sefton (submitted 1991). The method, which employs a fluorogenic substrate for thrombin, was more reproducible and provided more quantitative data than the traditional partial thromboplastin time (PTT) tests on which it is based. The test was developed to be sensitive to variations in surface properties given an unchanging pooled plasma supply. This is the inverse of the clinical application of the PTT test where one distinguishes between normal and abnormal samples of plasma given a constant activating surface (usually kaolin powder or ellagic acid).

Kallikrein generation (see Bots et al, 1986 and section 1.4.2) would be a more direct probe of surface activated coagulation than thrombin generation which is subject to more complex kinetics resulting from sequential and feedback reactions.

2.5.1 Surface Characterization by Thrombin Generation

Table 2.5.1: Materials for thrombin generation assay.

Silanized 12 mm x 75 mm culture tubes (see Silane Surface Preparation)
Pooled citrated human plasma (Canadian Red Cross, Toronto)
Rabbit brain cephalin (Sigma, St.Louis) abbreviated as RBCeph
NaCl, 0.85% (w/w) in water
BOC-val-pro-arg-7-amido-4-methyl coumarin (Sigma, St.Louis) 10 mM in dimethylsulfoxide, abbreviated as BMCA
$CaCl_2$, 0.025 M in deionized water
spectrofluorimeter (SPEX Nova, Baird Atomic, Braintree UK)

Fluorogenic substrates have a limited specificity for their respective enzymes (Lottenberg et al, 1981). The substrate for thrombin (BMCA, see Table 2.5.1) used in this study was first reported by Morita et al (1977). Some information with respect to cross reactivity was provided. Reactivities were reported as μmol hydrolyzed per minute per mg of enzyme. The values determined for the conditions of the experiment were 60.0 for thrombin, 0.3 for plasmin, 0.4 for Factor Xa and 0.0 for kallikrein. It is clear that BMCA has a high specificity for thrombin, but the fact that it shows some reactivity with other plasma enzymes means that the interpretation of data must be made with care. For example, the very slow substrate

cleavage observed at short times, before prothrombin is cleaved to form thrombin, may be influenced by the presence of these other enzymes. Data based on the initial slopes of BMCA cleavage kinetics may yield estimates for thrombin generation rate that are too high. True thrombin generation data can best be obtained during the period when thrombin concentration is highest, i.e. when BMCA cleavage is most rapid and the action of thrombin dominates.

Materials for the measurements made in the present work are indicated in Table 2.5.1. Blood plasma (0.5 mL) was placed in a silanized culture tube and incubated at 37°C for two minutes. Rabbit brain cephalin was prepared according to the supplier's instructions in 0.85% w/w NaCl and 1.0 mL was added to the plasma in the culture tube and vortexed. The culture tube was incubated at 37°C for an additional six minutes.

BMCA (20 μL) was mixed with 0.025 M $CaCl_2$ (0.5 mL) and added to the culture tube at time "zero". The tube was then placed in the spectrofluorimeter sample holder at room temperature and subjected to excitation at a wavelength of 380 nm. The cleavage of BMCA by thrombin was detected at 460 nm emission wavelength and quantified on an arbitrary fluorescence scale. Different sensitivities were required to monitor the fluorophore generation over the period of the experiment. At the beginning, a small, finite intrinsic fluorescence (about 60 to 70 arbitrary units in range 8) was evident in the plasma itself. As thrombin was created, the rate of fluorophore generation increased proportionally. The detector quickly became saturated and lower detector ranges (with a sensitivity of about one half for successively higher ranges) were required to monitor the sample from zero time to the completion of clot formation.

Readings were taken every twenty seconds and recorded along with the sensitivity range at which the measurement was made. These kinetic data were used to estimate the tendency of each model surface to promote coagulation.

2.5.2 Calibration of the Thrombin Assay

Calibration was required to attribute thrombin activity to the data and to obtain more accurate estimates of the sensitivity factors for each detector range than could be provided by the manufacturer. Table 2.5.2 lists materials used in this calibration.

Table 2.5.2: Materials for thrombin generation assay calibration

Clean glass 12 mm x 75 mm culture tubes (see Surface Preparation).
Phosphate buffered saline, PBS (10L H_2O, 87.7g NaCl, 61.0g Na_2HPO_4, 11.0g NaH_2PO_4, pH 7.4).
PEG 8000, 0.7 w/w% in PBS buffer.
Human thrombin, 200 U/mL, free of other clotting factors including plasmin and plasminogen according to the manufacturer (Sigma, St. Louis).
spectrofluorimeter (SPEX Nova, Baird Atomic, Braintree UK).

From the stock solution of thrombin (200 U/mL), dilutions of 1 in 50, 25, 12.5, 6.25, and 3.13 were prepared in PBS buffer. 2.0 mL of PEG/PBS solution were incubated for 2 minutes at 37°C in a glass culture tube. 20μL of the BMCA (see thrombin generation assay) and 20μL of the selected thrombin standard dilution were added to the PEG/PBS, vortexed and placed in the spectrofluorimeter. Substrate cleavage was measured in arbitrary fluorescence units for each of the five standard dilutions of thrombin. The kinetics of substrate cleavage were monitored in the spectrofluorimeter (Baird, Braintree U.K.) over a 5 to 20 minute period for the sensitivity ranges 8, 7, 6, 5, 4, 3, and 2.

The rate of substrate cleavage was approximately constant over the course of each experiment due to the constant level of thrombin present. However it was difficult to maintain a temperature of 37°C in the spectrofluorimeter and this may have had an effect on the kinetics. Despite the use of PEG 8000 to minimize it, thrombin adsorption at the glass or air interfaces may also have affected the kinetics of BMCA cleavage in solution.

3 Results and Error Analysis

3.1 Surface Chemical Analysis by XPS

3.1.1 XPS Error Analysis

Table 3.1.1: A comparison of XPS data for 0° takeoff angles obtained in Toronto and Seattle.

Surface	Element	Atom% Toronto	Atom% Seattle
Qz	C	25.1	19.4
Qz	O	44.1	50.5
Qz	Si	24.0	28.1
SO3	C	22.3	15.9
SO3	O	48.0	52.6
SO3	Si	27.2	28.8
C18	C	12.3	7.8
C18	O	56.4	59.0
C18	Si	31.3	33.2

For each of the surfaces examined at the University of Washington, three replicate measurements were done at a takeoff angle of 55°. The average standard deviation for carbon, silicon, and oxygen measurements was 1.3 atom% given 18 degrees of freedom. The variability was apparently not a function of the surface being tested, nor was it related to the element detected or the measured atom%. Therefore, for a single measurement of elemental composition, one can assume the value to be within approximately ± 2.6 atom% 95% of the time.

The results for a 90° detector angle obtained at Toronto (University of Toronto) and Seattle (University of Washington) can be compared for Qz, SO3, and C18 (Table 3.1.1). It is important to note that the surfaces were prepared separately using the same methods and that the discrepancies contain variation due to surface preparation procedures as well as random measurement error.

The average standard deviation of the elemental surface composition on separately prepared surfaces, tested at different sites was 2.1 atom% with 9 degrees of freedom. The measurements done at the University of Washington all detected significantly less carbon than was found at the University of Toronto.

3.1.2 Multiple Detector Angle XPS Data

The results of XPS studies done at University of Toronto on the initial eight model surfaces are listed in Table 3.1.2. The variable angle data helped to confirm the silanization reactions and to show that the silanes were confined to a thin surface layer.

Table 3.1.2: Variable angle XPS measurements of surface composition (in atom%) for the original eight model surfaces.

Surface-Takeoff Angle	C	O	Si	N	S	Cl	F	Na
Qz - 90°	25.1	44.1	24.0	1.57	-	-	4.17	1.02
- 30°	44.9	28.4	15.4	2.67	-	-	6.76	1.80
CH3 - 90°	4.73	62.2	33.1	-	-	-	-	-
- 30°	10.0	57.3	32.6	-	-	-	-	-
C18 - 90°	12.3	56.4	31.3	-	-	-	-	-
- 30°	22.5	48.4	29.2	-	-	-	-	-
SO3 - 90°	22.3	48.0	27.2	0.81	1.50	0.18	-	-
- 30°	40.8	34.5	21.0	1.06	2.46	0.19	-	-
NH2 - 90°	12.9	55.2	30.0	1.93	-	-	-	-
- 30°	25.7	45.0	27.2	2.09	-	-	-	-
Ep - 90°	7.55	60.3	32.2	-	-	-	-	-
- 30°	14.4	54.5	31.1	-	-	-	-	-
Ur - 90°	12.7	54.7	30.8	1.88	-	-	-	-
- 30°	23.7	45.8	27.2	3.32	-	-	-	-
SH #1 - 90°	9.0	60.2	30.8	-	-	-	-	-
- 30°	19.3	51.8	28.8	-	-	-	-	-
SH #2 - 90°	10.9	57.5	31.6	-	-	-	-	-
- 30°	22.1	48.8	29.1	-	-	-	-	-

Data collection was repeated only on the SH surface to confirm the observation that sulfur was not detectable. The results on both SH samples were found to be the same within experimental error and confirmed the absence of sulfur. The mercapto silane was not independently checked by NMR but the supplier (Union Carbide) specified the material to be greater than 99% pure. The amount of carbon on the SH sample suggested that silanization did occur and so the surface was used throughout the study as an independently prepared and unique surface. Any observed interactions between the SH surface and its environment could not, however, be attributed to the presence of the SH group.

It should be noted that the surfaces silanized with hydrocarbons (CH3 and C18) have lower carbon contents than all other samples including the "clean" standard material (Qz). This apparent paradox was confirmed by independent tests at the University of Washington and reported by them to be normal for such surfaces. High energy surfaces such as clean silica typically have a "hydrocarbon overlayer containing nitrogen and various functionalized carbon groups" (Leach-Scampavia et al, 1990) which is apparently stable even under the conditions of high vacuum required by XPS. The hydrophobic silanes on the other hand, limit this kind of adsorption from the air and as a result have a lower total surface carbon content than the pure silica. These effects make confirmation of surface chemistry less straightforward than expected, especially for those silanes containing only silicon, oxygen and carbon.

The success of reactions to produce NH2, Ur, and SO3 was more easily confirmed by the presence of nitrogen and sulfur. In addition, on the sulfonated surface, a distinct π to π^* transition satellite was observed in both the Toronto and Seattle experiments thus confirming the presence of the aromatic ring unique to SO3.

One of the features that is common to all surfaces is the oxygen to silicon ratio which varies only slightly in the vicinity of 1.8: 1 for a 90° detector angle and 1.7: 1 for 30°. In pure bulk silica, the ratio is 2 to 1 (SiO_2). There is therefore, an apparent enrichment of silicon on all surfaces. This is true even on the sulfonated surface which was expected to show the opposite trend due to the presence of three oxygens per silane molecule. Although XPS demonstrated that sulfur was present there was no accompanying evidence of increased oxygen at the surface of SO3.

A more detailed analysis of the XPS data (to estimate silane layer thickness) is included in section 4.1 of this thesis. The raw data tend to support the conclusion that fifteen chemically different surfaces were prepared. However, it was difficult to confirm absolutely the success of silanization on all surfaces without resorting to indirect interpretations. Only on the mercapto functionalized surface (SH) was there direct evidence that the desired surface chemistry was not produced.

Based on the results from the original eight model surfaces, seven additional materials were prepared as described in section 2.1.3. The results of XPS analysis of the new surfaces prepared for the extended study are listed in Table 3.1.3.

Table 3.1.3: Variable angle XPS measurements of surface composition (in atom%) for the seven model surfaces in the extended survey.

Surface	C	O	Si	N	S	Cl	F	Na
SO3b - 90°	21.5	45.9	24.2	1.05	1.28	.04	-	-
- 30°	48.6	31.3	18.1	1.1	0.91	-	-	-
SO3+NH2 - 90°	26.0	46.7	25.0	1.92	.43	.15	-	-
- 30°	51.0	28.6	16.5	3.14	.64	-	-	-
SO3>NH2 - 90°	34.3	40.3	23.2	1.8	.48	-	-	-
- 30°	52.4	27.2	17.4	2.91	.07	-	-	-
LYS - 90°	32.7	40.9	23.3	1.9	1.24	.02	-	-
- 30°	51.1	28.5	17.9	1.76	.73	-	-	-
PEG - 90°	39.7	38.6	17.7	.31	1.97	-	-	-
- 30°	52.8	29.3	13.4	.44	2.26	.04	-	-
NH2b - 90°	20.1	50.2	27.9	1.75	-	.09	-	-
- 30°	36.9	35.9	24.2	2.97	-	.014	-	-
Qzb - 90°	14.7	55.7	28.9	.48	.11	.01	-	-
- 30°	36.1	40.2	23.3	.48	-	-	-	-

3.2 Contact Angles

3.2.1 Contact Angle Error Analysis

Figure 3.2.1 shows that the range of advancing water contact angles observed on the eight original model surfaces was between 40 and 90°. The results of three individual advancing water contact angle experiments are plotted as a function of their average values. Each experimental point is representative of the average of ten measured advancing contact angles measured on the same day including both sides of a series of five water droplets. Experiments were made on three separate days during a two month period over which all contact angle measurements were performed. Error bars are not shown for each of the points, but the 95% confidence interval for contact angle measurement on all eight surfaces was ±4.37° for 16 degrees of freedom. The 95% confidence interval for the estimate of error itself was enclosed by 2.96° and 6.06° for the same data set. There was some evidence to suggest that error was greater for lower contact angle surfaces. It became evident during detailed data analysis (section 4.2.2) that the error was more constant as a function of the work of adhesion.

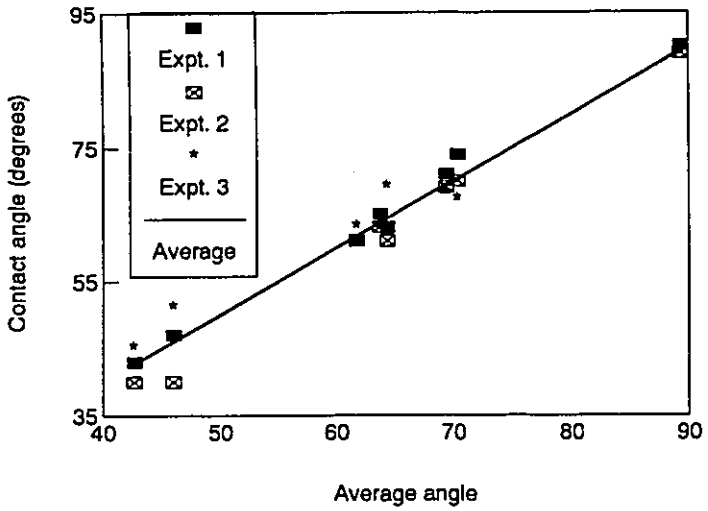

Figure 3.2.1: Variation in advancing water droplet contact angle data depicted by plotting the results of three individual experiments versus their average. The three experiments were done about a month apart during which the surfaces were exposed to a variety of liquids and storage methods.

3.2.2 Advancing and Receding Contact Angle Data

Table 3.2.1 lists the average advancing water contact angles for each of the original eight model surfaces tested. As expected the hydrocarbon surfaces were observed to be the most hydrophobic while the acidic surfaces (pure silica (Qz) and sulfonate (SO3)) were most hydrophilic. The hydrophilic surfaces, however, showed higher than expected contact angles suggesting that siloxane bonds, adsorbed hydrocarbons or other sources of hydrophobicity contributed to their surface properties.

Table 3.2.1: Advancing water contact angles (±4.4°) on model surfaces (n=3x10 expts.)

Surface	Contact angle (degrees)
C18	89.3
CH3	70.3
SH	69.3
NH2	64.3
Ep	63.7
Ur	61.7
Qz	46.0
SO3	42.7

Table 3.2.2: Advancing water contact angles (±4.4°) on model surfaces in the extended survey (n=1x10 expts.)

Surface	Contact angle (degrees)
SO3b	31.0
SO3+NH2	58.5
SO3>NH2	64.3
LYS	39.7
PEG	7.7
NH2b	72.9
Qzb	38.5

Table 3.2.2 contains the contact angle data on the seven surfaces prepared for the extended surface study. The data for similar surfaces in Tables 3.2.1 and 3.2.2 (SO3, SO3b; NH2, NH2b; Qz, Qzb) are comparable despite the fact that the surface preparation methods varied (see section 2.1.3). The Qzb surface was more wettable than the Qz probably because the sample was tested sooner after its preparation. The PEG grafted surface was the most wettable, and this observation helped to confirm the successful incorporation of PEG groups via the sulfonate group of the sulfonated silane. Interpretation of the XPS data on the same surface was less conclusive since the carbon and oxygen in PEO are also present on the underlying substrate.

Advancing angles are not identical to equilibrium contact angles as required in the Young equation, and thus it was important to measure the receding contact angles as well. Contact angle hysteresis, the difference between advancing and receding angles, is thought

to arise from a combination of physical roughness and chemical heterogeneity (Andrade, 1985c). All of the samples were visually smooth before and after silanization. ESCA studies revealed organosilane layers on the order of 0.5 to 1.5 nanometers thick (see section 4.1.1 for calculations). Both the physical and chemical sources of heterogeneity were thought to be small. Figure 3.2.2 shows that hysteresis was small (approximately 10°) on the hydrophobic surfaces and large (as much as 25°) on the hydrophilic ones. All surfaces demonstrated hysteresis significantly greater than experimental error.

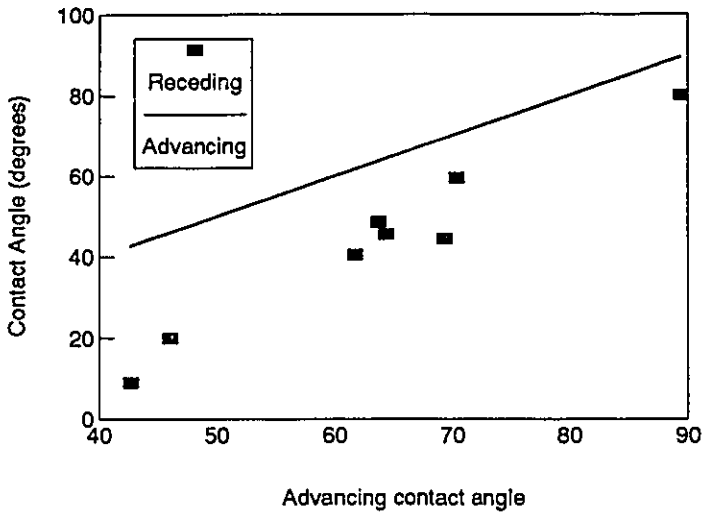

Figure 3.2.2: A comparison of advancing and receding water droplet contact angles on eight surfaces.

Advancing contact angles were measured on the fifteen model surfaces for glycerol in air (γ_{GA}=63.4 mN/m), dimethyl sulfoxide in air (γ_{DA}=44 mN/m) and n-octane (γ_{OW}=21.8 mN/m) in water. Table 3.2.3 shows the raw DMSO and glycerol data. The results for the original eight surfaces are plotted in Figure 3.2.3. Except for the water/air system (which is based on an average of 30 experiments), the contact angle data represent single experiments based on the average of 10 measurements. The relationships for all four systems were remarkably linear. There was no evidence of penetration of any of the liquids into the surfaces, nor did the properties of the surface appear to change after exposure to the liquids. To check the stability of the surfaces and detect any physical changes that may have been

induced by contact with the different liquids, the replicate water drop measurements in Figure 3.2.1 were performed at times before, between, and after the tests using DMSO and glycerol.

Table 3.2.3: Advancing contact angles for glycerol and DMSO on model surfaces (n=1x10 expts.)

Surface	Contact Angle (degrees)	
	Glycerol	DMSO
C18	78	51
CH3	61	37
SH	63	31
NH2	65	32
NH2b	58.9	25.8
Ep	57	28
Ur	57	30
SO3>NH2	51.5	22.5
SO3+NH2	48.6	14.6
Qz	48	21
SO3	44	18
LYS	30.8	8.9
Qzb	28.4	13.2
SO3b	20.2	6.4
PEG	9.8	0.0

The contact angles for captive octane droplets in water represent the water contact angle at the three phase line of contact (see Figure 3.2.3). This system has been used in conjunction with data for water droplets in air to determine the components of surface tension as proposed by Fowkes (Andrade et al, 1979). The relationship between the captive octane bubble, and water in air droplet angles in this study was linear. This observation is not consistent with the hypothesis that the surface tension components are independent of the total surface tension (see section 4.2.4 for discussion).

Figures 3.2.4 and 3.2.5 show data (analogous to those for water in Figure 3.2.2) for advancing and receding contact angles of glycerol and DMSO respectively on the model surfaces. The data for advancing angles are presented not as individual points but as a 45° line for comparison with the receding data. The hysteresis observed for glycerol (Figure 3.2.4) was similar to that for water varying from 10° for C18 to about 25° on the most hydrophilic surfaces. For DMSO, the hysteresis trends observed for water and glycerol

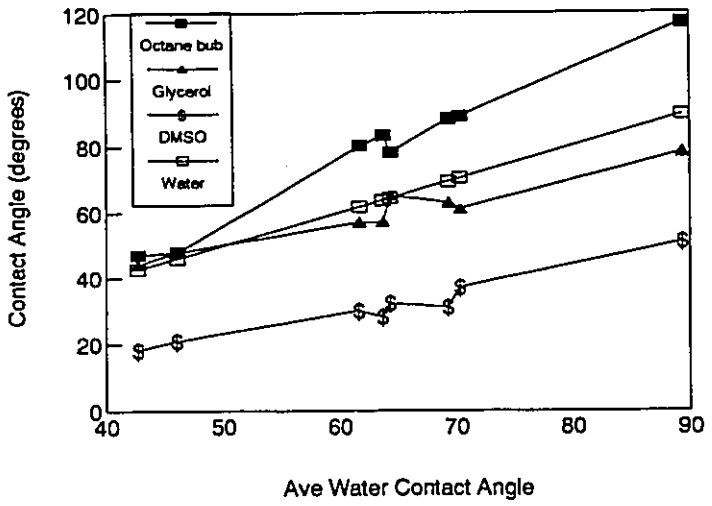

Figure 3.2.3: A comparison of advancing contact angles for four different liquid droplet systems: octane droplet in water, glycerol in air, dimethyl sulfoxide in air, and water in air.

could not be verified due to the fact that advancing contact angles on most surfaces were already very low. In addition, it was found that the measurement of contact angles less than 20° was of relatively low precision. The reason for this additional uncertainty was mainly a result of the difficulty in lining up goniometer crosshairs with the edge of a very thin spreading liquid droplet.

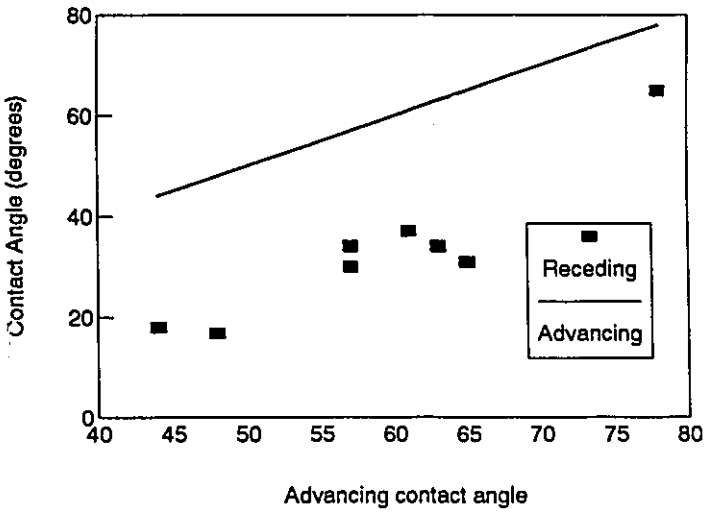

Figure 3.2.4: Advancing and receding glycerol contact angles.

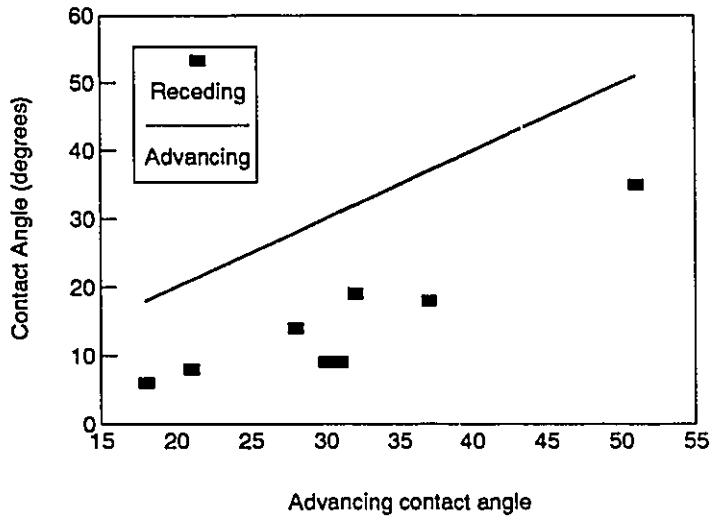

Figure 3.2.5: Advancing and receding dimethyl sulfoxide contact angles.

Figure 3.2.6 is similar to Figure 3.2.2 except that it also includes the data for captive air bubbles in water. The air bubble contact angle presented in Figure 3.2.6 is more precisely the angle between water and the surface (i.e. 180° minus the air/surface angle). It is interesting to note that the captive air bubble data more closely match the advancing than

the receding sessile drop contact angle. This is surprising in light of the fact that the introduction of an air bubble more closely resembles the protocol for a receding water droplet. One may speculate that the buoyancy of the captive air bubble or the pressure inside it promotes the displacement of the receding water film. Perhaps the advancing contact angle is more indicative of equilibrium wetting while the receding angle reflects irreversibility within the liquid itself (i.e. its tribological or lubricating properties). The data in Figure 3.2.6 also support the hypothesis that water is unable to alter the silane layer. Significant water penetration into, and swelling of the surface would have reduced the water contact angle to values near or less than the receding angle of the same surface. The angles were not observed to change appreciably during measurements made over a half hour period.

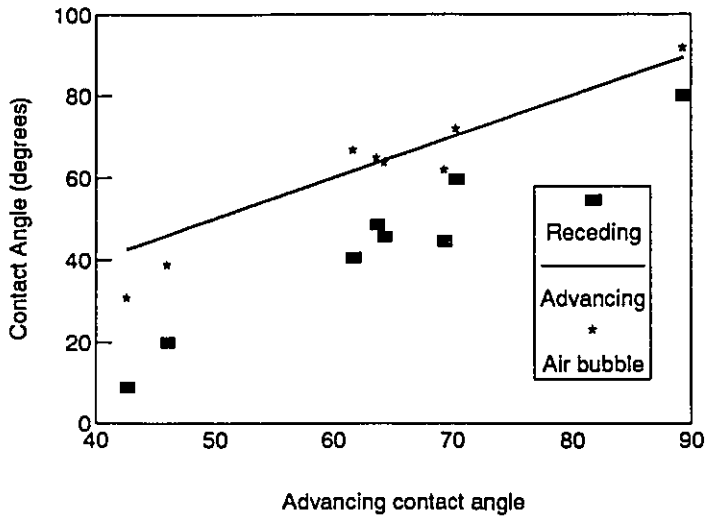

Figure 3.2.6: Same as Figure 3.2.2 except that data for captive air bubbles in water are included.

The contact angle data provided opportunities to characterize each surface and to test the validity of surface energetic theories for the interpretation of such data. In the absence of true equilibrium contact angle data the advancing angles were used instead.

3.3 Protein Adsorption

The adsorption of radiolabeled albumin and fibrinogen on the sulfonated (SO3) and octadecylated (C18) surfaces was measured under conditions designed to give optimum

information for kinetic modeling and surface characterization. In addition, 30 minute adsorption isotherms for both proteins on the other six surfaces (CH3, SH, Qz, Ep, NH2, Ur), were intended mainly for characterization purposes.

3.3.1 Protein Adsorption Error Analysis

Single protein adsorption studies on the SO3 and C18 surfaces consisted of six runs of ten experiments each. The sixty measured values contained nine pairs of replicates which were used in analysis of the measurement error. Since replicate experiments were always performed on separate days, the difference between them gave the best possible information about the total effects of error on protein adsorption measurements.

The average protein adsorption replicate error was found to be independent of the concentration of protein or the time of adsorption. Replicate error was, however, found to be related to the amount adsorbed. Figures 3.3.1 and 3.3.2 show the relationship between replicate error and adsorption for albumin and fibrinogen respectively. The average error for each protein appeared to be well fit by an increasing linear relationship with adsorption.

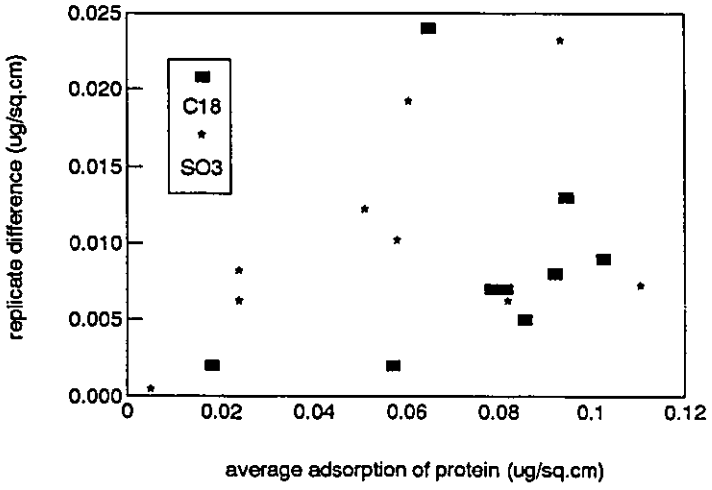

Figure 3.3.1: Replicate pair differences plotted as a function of average adsorption. Data are for albumin adsorption on octadecyl (C18) and sulfonated (SO3) silica.

As shown in Figure 3.3.1 the average error for albumin measurements was greater on the sulfonated than on the octadecylated surface. The data in Figure 3.3.2 for fibrinogen do not suggest a similar surface dependency of measurement precision.

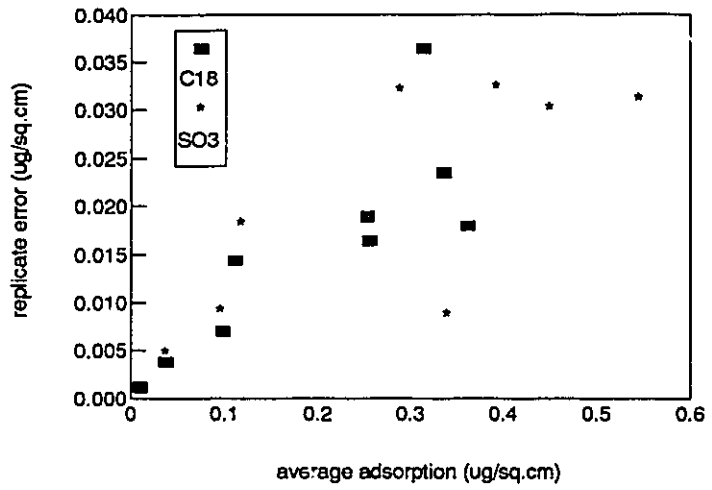

Figure 3.3.2: Replicate pair differences plotted as a function of average adsorption. Data are for fibrinogen adsorption on C18 and SO3 silica.

Figures 3.3.3 and 3.3.4 show the data in Figures 3.3.1 and 3.3.2 plotted as relative error versus adsorption. The relative error was defined to be the replicate difference divided by the average adsorption for each pair. Relative error data for albumin depicted in Figure 3.3.3 do not appear to be a strong function of any variable including the adsorbed amount. The average relative error for albumin on C18 was 12% and on SO3 the average was 21%. The average error for fibrinogen adsorption measurements was 9% on both surfaces. In the case of fibrinogen it may be argued that the relative error was a slightly decreasing function of adsorption.

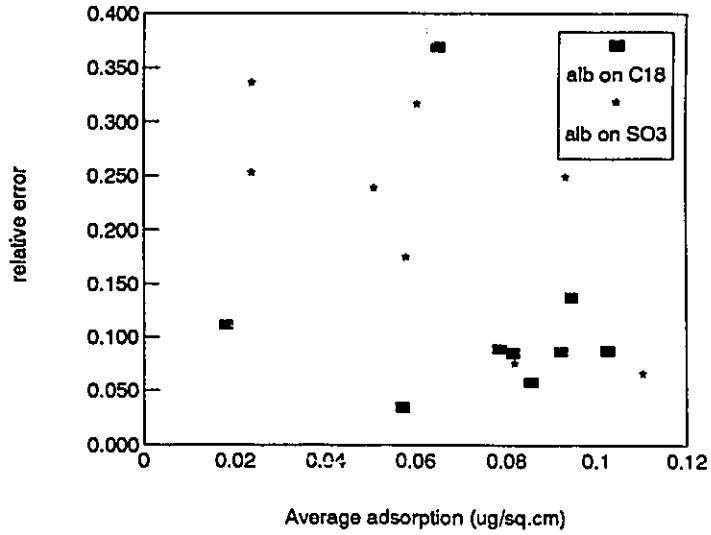

Figure 3.3.3: A plot of relative error for albumin adsorption versus average adsorption. Relative error appears to be independent of all variables.

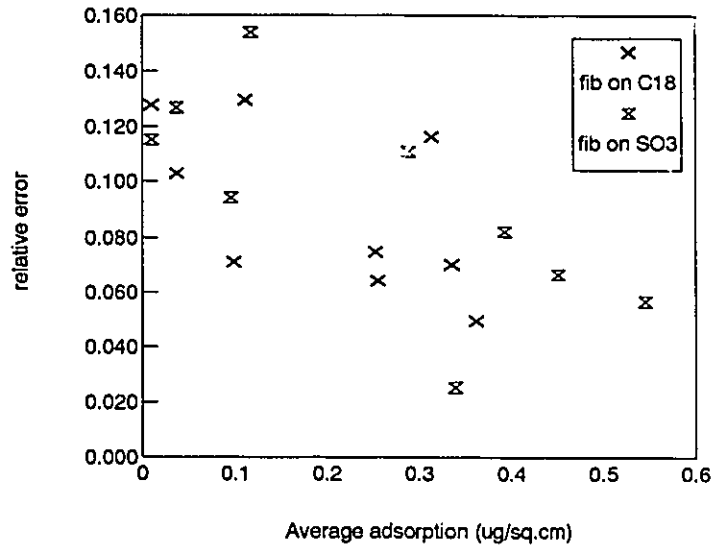

Figure 3.3.4: A plot of relative error for fibrinogen adsorption versus average adsorption. Relative error is at best a weak function of adsorption.

3.3.2 Albumin Adsorption Data for Mathematical Modeling

Albumin adsorption kinetics on octadecyl functionalized silica is depicted in Figure 3.3.5. The data show that albumin was rapidly adsorbed up to a level of about 0.07 μg/cm^2 after which adsorption proceeded more slowly. Typically, protein adsorption is diffusion limited at low surface coverage, and this is followed by a slower phase of uptake.

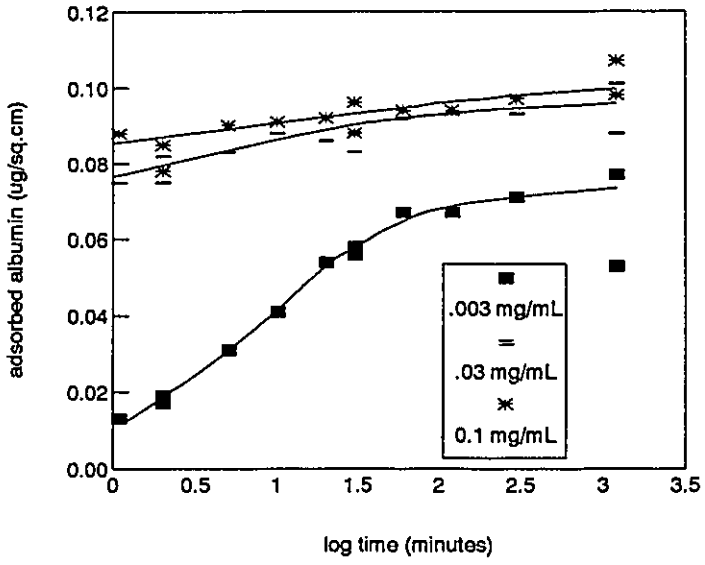

Figure 3.3.5: Kinetics of albumin adsorption on C18 from Tris buffer for three different albumin concentrations.

Albumin adsorption kinetics on sulfonated silica is presented in Figure 3.3.6. The rates of adsorption in this system were considerably slower than on C18. Surface binding rate (as opposed to diffusion rate) was a more dominant limitation on the overall rate of albumin uptake on SO3. There was no evidence of a plateau for albumin adsorption on SO3. The maximum observed adsorption was approximately 0.11 μg/cm^2, similar to the maximum level of adsorption observed on C18 at the same high concentration (1.0 mg/mL). The actual rates of adsorption after 24 hours, while greater than zero, were very slow and may have been the result of slow surface rearrangement and/or multilayer formation.

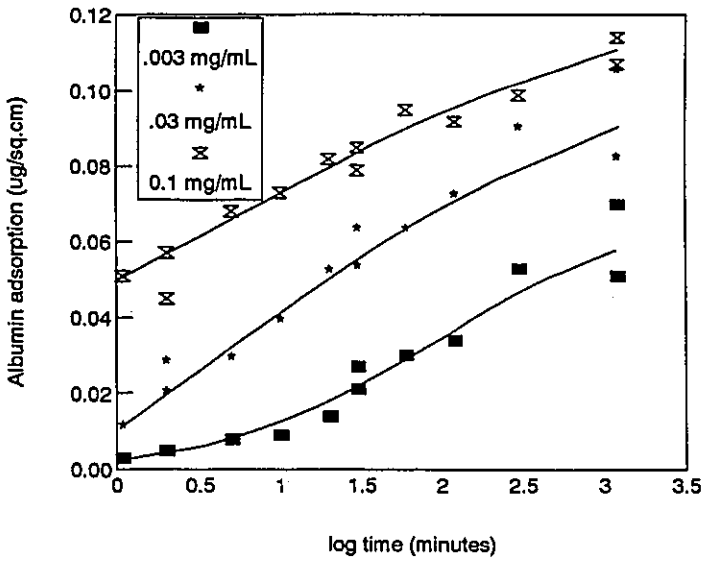

Figure 3.3.6: Kinetics of albumin adsorption on SO3 from Tris buffer for three different albumin concentrations. The lines are present to simply illustrate the trends more clearly.

Three albumin adsorption "isotherms" corresponding to 2 min, 30 min, and 20 h were determined on C18 and SO3 after for a series of protein solution concentrations chosen to cover the range 0.0005 to 1.0 mg/mL at roughly logarithmic intervals.

The albumin isotherms on C18 are shown in Figure 3.3.7. As in Figure 3.3.5, an intermediate adsorption plateau is observed in the range 0.08 to 0.10 $\mu g/cm^2$. Increased adsorption levels occurred at higher concentrations due possibly to multilayering, surface rearrangement, or perhaps inadequate rinsing of the high concentration solutions. The difference between the 30 min and 20 h data show that only a small but significant additional adsorption occurs after the first 30 minutes.

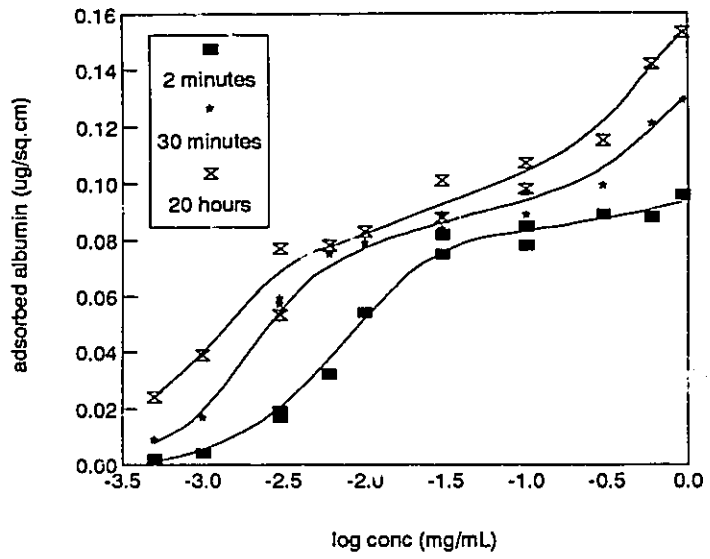

Figure 3.3.7: Albumin adsorption "isotherms" on C18 from Tris buffer for three different times.

The albumin "isotherms" on SO3 are shown in Figure 3.3.8. The levels of adsorption on this surface were much lower than on C18 in the low concentration range. For the kinetic data on SO3, there is no indication of a distinct primary adsorption plateau. However, a secondary increase in adsorption is evident above an adsorption level of approximately 0.08 $\mu g/cm^2$. Since this secondary adsorption occurs at the same level on the C18 surface, we may speculate that 0.08 $\mu g/cm^2$ represents a "critical" surface coverage which could be a "side-on" monolayer for example. The slope of the secondary adsorption phase on SO3 is proportional to the time of contact and was therefore assumed to be a real adsorption effect and not simply a "trivial" rinsing effect. The extent of the secondary adsorption was apparently much greater on SO3 than on C18 but this observation is heavily biased by the results at only two high concentrations.

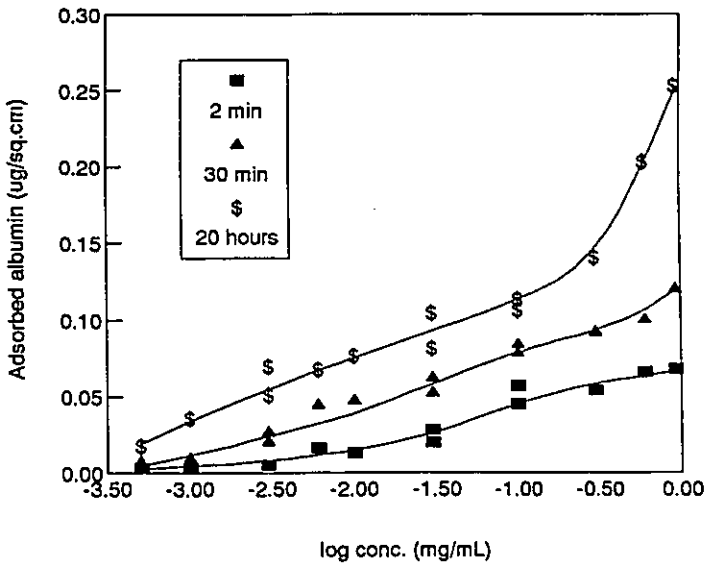

Figure 3.3.8: Albumin adsorption "isotherms" on SO3 from Tris buffer for three different times. Concentrations are not corrected to reflect solution depletion. The lines are present merely to illustrate the trends for each time of adsorption.

3.3.3 Comparative Albumin Adsorption Experiments

A limited study of albumin adsorption on other model surfaces was made based on thirty minute "isotherm" experiments. The four surfaces which showed the highest albumin adsorption are presented in Figure 3.3.9. C18 had the highest albumin affinity of all the surfaces tested. This supports the hypothesis that C18 chains have a specific affinity for albumin (Munro et al, 1983). At low surface coverage the rate of adsorption appeared to be mainly surface binding rate limited (rather than diffusion limited) since the overall rate of adsorption varied from surface to surface (c.f. fibrinogen adsorption data see section 3.3.5).

The adsorption trends on NH2 were quite different from the other surfaces in Figure 3.3.9. Initial adsorption was apparently of high affinity up to about 0.02 $\mu g/cm^2$. Between 0.02 and 0.08 $\mu g/cm^2$ adsorption was much slower than on the other surfaces, and above 0.08 $\mu g/cm^2$ the extent of "secondary" adsorption became relatively high.

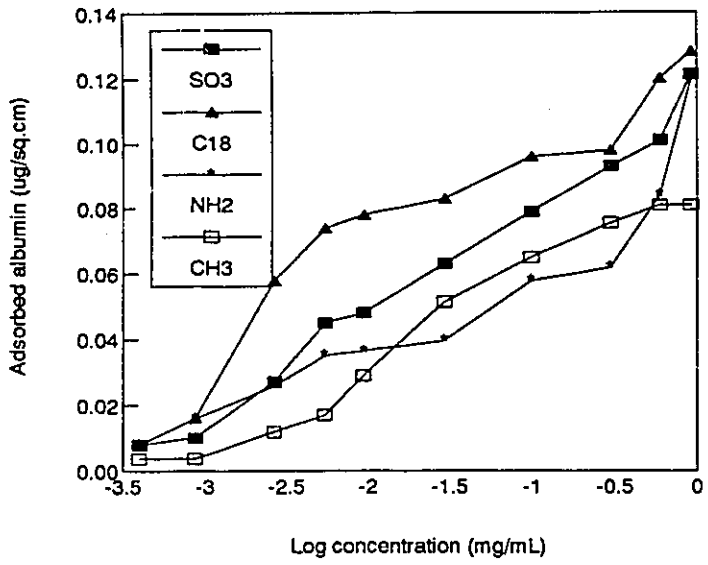

Figure 3.3.9: Thirty minute albumin adsorption isotherms on four high affinity model surfaces.

Figure 3.3.10 shows 30 minute albumin adsorption on the other four model surfaces. Albumin affinity, as indicated in the low concentration part of the isotherms appeared to be higher on the Ur and SH silanes than on CH3 but adsorption at high concentrations was lower. The initial adsorption on all five surfaces was apparently rate limited to a concentration of 0.01 mg/mL but the initial rates were not correlated with the maximum adsorbed amounts. Perhaps the SH, Ur, and Ep moieties were capable of excluding albumin from a fraction of the surface sites. Whatever the mechanisms, albumin adsorption apparently reached a plateau well below the primary monolayer level of 0.08 $\mu g/cm^2$ observed on C18 and SO3. Pure silica had by far the lowest affinity for albumin, and the adsorption was linear with respect to concentration over the entire range. The hydroxyl groups on Qz and Ep may be associated with their observed low affinity.

After comparing all the data in Figures 3.3.9 and 3.3.10 it was determined that with the possible exception of NH2, all surfaces could be uniquely characterized with respect to albumin adsorption by two quantities: (1) the initial slopes of the isotherms (affinity for

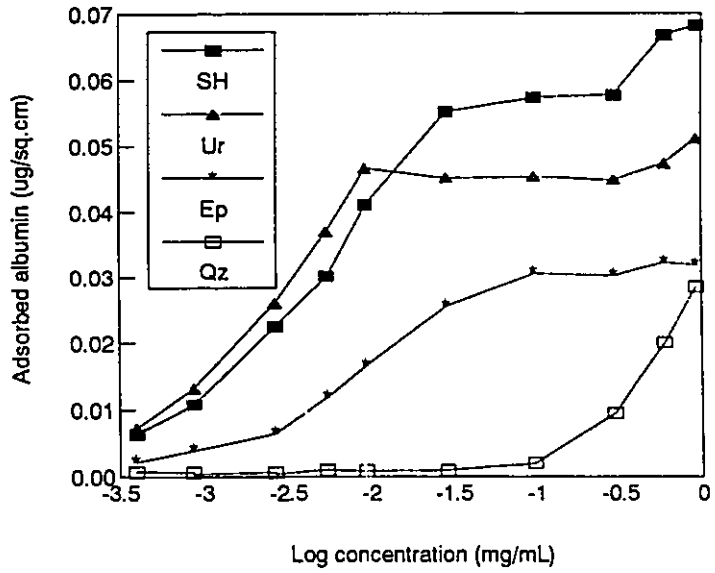

Figure 3.3.10: Thirty minute albumin adsorption isotherms on low affinity surfaces.

albumin) represented by the adsorption at a concentration of 0.003 mg/mL, and (2) the maximum adsorption (capacity for albumin) represented by the average of the two highest concentration conditions 0.6 and 1.0 mg/mL. These values are listed in Table 3.3.1.

Table 3.3.1: Surface characterizations representative of single component albumin adsorption.

Surface	Albumin Affinity $\mu g/cm^2$	Albumin Capacity $\mu g/cm^2$
Qz	0.0004	0.024
Ep	0.0064	0.032
CH3	0.0118	0.081
SH	0.0225	0.067
SO3	0.0240	0.111
Ur	0.0261	0.049
NH2	0.0256	0.098
C18	0.0570	0.124

Albumin adsorption data were not collected for the six surfaces prepared for the extended study.

3.3.4 Fibrinogen Adsorption Data for Mathematical Modeling

Extensive fibrinogen adsorption experiments were performed on the C18 and SO3 surfaces in order to obtain a database suitable for model fitting. The concentrations used were the same as those for albumin (on a weight/volume basis). The data were less influenced by random error than were the albumin data, with a standard deviation of about ±10% for each data point.

The kinetics of fibrinogen adsorption on C18 are shown in Figure 3.3.11. Adsorption is proportional to the square root of time for coverage less than 0.20 $\mu g/cm^2$. These data are consistent with a transport limited adsorption mechanism with an average fibrinogen diffusivity of $0.8 \pm 0.3 \times 10^{-7}$ cm^2/s. This is significantly less than the literature value of 2×10^{-7} cm^2/s (Andrade and Hlady, 1987).

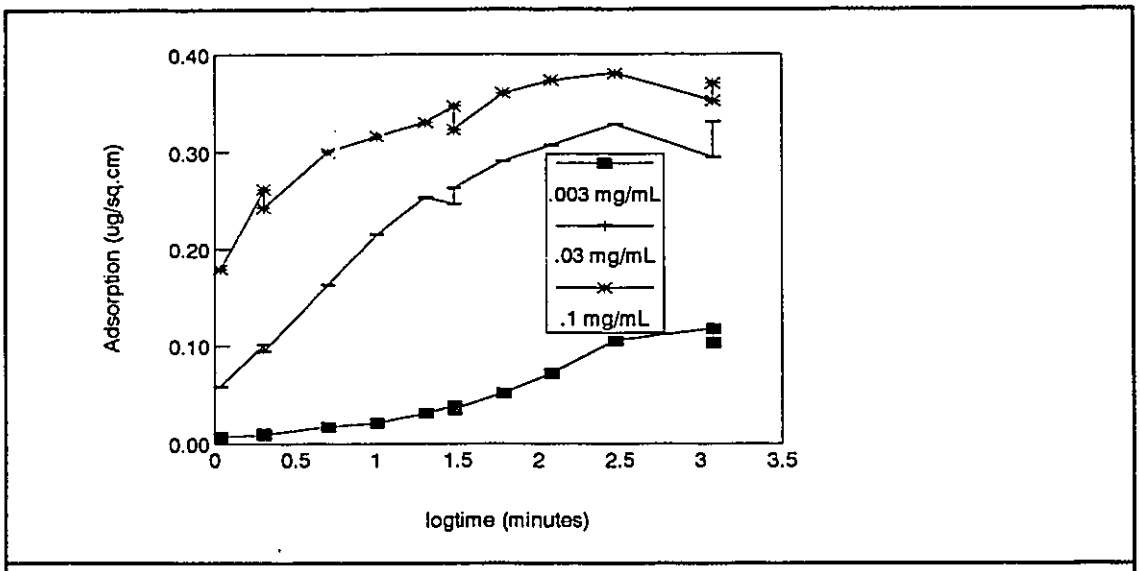

Figure 3.3.11: Kinetics of fibrinogen adsorption on C18 from Tris buffer for three different initial concentrations.

A maximum fibrinogen adsorption on C18 is approached after 20 hours with no apparent intermediate plateau as is observed for albumin. The mass of adsorbed fibrinogen was about three to four times higher than for the primary (0.08 $\mu g/cm^2$) albumin layer on the same surface. Despite the fact that no intermediate plateau is observed there is evidence

of at least two stages of adsorption. Adsorption up to 0.20 $\mu g/cm^2$ is apparently under diffusion control while higher coverages are achieved more slowly. A value of 0.20 $\mu g/cm^2$ is consistent with estimates of side-on monolayer adsorption of fibrinogen (see section 1.1.3).

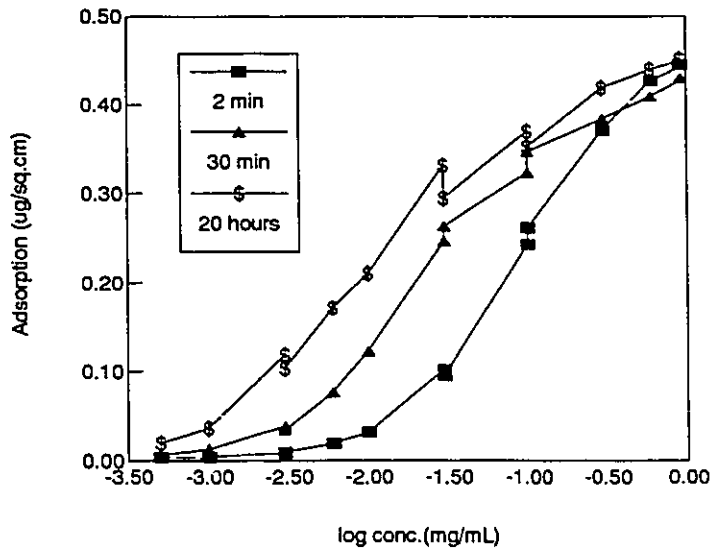

Figure 3.3.12: Fibrinogen adsorption "isotherms" on C18 for three different times. Concentrations are not corrected to reflect depletion.

After 20 hours there is some indication that the rate of adsorption approaches zero (i.e. the system may be close to steady state). For the highest concentration (0.1 mg/mL), this steady state is achieved after about one hour. For a concentration of 0.03 mg/mL the time to reach steady state time is about two hours and for the 0.003 mg/mL solution, at least five hours are needed. This demonstrates that if one chooses to determine the "affinity" of a surface for a given protein one must use long time data in static systems in order to ensure steady state. Diffusion limitations seem to persist as long as the adsorption of fibrinogen is less than 0.20 $\mu g/cm^2$.

Fibrinogen adsorption "isotherms" on the C18 surface are plotted in Figure 3.3.12 for 2 min, 30 min, and 20 h contact times. The maximum adsorption achieved for all times was approximately 0.45 $\mu g/cm^2$ at a concentration of 1.0 mg/mL (which is still only a third of

the fibrinogen concentraion found in normal plasma). Higher concentration data would be needed to determine if this were the ultimate adsorption plateau, but the expense of using concentrated solutions of fibrinogen made this impractical.

Fibrinogen adsorption "isotherms" on the SO3 surface (Figure 3.3.13) are very similar to those on C18 especially at low coverage (less than 0.20 $\mu g/cm^2$) and short times (2 minutes). The maximum adsorption achieved on SO3 is much higher than on C18, reaching a level of 0.87 $\mu g/cm^2$. The fact that adsorption is so high on a relatively hydrophilic surface runs contrary to conventional "rules of thumb" for protein adsorption. Others have found, however, that sulfonate groups do have a specific binding affinity for fibrinogen (Santerre et al, 1989).

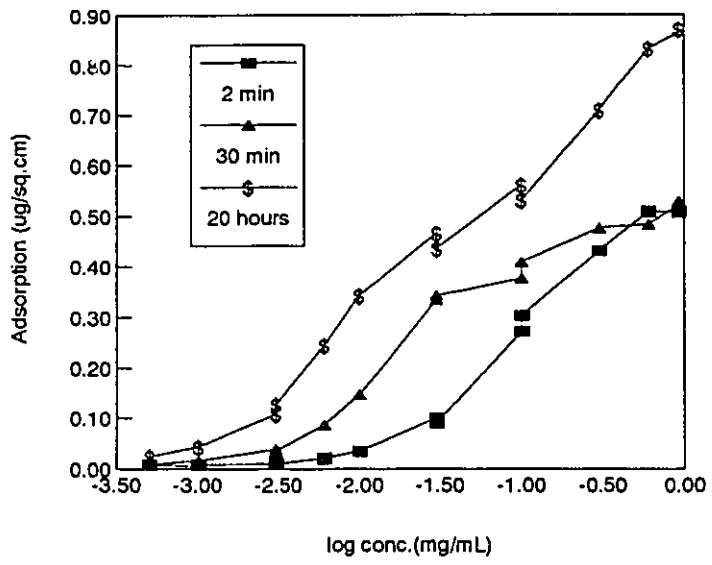

Figure 3.3.13: Fibrinogen adsorption "isotherms" on SO3 for three different times.

The fibrinogen adsorption kinetics of SO3 (Figure 3.3.14) suggest the existence of an intermediate plateau in the vicinity of 0.4 $\mu g/cm^2$ which was not apparent in the isotherm data. Adsorption above this level did not reach a new plateau suggesting that surface uptake continues, albeit very slowly, even after 20 hours. This was observed to be true even in the

lowest concentrations and thus no assumption of a steady state or "equilibrium" could be justified, even after 20 hours. Below 0.30 μg/cm^2 adsorption is apparently diffusion limited with a fibrinogen diffusivity similar to that found on the C18 surface ($0.8x10^{-7}$ cm^2/s).

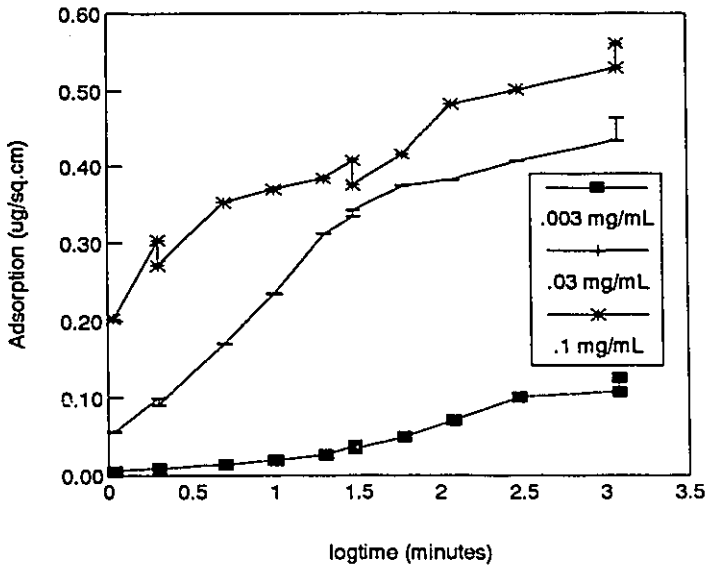

Figure 3.3.14: Kinetics of fibrinogen adsorption from Tris buffer onto SO3 for three different initial concentrations.

Fibrinogen adsorption data suitable for equilibrium model fitting would be difficult to obtain within a reasonable time frame especially at the low concentrations typically used to calculate affinity. It was this general observation which led to the exclusive use of kinetic rather than equilibrium models for the fitting of experimental data in this study (section 4.3.2). It is possible that steady state would be more easily achieved in a flow or well stirred particle system, but rapid initial events are more difficult to observe in such systems. Flow experiments would also have required large volumes of labeled protein solution for which the available preparation methods were not well suited.

3.3.5 Comparative Fibrinogen Adsorption Experiments

Thirty minute fibrinogen adsorption experiments were performed on the eight model surfaces employed in this study. Data for those surfaces which showed the highest adsorption are shown in Figure 3.3.15. As for albumin the two highest adsorbing surfaces were SO3

and C18. The highest uptake occurred on SO3 which was surprising given its relative hydrophilicity. However, work by Santerre et al (1989), and Grasel and Cooper (1989) has shown that sulfonate groups incorporated in segmented polyurethanes have a specific chemical affinity for fibrinogen. The C18, SH, and CH3 surfaces show similar adsorption perhaps due to their relatively similar hydrocarbon chemistry. Adsorption on the epoxy silane follows the same trend as that observed on the others but is significantly less.

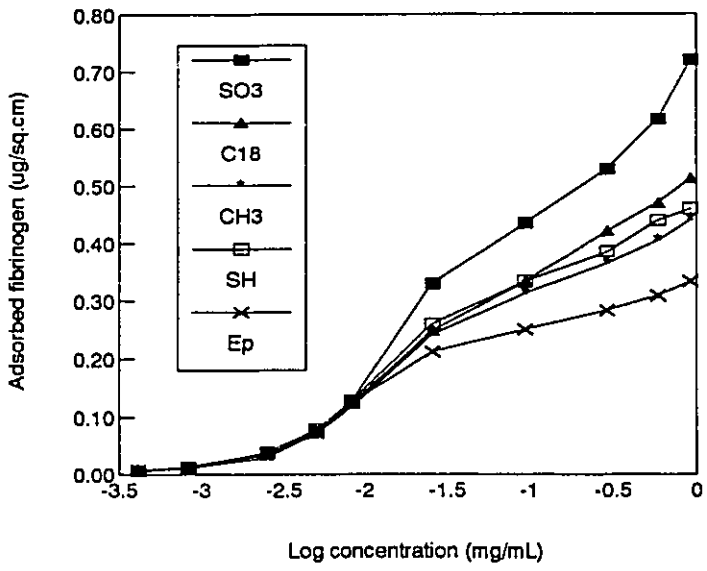

Figure 3.3.15: Thirty minute fibrinogen adsorption isotherms on five relatively high affinity surfaces.

The surfaces NH2, Ur, and Qz, all of which are relatively hydrophilic, show the least adsorption of fibrinogen after 30 minutes (Figure 3.3.16). The NH2 data do not conform to the trends observed on the other seven surfaces for concentrations above 0.03 mg/mL. It should be noted that albumin adsorption data in Figure 3.3.10 show the NH2 surface to have a unique effect on that protein as well.

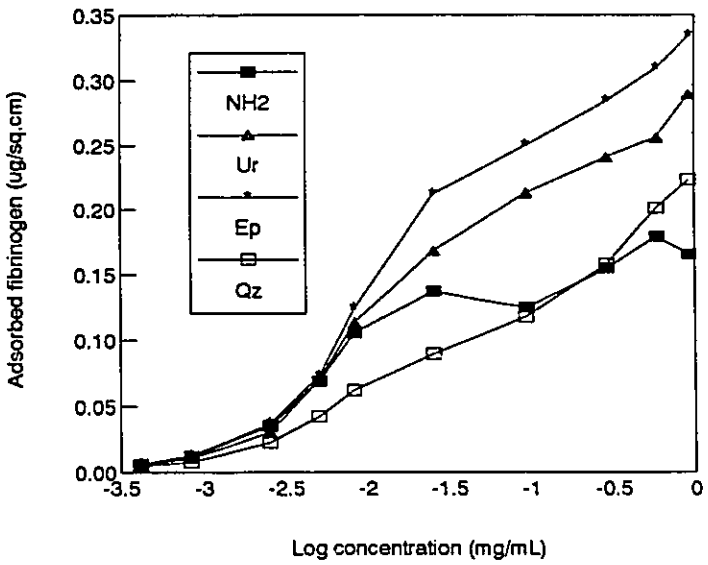

Figure 3.3.16: Thirty minute fibrinogen adsorption isotherms on four relatively low affinity surfaces.

Table 3.3.2: Surface Characterizations Representative of Single Component Fibrinogen Adsorption.

Surface	Fibrinogen affinity ($\mu g/cm^2$) [30 min. at 0.03 mg/mL]	Fibrinogen Capacity ($\mu g/cm^2$) [30 min. at 1.0 mg/mL]
Qz	0.090	0.224
NH2b	0.121	0.229
NH2	0.138	0.166
Ur	0.168	0.289
LYS	0.174	0.441
Ep	0.212	0.334
SO3>NH2	0.225	0.331
SO3+NH2	0.231	0.352
CH3	0.241	0.441
C18	0.248	0.513
SH	0.259	0.460
SO3b	0.302	0.815
SO3	0.330	0.720
PEG	0.390	0.967

Fibrinogen adsorption on all surfaces (except Qz) up to a concentration of 0.006 mg/mL is virtually identical suggesting a transport limitation on fibrinogen adsorption with a diffusivity of about $0.8 \pm 0.3 \times 10^{-7}$ cm^2/s. Adsorption of fibrinogen on silica was much slower than on the other seven surfaces. Clearly, surface binding rates were more limiting in the uptake of fibrinogen on silica.

The data presented in Figures 3.3.15 and 3.3.16 were used to characterize each surface with respect to fibrinogen adsorption. With the exception of NH2, it appeared that the surfaces could be differentiated by a single variable such as the maximum adsorption (at 1.0 mg/mL) representative of the capacity of the surface for fibrinogen. Adsorption at 0.03 mg/mL was chosen to be representative of affinity. These values are listed in Table 3.3.2.

3.3.6 Fibrinogen Adsorption from Blood Plasma

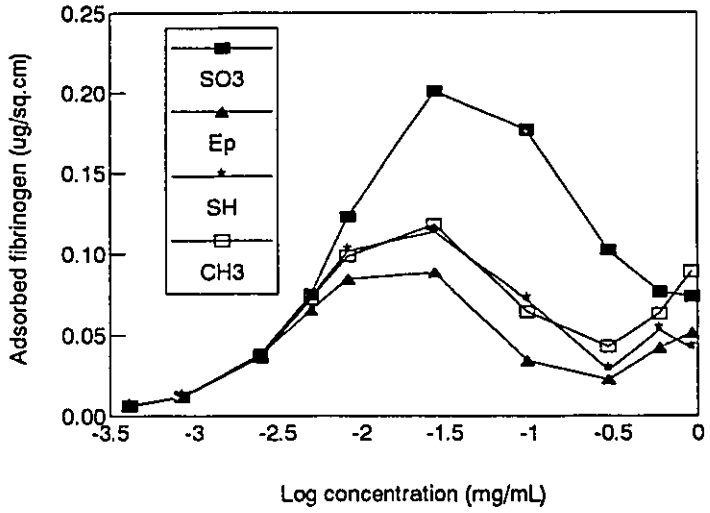

Figure 3.3.17: The Vroman effect for thirty minute adsorption of fibrinogen from diluted plasma onto four high affinity surfaces.

Thirty minute adsorption "isotherms" were obtained for fibrinogen adsorption from a single plasma pool onto the eight model surfaces (Figures 3.3.17 and 3.3.18). Evidence of the classical "Vroman Effect" was apparent in all eight cases. Diffusion limited adsorption at low concentrations was followed by a peak adsorption and then a slow "decay". One feature of these isotherms which has not previously been observed is a consistent and sig-

nificant upturn in adsorption for fibrinogen concentrations greater than 0.30 mg/mL, i.e. plasma concentrations of about 10% normal. This phenomenon may be a result of inadequate rinsing or, more probably, secondary fibrinogen adsorption upon a complete protein monolayer. This high concentration effect was not observed to occur on all surfaces and thus could not be directly attributed to the systematic effect of rinsing. The fibrinogen used in this study may have contained another protein impurity which, if present in the labeled fraction, may have been responsible for the calculated upturn in adsorbed fibrinogen.

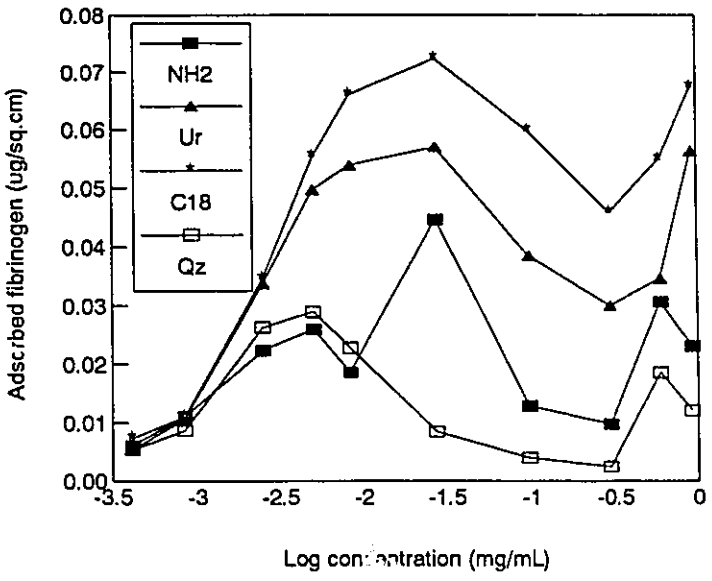

Figure 3.3.18: The Vroman effect for thirty minute adsorption of fibrinogen from diluted plasma onto four low affinity surfaces.

The initial slopes (for fibrinogen concentrations less than 0.003 mg/mL) were equal to those of the corresponding curves in Figures 3.3.15 and 3.3.16. This observation suggests that initial fibrinogen adsorption onto an empty surface is not altered by the presence of other plasma proteins, thereby contrasting conceptually with the sequence of adsorption first proposed by Vroman based on his observations in lens/slide systems (Schmaier et al, 1983). Clearly the initial stages of adsorption are governed by available surface area, surface binding rates, and diffusivities.

The mechanism for displacement of fibrinogen from the surface is unclear but the available evidence suggests that the effect is due more to the low concentration proteins than to albumin and IgG which are present in high concentration. In particular, HMWK, factor XII, and plasminogen have shown to be effective displacers on glass (Brash and ten Hove, 1984). It may be that there is a "displacement sequence" of proteins the order of which resembles the "adsorption sequence" proposed by Vroman. If surface activated clotting factors and cofactors are the best displacers, the Vroman Effect may provide a practical means for quantifying blood compatibility. The data in Figures 3.3.17 and 3.3.18 were characterized by a single parameter for each surface, namely the peak height or local maximum adsorption in the concentration range 0.003 to 0.1 mg/mL. The values are listed in Table 3.3.3.

Table 3.3.3: Quantitative characterizations of model surfaces with respect to the Vroman Effect. The numbers correspond to peak adsorption after 30 minutes.

Surface	Fibrinogen Peak Height ($\mu g/cm^2$)
NH2	0.026
NH2b	0.027
Qz	0.029
Ur	0.057
C18	0.070
Ep	0.088
SH	0.114
CH3	0.118
SO3b	0.134
SO3	0.201
LYS	0.208
PEG	0.223
SO3>NH2	0.267
SO3+NH2	0.304

As mentioned above, at high concentrations fibrinogen adsorption from plasma was consistently observed to increase at high concentrations, thus in a sense "reversing" the Vroman effect. This behavior was seen only at concentrations higher than 10% of normal plasma (i.e. fibrinogen concentration greater than about 0.3 mg/mL). Similar results have been reported by Slack and Horbett (1987) for fibrinogen adsorption from human plasma onto glass. Lindon et al (1987) showed that the Vroman effect did not occur when undiluted plasma was used but that it was observable at a dilution of 1% plasma in buffer. These

authors offer no explanation for this phenomenon. Two possibilities suggest themselves. First, the higher concentration solutions may not be fully rinsed from the tubing. This possibility seems relatively unlikely since large excess rinses are used in this laboratory (60 volumes) and in Horbett's (at least 20 volumes). The second more plausible hypothesis is that a second protein layer is able to adsorb from more concentrated plasmas. The possibility of bilayer protein adsorption is discussed at length in the mathematical modeling chapter of this thesis (section 4.3.2).

3.4 Surface Activated Coagulation Assay

3.4.1 Test Standardization

The Nova spectrofluorimeter was operated over a number of ranges which, according to the manufacturer, differ in sensitivity by a factor of approximately two. The output of the spectrofluorimeter was given as arbitrary absorbance units between 0 and 200 and thus required calibration in order to attribute thrombin activity (in units/mL) or thrombin generation rates to the data for plasma in contact with surfaces. The standardization procedure was also used to determine the reproducibility of the data and the linearity of the instrument's response given a simple, predictable system.

Sequential dilutions were made from a 200 U/mL stock solution to yield test solutions of 50, 25, 12.5, 6.25, and 3.12 U/mL thrombin concentration. For each test, the test solutions were added in a 1:100 ratio to the standardized substrate solution (0.1 mM Na-t-BOC-L-valyl-L-prolyl-L-arginine-7 amido-4-methyl coumarin). Range 5 was chosen to be a good intermediate range for the investigation of substrate cleavage kinetics by all five test solutions.

Figure 3.4.1 shows a plot of arbitrary fluorescence units (for range 5) versus time for four test solutions. Data from two separate experiments were obtained for the three lowest concentration test solutions. The data appeared to be quite linear for each individual experiment with systematic variation as high as 15% between the 12.5 U/mL repeats.

The production of fluorogenic substrate was designed to be pseudo first order with respect to thrombin, and thus the fluorescent response divided by concentration should yield a unique linear relationship for each range. The slopes of these lines with respect to time

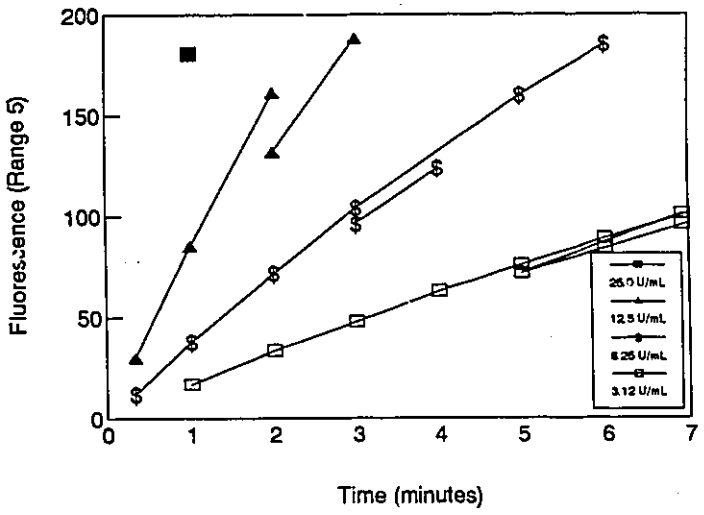

Figure 3.4.1: Thrombin generation assay of standard solutions by a fluorogenic substrate. Four standard thrombin solutions were prepared and tested at a single sensitivity (range 5) on a Nova Spectrofluorimeter.

were expected to be constant representing the conversion factor for calculating the thrombin concentration from fluorescence data. It was observed, however, that the slope was not constant and appeared to decrease slightly with time (Figure 3.4.2). In fact the instrument appeared to have a unique calibration curve for each point in time. At the shortest times (less than one minute) the sensitivity ratio between ranges was apparently only slightly greater than 2 (the manufacturers approximation) with an average value of about 2.15. At long times (6 and 7 minutes) the ratio appeared to be about 3.63. It must be pointed out that the estimated slope was not a local value but was based on a line from the origin (time and fluorescence equal to zero) and therefore on the assumption of linearity with respect to time. Even so the qualitative observation that the calibration "constants" varied with time was relevant.

The decrease in thrombin generation rate over time may be attributed to a drop in enzymatic activity correlated with a drop in temperature from the initial 37°C toward a room temperature of 23°C. (The sample holder in the spectrofluorimeter was not heated). This phenomenon can explain the decreasing thrombin production but not the changing relationship between sensitivity ranges with time. A temperature/time effect on fluorescence

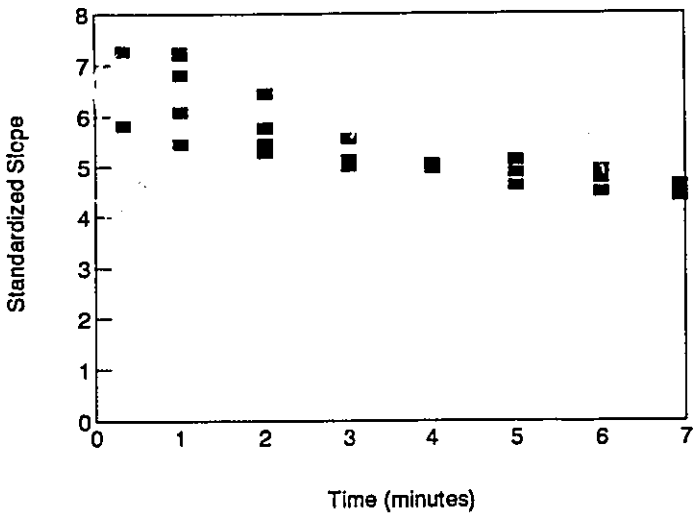

Figure 3.4.2: Thrombin calibration "constant" as a function of time for data collected in Figure 3.4.1. The calibration apparently changes significantly over time.

could easily be modeled empirically but for the purposes of this study a detailed interpretation of the kinetic data was not required. The data were used instead to obtain a single parameter equivalent to a clotting time in traditional assays. If quantitative interpretation of the kinetics of thrombin production on artificial surfaces were required, better data could perhaps be obtained using a temperature controlled spectrofluorimeter.

3.4.2 Thrombin Generation Assay on Model Surfaces

By reconstituting citrated, platelet poor plasma with platelet phospholipids and calcium ions, and bringing it in contact with the various surfaces, the intrinsic clotting pathway was initiated. The activating surfaces used in this study were the inner walls of silanized glass test tubes. The difficulty in calibrating the system to provide reliable quantitative values for the rate of thrombin generation did not make the assay less useful. The results were interpreted quantitatively to give a characteristic clotting time for each experiment.

Fluorophore generation was monitored at least four separate times on each model surface. The evolution of fluorescent product proceeded exponentially on each of the eight surfaces. The data were collected over three ranges of sensitivity 32, 4, and 8 which are nominally related by the conversion factors 32,4 and 1 respectively. Due to the calibration,

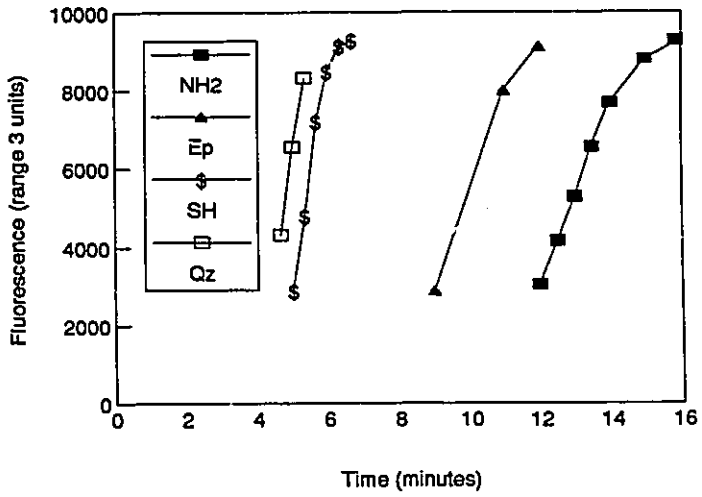

Figure 3.4.3: Thrombin generation data on four model surfaces. Data were extrapolated (to fluorescence = 0) in order to obtain a "clotting time". Data were collected in range 3.

these numbers were inappropriate. Factors capable of describing a smooth function over all ranges were used instead. The data were found to produce fairly smooth curves using the conversion factors 160, 10, and 1 for ranges 3, 5, and 8 respectively. These numbers were compromise values which worked reasonably well for all surfaces despite the fact that the range transitions on each occurred at different times. The essentially arbitrary selection of these conversion factors would have a profound and complex effect on the quantification of thrombin generation kinetics. Data interpretation was therefore simplified to avoid the need for calibration.

In order to quantify intrinsic activation, only the measurements obtained during the most rapid phase of substrate cleavage (in range 3) were used. Figures 3.4.3 and 3.4.4 provide examples of the kind of data that was used. The fluorescence versus time data were extrapolated linearly to zero fluorescence to give a characteristic "clotting time". The "clotting time" as described here does not represent the time at which a visible clot is formed (in fact it is probably a few minutes shorter than the time required for actual clot formation)

but is simply a parameter extracted from the graphical fluorescence versus time data. The average values and associated standard deviations were determined for each surface (Table 3.4.1).

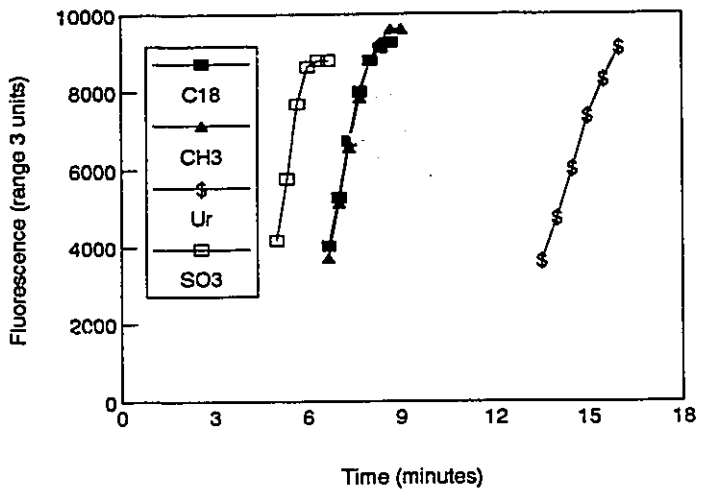

Figure 3.4.4: Thrombin generation results on four model surfaces collected in range 3. Data were extrapolated (to fluorescence = 0) in order to obtain a "clotting time".

Table 3.4.1: Clotting Times on Silanized Surfaces

Surface	Average Clotting Time (min.)	Number of Experiments	Fitted Standard Deviation (min.)	Estimated Standard Deviation (min.)	Error ±95% (min.)
SO3	3.9	4	0.45	0.35	0.83
Qz	4.0	6	0.50	0.35	0.58
CH3	4.1	5	0.52	0.98	0.72
SH	4.7	4	0.69	0.58	1.3
C18	5.1	4	0.81	0.58	1.5
Ep	8.6	4	1.8	2.2	2.5
Ur	9.0	6	1.9	1.9	2.2
NH2	9.6	4	2.1	1.8	3.9

The variability in measurements of clotting time was apparently proportional to the clotting time. As a result a second pooled estimate of the standard deviation is included in Table 3.4.1 as the "fitted standard deviation". This value was in turn used to estimate the 95% confidence limits for each average clotting time given degrees of freedom ranging from

3 to 5. The results demonstrate that there was a significant difference between the shortest and longest clotting times. The materials made for the extended study were also tested but with only four repeats. The average clotting times on these surfaces are listed in Table 3.4.2.

Table 3.4.2: Clotting Times on Silanized Surfaces of the Extended Survey.

Surface	Average Clotting Time (min.)
SO3b	3.2
LYS	5.5
PEG	7.0
NH2b	8.75
SO3+NH2	8.75
SO3>NH2	10.5

Average clotting times on all model surfaces ranged from 3.2 (SO3b) to 10.5 minutes (SO3>NH2). The ranking of these times was found not to be directly correlated with any of the measurements of surface chemistry, contact angles or protein adsorption. There is a possibility, especially evident in Table 3.4.1, that the clotting time may be correlated with surface charge. The presumably negatively charged surfaces SO3 and Qz apparently promoted rapid clotting while the positively charged surfaces containing amino groups were the slowest activators of clotting. The hydrophobic, uncharged hydrocarbon surfaces were intermediate in their activation of coagulation. No analytical method was used to determine independently the actual surface charge on each of these materials.

The thrombin generation kinetics for different surfaces were not observed to cross over one another at any point including at short times. Therefore the clotting times in Table 3.4.1 are values which rank the contact activating properties of all surfaces independent of time. The possibility that the initial rates of thrombin generation may be independent of the rates during the later stages was considered. If a surface exerts a specific influence on individual elements of the coagulation cascade, cross-over of the kinetics curves may occur. In particular, the sulfonated surface (SO3) may have promoted a heparin-like inhibition of thrombin such as has been observed on sulfonated polystyrene (Douzon et al, 1987). No such inhibition of the later stages of clot formation was evident on the sulfonated surfaces prepared for this study.

The random error involved in clotting time measurements was relatively large and thus not all surfaces could be quantitatively distinguished from one another by this method. Nonetheless the clotting time was retained as a useful biological parameter to be compared with the chemical and physical parameters measured in this study. In the future many more tests could be done on each surface by focusing only on data obtained in range 3. The time spent collecting and interpreting data in the more sensitive ranges did not yield any more useful information about the individual surfaces or the process of thrombin generation on them.

4 Analysis and Discussion

4.1 XPS Data Analysis and Estimation of the Thickness of Silane Monolayers

The C18, CH3, and Qz model surfaces were best suited for a semiquantitative analysis of the thickness of the silane layer. All three consisted of an essentially pure layer of carbon on pure silica (SiO_2).

The C18 surface consisted of an 18 carbon chain grafted to pure silica by means of a single siloxane bridge. The silane used (octadecyl dimethyl chlorosilane) has only one chlorine available to react with silica and therefore was capable of forming, at most, only a monolayer on the silica substrate. Carbon-carbon bonds in this molecule are approximately 0.154 nm with a bond angle of 109.5°. A "brush-like" monolayer of zig-zag C18 chains would produce a 2.3 nm monolayer. This conformation is unlikely, especially under the vacuum conditions of the experiment. Under these conditions the octadecyl groups would self-associate and tend to lie flat on the surface. The *a priori* expectation for the C18 layer thickness would have to be significantly less than 2.3 nm.

The variable angle XPS data are shown in Table 3.1.2. These data were used to estimate the thickness, t, of a polyethylene-like overlayer on C18, CH3, and the "clean" standard Qz. For each model surface, four estimates of the layer thickness could be obtained from the silicon and oxygen data at 30° and 90°.

The ratio of the number of electrons escaping from the pure silica surface, N_o, to the number escaping from the overlayer, N, is related to the mean free path, λ, for the electrons emitted by a given element (Andrade, 1985a). Equation 4.1.1 is an empirical expression for this relationship at a given angle of incidence (detector angle), θ, relative to the surface plane.

$$N/N_o = e^{-t/\lambda \sin\theta} \qquad [4.1.1]$$

λ is the distance through which 63% of all electrons emitted by a certain element can penetrate. For Si-2p electrons this distance is 4.4 nm and for O-1s electrons, it is 3.3 nm through polyethylene.

If the underlying substrate is pure silica, then we presumably may be able to assume that N_o is 66.7% for O -1s and 33.3% for Si-2p electrons. In order to use the data in Table 3.1.2, it is necessary to assume that the total number of electrons emitted from the theoretically pure silica and the real coated samples are essentially equal. The approach is semi-quantitative and provides a rough estimate of the thickness, t. The values are tabulated in Table 4.1.1.

Table 4.1.1: Estimates of silane (or organic) overlayer thickness on three model surfaces

Surface	Thickness (nm)	
	Estimate from Si-2p	Estimate from O-1s
C18	0.29	0.54
CH3	0.04	0.24
Qz	1.52	1.38

It should be noted in Table 4.1.1 that the estimated thickness was significantly different for a given sample depending on whether the Si-2p or O-1s data were used. The estimates were found to be sensitive to the values assumed for N_o based on a 2:1 atomic ratio (66.7% O : 33.3% Si) in silica. If the values were slightly altered to give a 65:35 ratio, the estimate of t was largely independent of the type of electron. Table 4.1.2 lists these estimates for t.

Table 4.1.2: Estimates of silane (or organic) overlayer thickness on silica assuming a standard Si to O ratio of 35:65

Surface	Thickness (nm)
C18	0.46
CH3	0.19
Qz	1.53

There is another possible interpretation of the data in Table 4.1.1. For the two silanes, the discrepancy in t is about 0.2 nm which is similar to the length of the Si-O bond (0.164 nm, Handbook of Chemistry and Physics, 62nd edn.). Since the silanes contain silicon and not oxygen, it is possible that the apparent discrepancy reflects the fact that a layer of silicon atoms lies directly above the oxygens to which they are attached.

The C18 layer has an apparent thickness on the order of 0.5 nm. It is possible that this represents a patchy monolayer of C_{18} chains oriented perpendicular to the surface (2.3 nm) or a nearly complete monolayer of octadecyl groups lying flat on the surface with a maximum depth of about four carbon atoms. The CH3 surface thickness was estimated as 0.2 nm which closely matches the Si-C bond length of 0.186 nm. The C18 likely contains some CH3 groups since HMDS (see section 2.1.2) was used as a blocking agent on all surfaces. Partial coverage of the C18 surface by CH3 may have lowered the value of t measured. While these estimates cannot be used to confirm the existence of complete substrate coverage, they it do show that "t" was in the vicinity of a monolayer and by analogy, all the model surfaces were also assumed to have near-monolayer coverage.

The "pure" silica control, Qz, was estimated to have an organic overlayer of approximately 1.5 nm or about twelve carbon atoms deep. Surprisingly Qz was observed to contain more carbon than any of the silanized model surfaces. As a "rule of thumb", one may estimate the thickness of an organosilane overlayer on pure silica by dividing the total percentage of all elements other than Si and O (detected at 90°) by three to obtain the depth in number of carbon atoms (in layers of approximately 0.125 nm each). In all cases, the monolayer thickness was estimated to be similar to the size of the silane molecules used. Thus it may be concluded that attempts to avoid multilayering were successful.

4.2 Contact Angle Analysis

4.2.1 Normalized Contact Angles for Surface Characterization

A simple parameter was defined to quantify the raw contact angle data on each model surface. Experimental data demonstrated an apparently linear relationship between the contact angles for various liquids and those for water (see Figure 3.2.3). There was little evidence that any of the liquid-solid pairs showed particular affinity (or incompatibility) beyond the more general correlation between contact angle and liquid surface tension. The fact that the surfaces were non swellable precluded the occurrence of solvent penetration that can be quite common on polymeric materials.

The new parameter, called the "equivalent water contact angle", assigned to each surface a single value that was based on the contact angle data for all the liquids. Data sets for four liquids (water, glycerol, DMSO, and octane in water) were normalized to produce four new data sets with a mean of 0.0 and a standard deviation of 1.0. These four data sets were in turn averaged to yield a single data set which could be converted back to "equivalent contact angles" for each liquid system. Table 4.2.1 lists the equivalent advancing water contact angle for all eight model surfaces.

Table 4.2.1: The normalized or "equivalent" water contact angle for the eight model surfaces. Values are based on contact angle data for water, glycerol, DMSO and octane in water.

Surface	Equivalent Water Contact Angle (degrees)	Measured Water Contact Angle (degrees)
C18	89.5	89.3
CH3	69.5	70.3
SH	67.7	69.3
NH2	65.9	64.3
Ep	62.4	63.7
Ur	62.1	61.7
Qz	46.8	46
SO3	43.4	42.7

Figure 4.2.1 shows the relationship between experimental data and equivalent contact angles including the 95% confidence interval for the data. The error limits were found to be ± 4.65°. This value is not significantly different from the ± 4.37° interval found for the replicate water droplet experiments. The lack of model fit was not statistically greater than measurement error. One may adequately predict the contact angles for glycerol, DMSO or octane in water given only the "equivalent water contact angle". There was little evidence to support the hypothesis that microscopic interactions between certain solid-liquid pairs caused the observed contact angle to deviate from the simple empirical correlation described here.

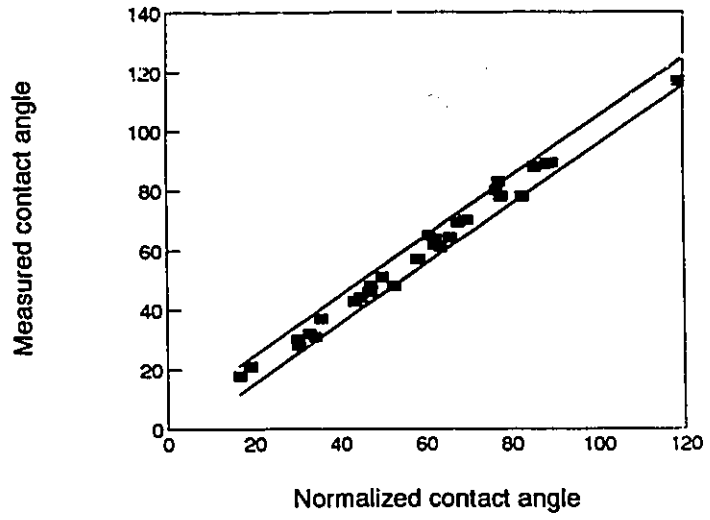

Figure 4.2.1: Measured contact angles plotted against their normalized values for water, glycerol, and DMSO on the eight original model surfaces. Upper and lower 95% confidence limits for data are also shown.

4.2.2 Work of Adhesion; Advancing and Receding Angles

The contact angle ($\theta_{L/S/A}$) data presented in section 3.2.2 may be used to obtain work of adhesion ($W_{\underline{SL}}$) values using the Young-Dupré equation (Adamson, 1990).

$$W_{\underline{SL}} = \gamma_{LA}(1 + \cos\theta_{L/S/A}) \qquad [4.2.1]$$

given the liquid surface tension, γ_{LA}.

The first data to be investigated using the work of adhesion parameter were the advancing and receding results for glycerol, water, and DMSO. The advancing and receding data are compared in Figure 4.2.2. The data for water and glycerol were spread over a wide range but the DMSO data were confined to a much narrower one since the contact angles obtained with this liquid were generally low. The receding angles for DMSO gave approximately constant work of cohesion values of about 90 mN/m. The results for water

and glycerol are more interesting because they demonstrate an apparently constant hysteresis value on all surfaces of 18.6 ± 2.4 mN/m (95% confidence interval for 15 degrees of freedom based on an assumption of constant hysteresis).

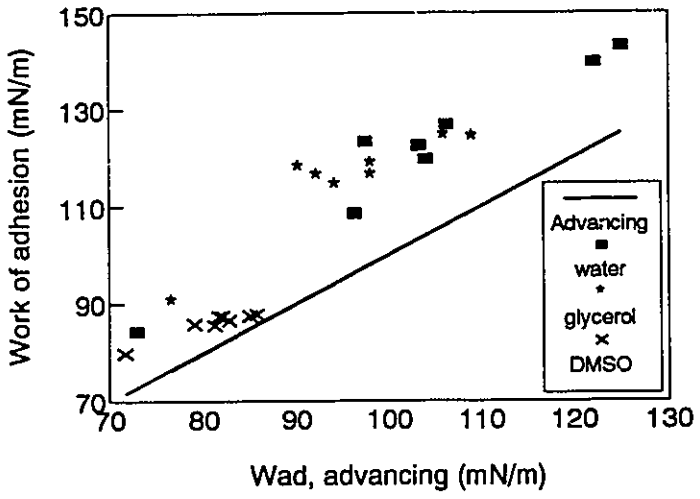

Figure 4.2.2: Work of adhesion for receding contact angles as a function of work of adhesion for advancing angles. The y = x line is included for comparison.

It should be pointed out that the relationship between work of adhesion and contact angle given by equation 4.2.1 is almost exactly linear over the range of contact angles between 20° and 100°. So by arbitrarily choosing work of adhesion to characterize solid surface tension, one has a number which offers no more information than could be obtained directly from raw contact angle data. The main advantage of using work of adhesion comes from the ability to use the parameter in thermodynamically defined relationships and thus in the testing of theory.

The most commonly considered theories for contact angle hysteresis suggest that it arises from an irreversible "pinning" of the three phase line (de Gennes, 1985) due to physical roughness and chemical patchiness (Andrade, 1985a). Neumann has prepared certain very hydrophobic surfaces (Neumann, Good et al, 1974) to be used in his equation of state. Hysteresis apparently cannot be avoided on higher energy surfaces presumably because they spontaneously adsorb low energy components from the atmosphere, which results in chemical heterogeneity. The chemistry of all the model surfaces was designed to provide

surfaces as homogeneous as possible, but still these surfaces showed significant hysteresis which increased as a function of decreasing contact angle. Thus it is clear there may be other sources of hysteresis in addition to physical roughness and chemical heterogeneity. The precursor film (de Gennes, 1985; Cazabat and Heslot 1990) known to precede an advancing liquid front may be a source of the hysteresis. It may be more difficult to retract this thin film than to create it due to the short range forces that are involved in maintaining its stability. The effect of a precursor film is progressively more important on more wettable surfaces. On nonwettable surfaces, the film may entirely disappear (Marmur, 1983) at equilibrium.

The effect of the precursor film is to lubricate a solid surface in preparation for the advancing liquid front. The thickness of this film is on the order of 100 Å (Heslot et al, 1990). De Feijter (1988) has suggested that the macroscopic contact angle is the result of a difference in surface tension between the precursor film and the liquid drop. The properties of the solid surface are only indirectly reflected in those of the interfacial film.

On the solid surfaces prepared for this study, hysteresis in terms of the work of adhesion was approximately constant. From this observation, one would favor the hypothesis that the source of hysteresis is largely physical since it is similar on all of the surfaces investigated. An effect of surface chemistry may also exist but appears to be small in comparison to the general source of hysteresis that is manifest in an essentially constant work of adhesion.

4.2.3 Work of Liquid Adhesion on Model Surfaces

Work of adhesion was chosen over contact angle as a parameter to compare the physical interactions between liquids and the model surfaces due to the fact that it could be used in, and compared with, thermodynamic relationships. Only advancing contact angle data were used in this connecton.

In Figures 4.2.3 and 4.2.4, work of adhesion data for the eight model surfaces are plotted as a function of liquid surface tension. Three liquids (water, glycerol, and dimethyl sulfoxide) were used. A striking pattern emerges from these data. C18, the most hydrophobic surface, shows approximately the same work of adhesion for all three liquids, whereas the other surfaces show increasing work of adhesion with increasing liquid surface tension.

SO3, the most hydrophilic surface, approaches most closely the $W_{\underline{SL}} = 2\gamma_{LV}$ limit.

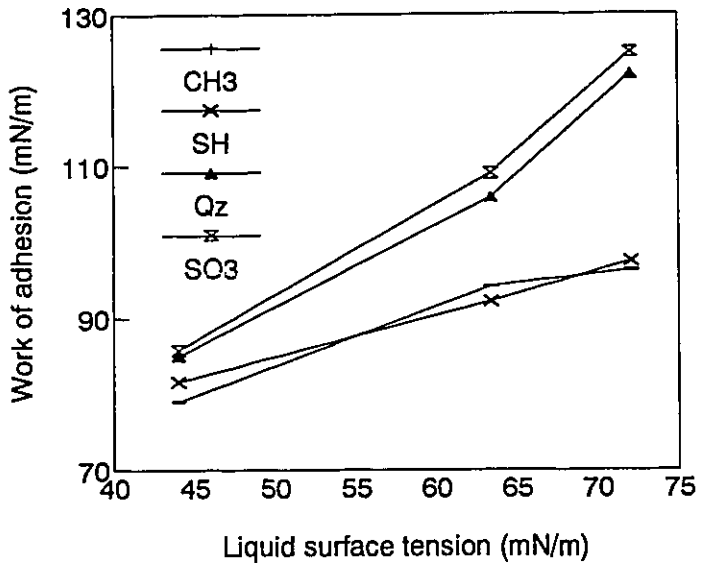

Figure 4.2.3: Work of adhesion for advancing contact angles versus total liquid surface tension of the test droplets. Data for SO3, the most hydrophilic model surface, Qz, SH, and CH3.

Figure 4.2.5 depicts the same data as in Figures 4.2.3 and 4.2.4 plotted against the work of adhesion for water. Here we may see the relationship between different liquids used to characterize the solids. The relationships between the work of adhesion for different liquids are nearly linear and appear to intersect in the vicinity of $W_{SL/V}$=75 mN/m, the value for C18 (see Figure 4.2.4). There is evidence of a simple relationship between contact angle and liquid surface tension, for all solid surfaces. There appear to be no strong specific liquid-solid interactions resulting in significant deviations from these simple trends. A surface which was wettable by water was wettable by any other liquid regardless of its surface chemistry.

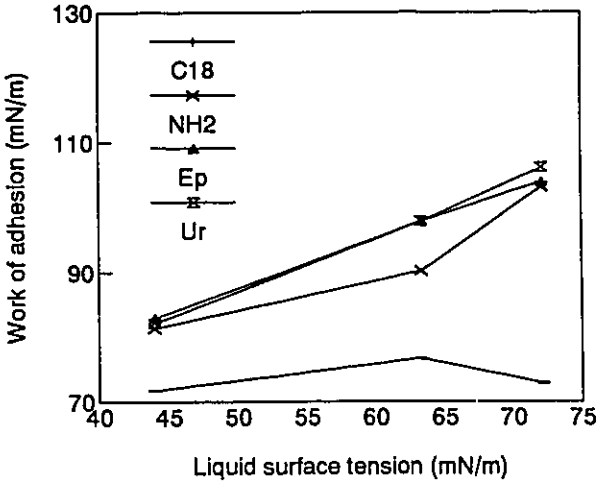

Figure 4.2.4: Work of adhesion for advancing contact angles versus total liquid surface tension of the test droplets. Data for C18, the most hydrophobic model surface, NH2, Ep, and Ur.

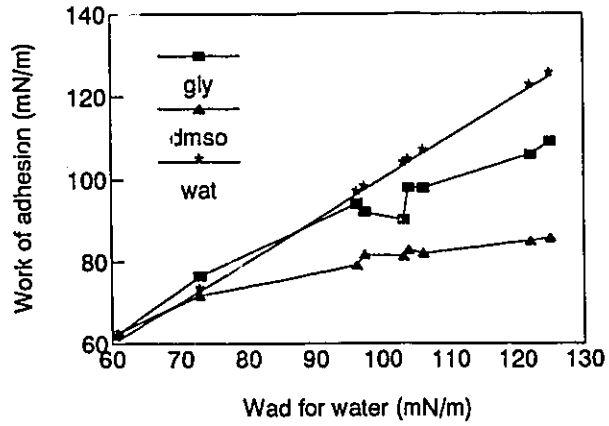

Figure 4.2.5: Work of adhesion for water, glycerol, and DMSO versus work of adhesion for water on the eight model surfaces. A strong correlation exists among the three liquids.

4.2.4 Use of Work of Adhesion Equations to Predict Octane Bubble Contact Angles

The water-in-air and octane-in-water contact angle experiments were initially performed so that the methods of Andrade et al (1979) could be used to determine the polar and disperse components of solid surface tension as defined by Fowkes (1964). The raw contact angle data for both systems were surprisingly well correlated by a straight line. The work of adhesion for water on the solid differed by a constant value in the octane and air environments (see Figure 4.2.6), the average difference being 43±3 mN/m (7 degrees of freedom) which is coincidentally very close to the work of cohesion for pure n-octane at 43.6 mN/m. The fundamental work of cohesion and adhesion equations were employed in order to find a possible explanation.

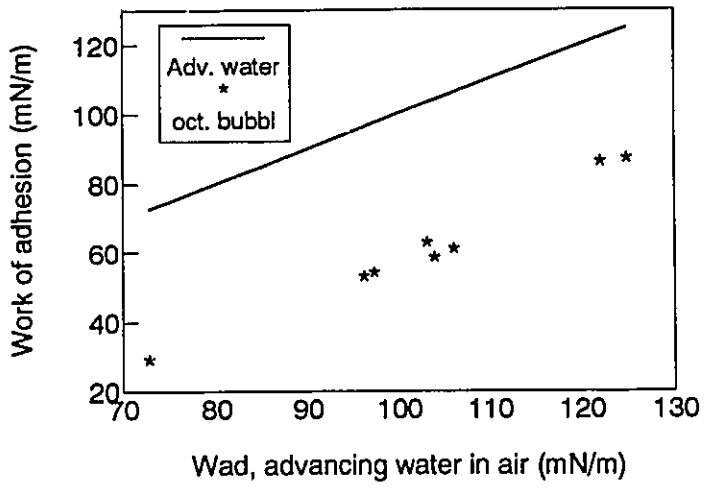

Figure 4.2.6: Work of adhesion for octane in water versus that for water in air. The y = x line is included for comparison.

The work of adhesion for water on a solid in air $W_{\underline{ws}}$ is given by,

$$W_{\underline{ws}} = \gamma_{SA} + \gamma_{WA} - \gamma_{WS} \qquad [4.2.2]$$

and for water on a solid in octane by,

$$W_{\underline{WS}}{}_{O} = \gamma_{SO} + \gamma_{WO} - \gamma_{WS} \qquad [4.2.3]$$

By subtracting 4.2.3 from 4.2.2 we obtain,

$$W_{\underline{WS}}{}_{A} - W_{\underline{WS}}{}_{O} = \gamma_{SA} + \gamma_{WA} - \gamma_{SO} - \gamma_{WO} \qquad [4.2.4]$$

Experimentally, we have shown that the left hand side of equation 4.2.4 has a value of 43 mN/m. The right hand side contains two unknowns involving the solid surface. We may take advantage of another work of adhesion equation (equation 4.2.5) for the solid and octane in air, to simplify further.

$$W_{\underline{OS}}{}_{A} = \gamma_{SA} + \gamma_{OA} - \gamma_{OS} \qquad [4.2.5]$$

Equations 4.2.4 and 4.2.5 may be combined to eliminate γ_{SA} and γ_{SO} to yield:

$$W_{\underline{WS}}{}_{A} - W_{\underline{WS}}{}_{O} = \gamma_{WA} - \gamma_{WO} + W_{\underline{OS}}{}_{A} - \gamma_{OA} \qquad [4.2.6]$$

For the water-octane pair it happens fortuitously that $\gamma_{WA} - \gamma_{WO} - \gamma_{OA} = 72.8 - 51.0 - 21.8 = 0$, and thus we have the special case given by equation 4.2.7.

$$W_{\underline{WS}}{}_{A} - W_{\underline{WS}}{}_{O} = W_{\underline{SO}}{}_{A} \qquad [4.2.7]$$

Octane was found to be completely wetting for all of the eight test materials with contact angles near zero degrees in all cases. This means that the term $W_{\underline{OS}}{}_{A}$ has a value of 43.6 mN/m, the work of cohesion for octane. This value is well within the 95% confidence interval found experimentally for the left hand side of equation 4.2.7.

The above demonstration uses the fundamental work of adhesion equations to explain observations in experimental data. A number of other observations and hypotheses may be made in its aftermath. First, the solid surface tension is still impossible to determine independently, even given water/solid systems in different environments. This is due to the fact that each new environment introduces a new unknown interfacial tension with the solid. It is possible to obtain information only about the interaction between solid and liquid.

Second, if we assume the above treatment to be valid, we may speculate that the work of adhesion may not exceed the value for the work of cohesion of the liquid. It follows therefore that complete wetting represents a limit of interaction, a maximum work of adhesion. This is consistent with Neumann's hypothesis of a minimum interfacial tension of zero between a solid and a completely wetting liquid (Neumann, Good et al, 1974) but disagrees with other ideas suggesting that negative interfacial tensions may be possible between chemically interacting liquids and solids (van Oss, Ju et al, 1989).

The above demonstration needs to be verified using another water-immiscible liquid with a significantly greater surface tension such as toluene (γ=28.5 mN/m). Based on the observations and theory discussed in this report, the difference between water-solid adhesion values in toluene and air environments should average about 50 mN/m. The average water contact angle in a toluene-water system should then be in the range of 6° higher than in a water-octane system. The situation may be somewhat more complicated if toluene is unable to completely wet the test solids, as was the case in the toluene/C18 in air system.

4.2.5 Established Models for the Determination of Solid Surface Tension

A good theory for the interpretation of contact angle data would be able to characterize a solid uniquely using a parameter (e.g. solid surface tension) which is independent of the probing liquids used to obtain contact angles. The following section is an extensive review of the theories most often used to determine "solid surface tension" and their relationship to the work of adhesion based on contact angle data for teflon taken from the text by Wu (1982). The weaknesses and strengths of each theory are discussed in advance of their application to data obtained for the model surfaces used in this study.

Equation 4.2.8 describes the work of adhesion for a liquid, L on a solid, S in an environment, V.

$$W_{\underline{LS}}_{V} = \gamma_{SV} + \gamma_{LV} - \gamma_{LS} \qquad [4.2.8]$$

This thermodynamic quantity serves as the framework for the comparison of contact angle theories and their ability to describe real data. The work of adhesion is a quantity which may be determined experimentally and manipulated theoretically. The solid surface tension may not be measured directly and thus cannot be used in the same manner.

The mathematical models used to estimate γ_{SV} may all be compared using the data for liquids on teflon (W_N). Each model may be expressed as a function defining $W_{\underline{LS}}$.
$\overline{V}$

4.2.5.1 Zisman's critical surface tension

Zisman's correlation extracts a single parameter from contact angle data for a wide variety of liquids on a given solid (Fox and Zisman, 1950). Contact angle data may be linearly extrapolated in the limit as $\cos\Theta_{\underline{SL}}$ approaches 1 to a characteristic liquid tension
$\overline{V}$

known as the critical surface tension, γ_C. The relationship exploited by Zisman's method may be expressed mathematically for a given solid as:

$$\cos\theta = 1 - k_C(\gamma_{LV} - \gamma_C) \qquad [4.2.9]$$

where k_C is the slope of the Zisman plot, typically in the range 0.02 to 0.04 m/mN for most solids. By incorporating [4.2.9] in [4.2.8] we may estimate the work of adhesion on a given solid for a limited range of liquid surface tensions.

$$W_{\underline{SL}} = \gamma_{LV}(2 - k_C(\gamma_{LV} - \gamma_C)) \qquad [4.2.10]$$
$\overline{V}$

Equation 4.2.10 is plotted versus data for teflon (Wu, 1982) in Figure 4.2.7. γ_C was assumed to be 20 mN/m and k_C to be 0.035 m/mN in order to best fit the data for low surface tension liquids. The fit is quite good for liquids ranging from 20 to 40 mN/m but quickly deviates from the experimentally determined data beyond 40 mN/m. The data for teflon suggest that a maximum work of adhesion of about 56 ± 5 mN/m is approached for liquids with a high surface tension. This would imply a contact angle of approximately 152° for mercury (γ_{LA} = 484 mN/m) on teflon using equation 4.2.1. Mercury is not, however, the best liquid for estimating the work of adhesion since, for the Hg/teflon system a typical measurement error of ±4° can change the work of adhesion estimate by 30%.

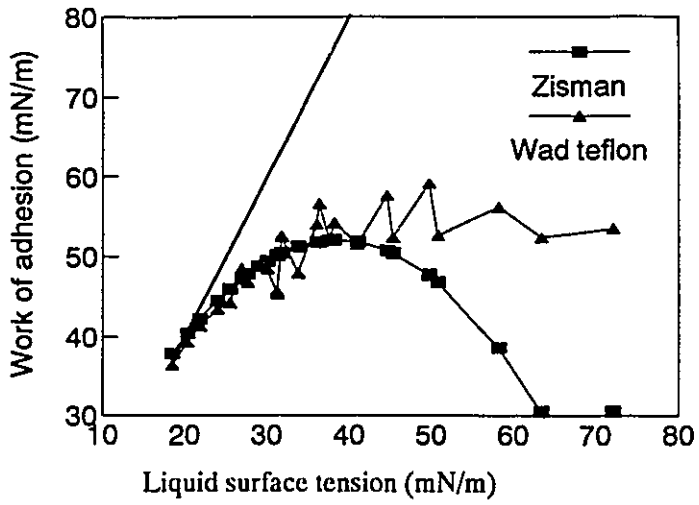

Figure 4.2.7: Work of adhesion for liquids on teflon. Zisman model based on critical surface tension of 20 mN/m and a cos θ versus γ_L slope of -0.035 m/mN. The y = 2x line represents the upper limit of liquid cohesion (i.e. θ = 0°).

4.2.5.2 The Good Interaction Parameter, ϕ

The Good interaction parameter, ϕ (Girifalco and Good, 1957) was used to characterize the interaction between solid/liquid pairs. Values of ϕ were chosen in order to fit the following model for the work of adhesion (using surface rather than interfacial tensions):

$$W_{\underset{\sim}{SL}} = 2\phi\sqrt{\gamma_S\gamma_L} \qquad [4.2.11]$$

ϕ values were close to 1.0 for low energy liquids on low energy solids and were less than 1.0 for other solid/liquid pairs. The value of ϕ was rationalized in each case by microscopic arguments concerning the adhesive and cohesive molecular interactions. Equation 4.2.11 is plotted in Figure 4.2.8 along with data for teflon (γ_S = 20 mN/m, ϕ = 1.0). γ_S could be estimated assuming ϕ = 1 for low surface tension liquids. The fit for liquids with surface

tensions less than 40 mN/m was very similar to that given by the critical surface tension relationship (Figure 4.2.7). For higher γ_{LV} values equation 4.2.11 overestimates the work of adhesion while equation 4.2.10 underestimates it.

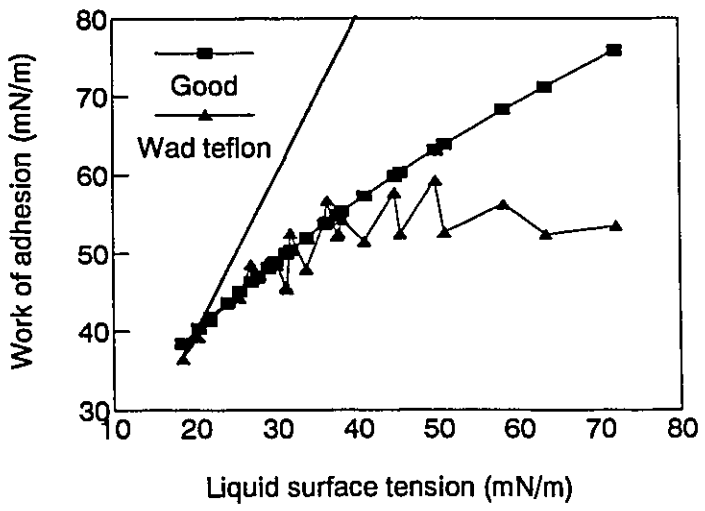

Figure 4.2.8: Fit of Good interaction parameter model to teflon data. The model assumes a solid surface tension of 20 mN/m for teflon and a Good interaction parameter of 1.0. The y = 2x line represents the upper limit of liquid cohesion.

When the liquid surface tension is high, the value of ϕ used in equation 4.2.11 must be adjusted to fit the $W_{SL/V}$ estimates from contact angle data (equation 4.2.1). Equation 4.2.11 cannot be used to predict the work of adhesion between previously untested solid/liquid pairs but it does provide the conceptual foundation and model form for the theory of surface tension components used by Fowkes to characterize uniquely the individual components of solid and liquid surface interactions (Fowkes, 1964).

4.2.5.3 Fowkes Surface Tension Components

Fowkes proposed that the surface tensions of individual solids and liquids are composed of the sum of many individual components including those due to dispersive forces, dipole-dipole, pi-bonds, and others (Fowkes, 1964). For most liquids and solids, however, it was assumed that surface tension could be well approximated by the sum of two com-

ponents: polar and non-polar (dispersive). Interfacial tensions could be predicted by assuming a mathematical model quantifying the interaction between components. Two model forms for the work of adhesion have found wide application, the geometric mean:

$$W_{\frac{SL}{V}} = 2\sqrt{\gamma_S^p \gamma_L^p} + 2\sqrt{\gamma_S^d \gamma_L^d} \qquad [4.2.12]$$

and the harmonic mean:

$$W_{\frac{SL}{V}} = \frac{4\gamma_S^p \gamma_L^p}{\gamma_S^p + \gamma_L^p} + \frac{4\gamma_S^d \gamma_L^d}{\gamma_S^d + \gamma_L^d} \qquad [4.2.13]$$

where,

$$\gamma^p + \gamma^d = \gamma \qquad [4.2.14]$$

The superscripts p and d refer to the polar and dispersive (nonpolar) components of solid or liquid surface tension. Wu (1982) favors the use of equation 4.2.13 while others (Dalal, 1987; Owens and Wendt, 1969) have suggested that equation 4.2.12 is better for characterizing solid surface tensions. Since the components of surface tension are theoretically independent of the total surface tension, they may be adjusted in order to fit contact angle data for liquids on a known solid. Teflon has traditionally been used as the standard nonpolar solid surface. In Figure 4.2.9 equations 4.2.12 and 4.2.13 are compared with data for teflon assuming $\gamma_S^d = 20$ mN/m and $\gamma_s^p = 0$. The ratio γ_L^p/γ_L^d was arbitrarily assumed to have a constant value of 0.1 for the purpose of plotting Figure 4.2.9. Both models fit the data reasonably well for liquid surface tensions less than 40 mN/m as did the previously presented models. Unlike the previous two models the adjustable parameters γ_s^p and γ_s^d can be altered to fit the data yielding parameters unique to the solid and valid for the prediction of contact angles in contact with any other liquid whose surface tension components are known.

The difference observed in Figure 4.2.9 between the data and the models is consistent with the fact that the polar component of liquid surface tension increases with increasing total surface tension. This contradicts the supposition that the polarity of a liquid is related to its chemistry and is independent of its total surface tension. Available data suggest that liquids with surface tensions less than 50 mN/m have little or no polar component. Dimethyl sulfoxide, for example, is known to be a highly polar solvent but its polar component of surface tension (determined using teflon contact angles) is of the order of 3 mN/m. Good,

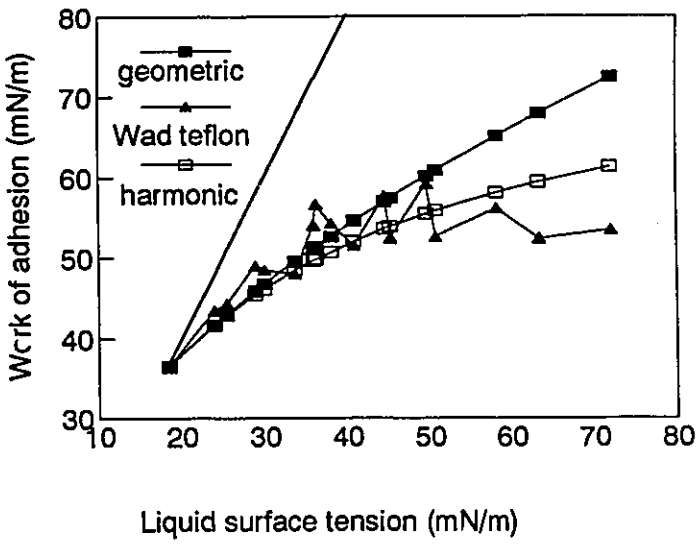

Figure 4.2.9: Models for Fowkes surface tension components based on the harmonic and geometric mean. Teflon was modeled as entirely dispersive (20 mN/m) while the liquids were all arbitrarily assumed to have a dispersive to polar ratio of 10:1. The harmonic mean model fits better on low energy surfaces like teflon.

Van Oss, and Chaudhury (van Oss et al, 1987) have attempted to explain this paradox with their new microscopic theory (see section 4.2.5.5) and suggest that DMSO may be a "monopolar" liquid, able to interact only with surfaces containing an opposite monopole.

The difference between equations 4.2.12 and 4.2.13 can be seen in their mathematical form and in Figure 4.2.9. The harmonic mean reaches a plateau, a maximum work of adhesion of high liquid tensions, similar to the plateau achieved by the actual teflon data. The geometric mean equation predicts an increasing work of adhesion even at high γ_L values. Wu has suggested that the harmonic mean works better than the geometric mean on "low energy" surfaces such as polymers. The geometric mean was recommended for characterizing high energy surfaces such as metals, glass, and ceramics.

One potential problem with the surface tension components method is that two different liquid contact angles must be measured on the solid being tested. The components estimated contain experimental error, solvent penetration effects, and other systematic influences along with purported properties of the surface. Dalal (1985) attempted to avoid the problems of

experimental error by performing a least squares fit of six contact angles on a given solid to the harmonic and geometric mean equations. He concluded that the geometric mean fit the data better than the harmonic mean although the criteria for reaching this conclusion were not made clear.

The theory of surface tension components is most easily shown to be deficient when attempting to predict liquid/liquid interfacial tensions. The inconsistencies observed both experimentally and theoretically led to the development of a competing macroscopic theory (Ward and Neumann, 1974) and more recently to an extension of the microscopic theory (van Oss et al, 1987, 1988, 1990).

4.2.5.4 Neumann's Equation of State

The contact angle that is measured with a goniometer is a macroscopic property with a much more complicated microscopic structure on the molecular scale (de Gennes, 1985). An arguably more appropriate macroscopic approach to the interpretation of contact angles has been proposed by Neumann (Ward and Neumann, 1974: Neumann et al, 1974). The Neumann "equation of state" has been the source of controversy since its formulation is based on the assumption that the interfacial tension between a completely wetting liquid and the wetted solid is zero. One has only to look to analogous liquid-liquid systems to show that this need not be true (e.g. octane spreads on water, and γ_{WO}=51 mN/m not 0 mN/m).

The Neumann equation of state for the work of adhesion between liquids and solids has the form:

$$W_{\frac{SL}{V}} = \gamma_{SV} + \gamma_{LV} - \frac{\left[(\gamma_{SV})^{\frac{1}{2}} - (\gamma_{LV})^{\frac{1}{2}}\right]^2}{1 - 0.015(\gamma_{SV}\gamma_{LV})^{\frac{1}{2}}} \qquad [4.2.15]$$

The model is empirical and is based on contact angle data for a wide variety of liquids on relatively low energy polymer surfaces. It is not surprising therefore, that equation 4.2.15 fits the data for teflon as well as it does (see Figure 4.2.10). Neumann hypothesized that deviations from the equation of state model are due to improperly controlled interactions between the solid and liquid, which alter their physicochemical properties. It is difficult to precisely monitor such localized changes at the interface. Many polymers are able to absorb

small amounts of solvent into the solid matrix, thus invalidating the assumption of two distinct phases separated by an interface. The measured contact angle in such a system would be lower than expected for a non-interacting pair.

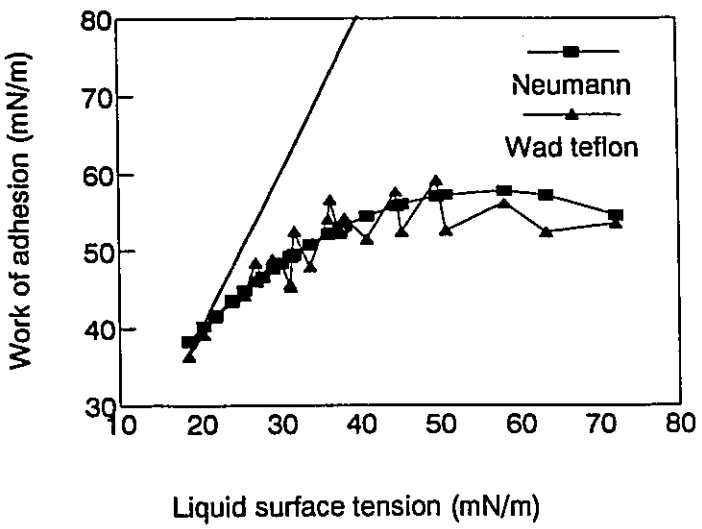

Figure 4.2.10: Neumann's empirical equation of state model for a solid surface tension of 20 mN/m. This model fits the teflon data very well. The empirical model was derived on surfaces similar to teflon and cannot fit data for surfaces with a water contact angle much lower than 90°.

Johnson and Dettre (1989) have presented data refuting Neumann's hypothesis that the contact angle on a given surface is a function of only one variable, namely the surface tension of the liquid droplet. They claim that the data they have obtained show deviations from Neumann's model greater than experimental error. However, the fact that their data disagree with the widely held belief that octane and heptane are able to spread on water, casts some doubt on their conclusions. A relatively high degree of precision is required to prove or disprove Neumann's hypothesis that contact angle is a unique function of total liquid surface tension. Given the current limitations in controlling precision of measurements, cleanliness of surfaces and penetration of solvents such proof is difficult to obtain. In practice experimental data do not often deviate far from Neumann's model.

Another of the crucial hypotheses on which Neumann's theory rests is one that states that the interfacial tension is zero when the contact angle is zero. The case of octane spreading on water has been often presented as evidence contrary to this theory. However, there may be a fundamental difference between liquid-liquid and liquid-solid interfaces and the assumption may still be valid. Liquid-liquid interfacial tensions are the sum of two surface tensions on either side of the interface. For octane on water the interfacial tension is 51 mN/m. It is possible that the surface tension of octane on water is zero while the surface tension for water on octane is 51 mN/m. This would explain the contradiction between Neumann's hypothesis and measurements on liquid-liquid systems. By analogy, if there are two surfaces at the liquid-solid interface the interfacial tension can be modeled as the sum of two surface tensions:

$$\gamma_{\underline{L}} = \gamma_{LV} - \frac{1}{2} W_{\underline{LS}} \qquad [4.2.16]$$

$$\gamma_{\underline{S}} = \gamma_{SV} - \frac{1}{2} W_{\underline{LS}} \qquad [4.2.17]$$

and,

$$\gamma_{LS} = \gamma_{\underline{L}} + \gamma_{\underline{S}} \qquad [4.2.18]$$

where $\gamma_{L/S}$ is the surface tension of the liquid phase in contact with the solid. A liquid surface will reorient due to the free mobility of its molecules to attain the most energetically favorable configuration. For a rigid solid surface, changes in the molecular orientation are not possible since it can support externally applied force as surface stresses. By this rationale it is not appropriate to interpret solid-liquid interfaces in the same way as liquid-liquid interfaces because a solid cannot contribute to the interfacial tension, only to the surface tension of the liquid in contact with it.

The vapor phases do not contribute any short range forces to the conditions at solid-vapor, or liquid-vapor interfaces. One may thus assume that $\gamma_{V/S}$ and $\gamma_{V/L}$ are equal to zero, and thus the interfacial tensions γ_{VS} and γ_{VL} are equal to $\gamma_{S/V}$ and $\gamma_{L/V}$ respectively. Thus the nomenclature for these interfaces is less susceptible to the confusion that exists at the liquid-liquid or liquid-solid interface, where two surfaces contribute to the interfacial tension.

Neumann's key assumption that a zero interfacial tension, γ_{SL} exists between a wetting liquid and a solid may be a correct one for the practical purposes of interpreting contact angles, but incorrect in its nomenclature. A wetting liquid may have zero surface tension in contact with the solid $\gamma_{L/S}$ but the total interfacial tension must be greater than zero in order to maintain the stability of the interface.

The macroscopic, empirical approach of Neumann et al may well have broad practical application in the characterization of solid surfaces. Currently its use is constrained by an empirical model whose range of usefulness is limited to very low energy surfaces like teflon.

4.2.5.5 The Good, Van Oss, and Chaudhury (GVC) Theory

Proponents of microscopic theory have acknowledged the deficiencies of the Fowkes model for surface tension components (Morra et al, 1990). The Fowkes model often does not predict liquid-liquid solubilities such as water ($\gamma^p = 51.0, \gamma^d = 21.8$) in dimethyl sulfoxide ($\gamma^p = 3, \gamma^d = 41$). DMSO is a highly polar solvent which is easily miscible with water but the Fowkes theory predicts a stable interface between the two liquids.

Good, Van Oss, and Chaudhury (GVC) modified Fowkes' mathematical model for the polar component of surface tension to allow for acid-base interactions (van Oss, Good, Chaudhury et al 1987 and 1988). Molecules can have electron-donor or electron-acceptor capabilities or both. The new model defines two new surface tension "parameters" (γ^+, γ^- not true surface tensions) which combine to yield the acid-base component of surface tension γ^{AB} (essentially a new name for γ^p). The dispersive component of surface tension is more precisely named the Lifshitz-Van der Waals component of surface tension. In order to fully define the surface tension parameters for a solid, the contact angles for three liquids (for which all three components are known) must be measured and used with the following model for the work of adhesion.

$$W_{\underline{SL}}_{\overline{V}} = 2\sqrt{\gamma_S^{LW}\gamma_L^{LW}} + 2\sqrt{\gamma_S^+\gamma_L^-} + 2\sqrt{\gamma_S^-\gamma_L^+} - 2\sqrt{\gamma_S^+\gamma_S^-} - 2\sqrt{\gamma_L^+\gamma_L^-} \qquad [4.2.19]$$

The fitted parameters are highly susceptible to experimental error. The "known" parameter values for a small number of liquids are not absolutely confirmed, not even for water, so the meaning of estimated solid surface tension parameters is equally uncertain.

Parameter estimates made using the GVC model are even more susceptible to error than those from the simpler Fowkes model due to the effects of solvent absorption and random measurement error.

4.2.5.6 McGuire, Lee, and Sproull Model

A new model has recently been proposed (McGuire et al, 1990) based partly on the theory of Fowkes and partly on an empirical treatment of experimental observations. The model takes the form:

$$\frac{W_{SL}}{\overline{V}} = 2\sqrt{\gamma_L^d \gamma_S^d} + k\gamma_L^p + b \qquad [4.2.20]$$

where γ_L^d, γ_S^d, and γ_L^p are surface tension components similar to those in equations 4.2.12 and 4.2.13. The constants k and b are specific to the solid being tested. Therefore the solid must, as in the GVC model, be characterized by three parameters, in this case γ_s^d, k, and b. The parameters are, however, less constrained by physical meaning and can be used less critically than the γ^+ and γ^- values in equation 4.2.19. The form of the McGuire, Lee and Sproull et al model is consistent with the data trends observed in Figures 4.2.3, 4.2.4 and 4.2.5. However those data and the data presented in the McGuire paper call into question the independence of the three parameters involved.

In their paper, McGuire et al found γ_s^d to be approximately 30 ± 3 mN/m for materials as varied as high density polyethylene (HDPE), stainless steel, nylon, copper, and glass based on contact angle data. The major variation among materials arose almost entirely in the k parameter. There is in general little evidence to suggest that three independent parameters are needed to adequately characterize a wide variety of solid surfaces. One parameter may work nearly as well.

4.2.6 Fitting of Solid Surface Tension Models to Data for Silanized Quartz

4.2.6.1 Estimates of Solid Surface Tension by Neumann's Equation of State

Advancing contact angle data for the eight model surfaces and three liquids were used to estimate solid surface tensions by Neumann's equation of state. The estimates for each liquid on the eight model surfaces are plotted as a function of the normalized contact angle (see Table 4.2.1) in Figure 4.2.11. If Neumann's equation of state is correct, the estimates given by the three liquids should be the same. The hypothesis appears to be true on C18 and teflon (with contact angles of about 90° and 100° respectively), but on all other surfaces a consistent divergence of solid surface tension estimates is evident. Apparently, Neumann's theory gives valid results only for a limited range of fairly hydrophobic materials.

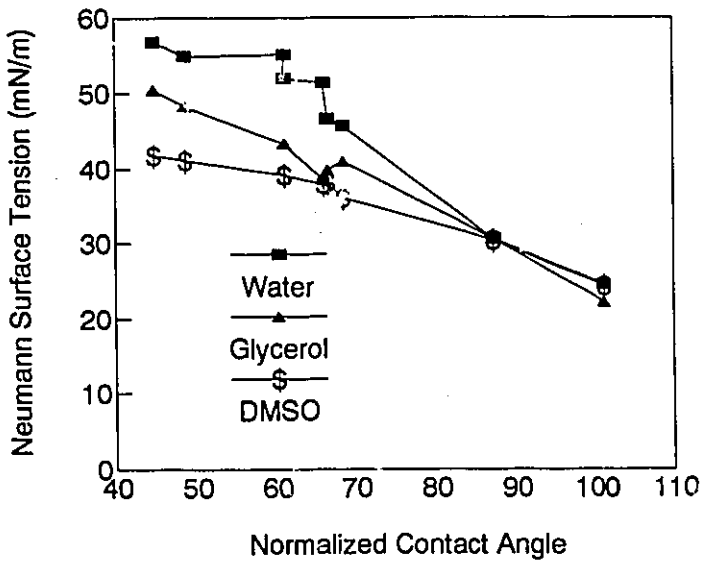

Figure 4.2.11: Neumann equation of state estimates of solid surface tension for the eight model surfaces and teflon using water, glycerol, and DMSO. The three lines should be coincident if the Neumann model is correct.

4.2.6.2 Estimates of Solid Surface Tensions by Fowkes Component Theory

Three different liquid-liquid pairs, water-glycerol, water-DMSO, and water/octane-water, provided the data necessary to determine the solid surface tension components of the model surfaces. The surface tension data for each liquid are given in Table 4.2.2.

Table 4.2.2: Liquid Surface Tension Components

Liquid	γ_{LV} (mN/m)	γ_L^p (mN/m)	γ_L^d (mN/m)
Water	72.8	51.0	21.8
Glycerol	64	30	34
DMSO 1	44	3	41
DMSO 2	44	9	35
Octane	21.8	0	21.8

(references: Dalal, 1985; van Oss et al, 1987; Wu, 1982; Andrade, Ma et al, 1979). The van Oss et al reference contains two estimates for the polarity of DMSO and so both are included in this table as DMSO 1 and 2.

The total solid surface tensions determined using the Fowkes theory for three systems are compared in Figure 4.2.12 along with the GVC (Good, van Oss, Chaudhury) estimates for the same surfaces using the water-glycerol-DMSO system. The estimated values of γ_{SV} were consistently different in each case and thus the validity of Fowkes' theory cannot be supported by the data collected in this study. The simple linear relationship between the normalized contact angle and Fowkes' estimate of the solid surface tension should be noted.

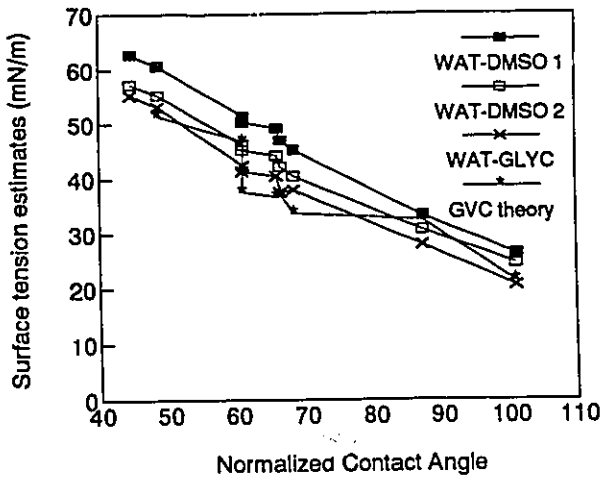

Figure 4.2.12: Estimates of total solid surface tension based on component theory including Fowkes and GVC theories. The polar component of DMSO was estimated to be 3 mN/m in case I and 9 mN/m in case II. Note the linearity of all estimates as a function of the contact angle.

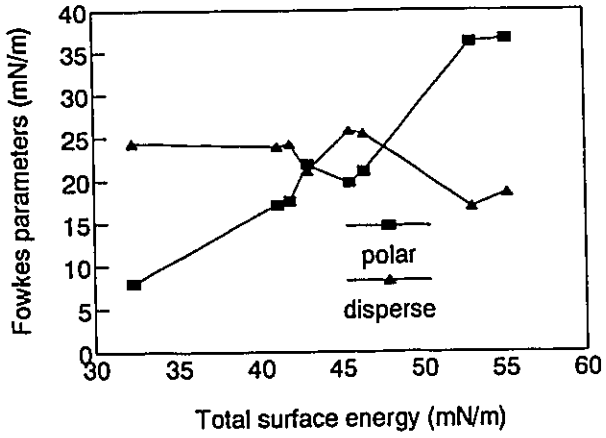

Figure 4.2.13: Magnitude of estimated polar and dispersive components of solid surface tension as a function of the total surface tension. Note that almost all variation in total surface tension among surfaces is manifest in the polar component.

The estimated components of surface tension for the water-octane/water data are presented in Figure 4.2.13. The trends seen in this figure are typical of all liquid-liquid pairs. The estimated disperse component was approximately the same for all surfaces although the actual value was different for each liquid pair used to calculate the components. Only the polar component varied significantly from surface to surface and thus total solid surface tension was directly correlated with it. The Fowkes model was able to determine one, (not two) independent component of surface tension on the eight model surfaces. Neumann attempted to show that the dispersive component of solid surface tension was in fact a function of the liquids used (Spelt and Neumann, 1987). This idea is consistent with the constant γ_S^d observed in the systems presented in this thesis.

4.2.6.3 Estimates of Solid Surface Tension by Acid-Base Theory

Contact angle data for water, glycerol, and DMSO droplets in air were used to determine the three surface tension "parameters" proposed by Van Oss, Chaudhury and Good (1988). Table 4.2.3 lists the components of surface tension for each of the liquids.

Table 4.2.3: GVC Components of Liquid Surface Tension (van Oss et al, 1988)

Liquid	γ_L mN/m	γ_L^{LW} mN/m	γ_L^+ mN/m	γ_L^- mN/m
Water	72.8	21.8	25.5	25.5
Glycerol	64	34	3.92	57.3
DMSO	44	41	.064	42.4

The absolute values of γ^+ and γ^- are not known, but GVC have suggested equal values of 25.5 mN/m for water as a first approximation. Little is known on an absolute basis in the GVC theory and the estimated parameters are frequently updated as more studies are done. The parameter estimates in Table 4.2.3 were the best currently available at the time of writing.

The estimated GVC surface tension parameters are plotted in Figure 4.2.14 as a function of the normalized contact angles. As was seen for the Fowkes components, only one parameter, in this case γ_S^-, appears to be responsible for the variation in total surface tension. The other two parameters, γ_S^{LW} and γ_S^+, were approximately the same for all surfaces, and in addition, they quite obviously were highly correlated (note how γ_S^{LW} and γ_S^+ balance

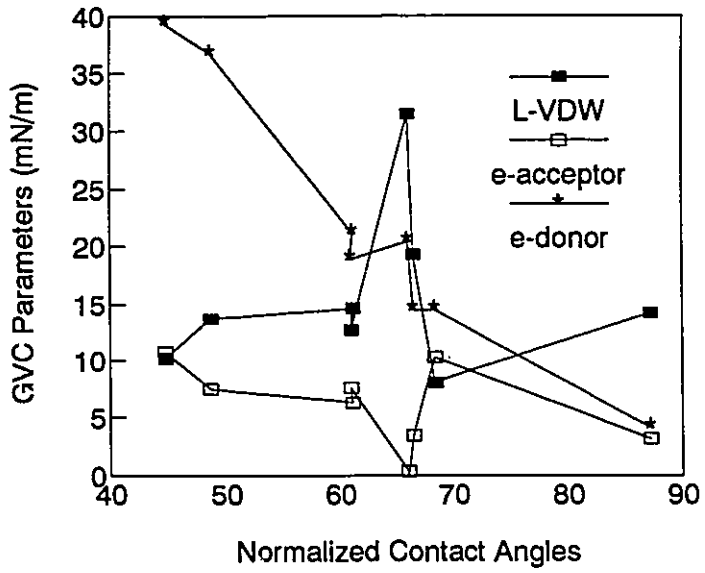

Figure 4.2.14: Magnitude of GVC components as a function of the normalized contact angle. Note how the Lifshitz-van der Waals and electron-acceptor components appear to offset one another. Almost all variation is found in the electron donor (negative) component.

each other out in Figure 4.2.14). This is further evidence that a surface tension may conceivably be characterized by a single independent parameter rather than the two or three required by microscopic theories.

4.2.6.4 Summary of Surface Energetic Theory Evaluations

All three theories (Neumann, Fowkes, Good et al) for the interpretation of contact angles appear to be unable to provide a unique value representing the surface tension of the model materials made for this study. The probable reason for the failure of these theories lies in their fundamental unproven assumptions regarding the interactions at the solid-liquid interface.

For the microscopic theorists, one important yet unproven assumption states that liquid-liquid theory may be extrapolated to liquid-solid interactions. Another assumption requires that teflon have no polar component of surface tension. This affects all the solid surface tension components estimated by Fowkes theory since most of the polar and disperse

components for liquid surface tension are obtained indirectly using contact angle data on teflon. The result is an inductive argument which has not been independently verified by the kind of critical evaluation attempted here.

Some of Neumann's hypotheses appear to be valid including the one which states that it is possible to characterize a solid surface tension uniquely with one contact angle measurement. However, there is no evidence that Neumann's equation of state holds for more than a few hydrophobic surfaces. Even on the low energy surfaces where the equation of state seems to work, there is no proof that the estimate of surface energy obtained is in any way related to the surface tension of the solid being characterized. It may simply be a parameter related to the work of adhesion or the critical surface tension.

All the theories tested were unable to characterize the model surfaces in such a way as to be able to predict their interaction with different liquids. The ability to predict interactions between solids and liquids is the goal of all the theories of surface energetics that were evaluated. A new more appropriate way to characterize surfaces based on contact angles was desired. The "normalized contact angles" described in Section 4.2.1 were adequate for the purpose of the eight model surfaces considered there, but for broader application the relationship between liquid surface tension and contact angle data on solid surfaces required a more general form. The following section (4.2.7) outlines the development of just such an empirical relationship.

4.2.7 A New Model for Interpreting Contact Angle Data

An extended set of model surfaces was created in order to investigate the development of a new mathematical model for the interpretation of contact angle data. In addition to the original eight surfaces, teflon, a new pure silica sample, and six new silanized surfaces were prepared. The preparation method for the new silanized silicas was slightly different from that for the original eight (see section 2.1.3) but the results were similar. For the purpose of contact angle studies, a precise knowledge of surface chemistry was not initially important. The goal was to produce a series of materials with widely varying surface properties to be used in a comparative analysis of contact angles employing different liquids. The advantage of silanized silicas lies mainly in their smoothness and resistance to liquid penetration.

The original eight surfaces were found to have contact angles with different liquids that were very highly correlated with one another. Analyses demonstrated that contact angles can be predicted better and more simply than is possible with currently available theoretical models. A general relationship has not yet been found directly using thermodynamic theory but the data collected in this study provided a basis for the development of a new empirical relationship.

On consideration of all the data, the simplest relationship found was an apparently constant difference between the measured contact angle on a given surface using different liquids. Moreover, the difference in contact angle between two liquids was apparently the same regardless of the solid surface being tested. The same relationship could not be justified for the cosine of the contact angle as well as for the angle itself. Also, the relationship was limited to those surfaces whose contact angle for all liquids was greater than 10°. Precise measurements of smaller angles were not possible. No attempt was made to justify the observed relationship on anything other than statistical grounds.

The average difference between water and glycerol contact angles on a given surface, $\Delta\theta_{wg}$ was 6.84 ± 2.80° for 14 degrees of freedom. Between water and DMSO the average difference, $\Delta\theta_{wd}$, was 34.4 ± 3.87° for 9 degrees of freedom. A standard water contact angle (θ_{w^*}) was defined using data for all three liquids. For a given solid:

$$\theta_{w^*} = [\theta_w + (\theta_g + \Delta\theta_{wg}) + (\theta_d + \Delta\theta_{wd})]/3 \qquad [4.2.21]$$

The standardized contact angles for glycerol (subscript "g") and DMSO (subscript "d") are similarly defined as:

$$\theta_{g^*} = \theta_{w^*} - \Delta\theta_{wg} \qquad [4.2.22]$$

$$\theta_{d^*} = \theta_{w^*} - \Delta\theta_{wd} \qquad [4.2.23]$$

If we use θ_{data} to represent all contact angle data and θ_* to represent all model predictions, then we may compare the two in order to see the quality of fit. Figure 4.2.15 shows the relationship between θ_{data} and θ_*, including the constant 95% confidence interval for all data. The assumption of constant variance appeared to be justified for the surfaces studied. From this relationship it is possible to predict the contact angle for any liquid on a specified solid given $\Delta\theta_{wL}$ and a water contact angle on that solid. The 95% confidence interval for

Figure 4.2.15, of ± 6.4°, gives an indication of the precision that may be expected for smooth surfaces. This error is only slightly larger than that found for replicate experiments using water (± 4.4°). Figure 4.2.15 demonstrates that the macroscopic advancing contact angle can be predicted knowing only the type of liquid (i.e. its $\Delta\theta_{wL}$ value) and the type of solid (i.e. its θ_{w^*} value). No prior knowledge of surface or liquid chemistry is necessary to achieve reasonable precision, nor is any knowledge of the physical properties of the surface such as zeta potential or surface charge necessary. In large measure, the contact angles of a series of liquids on a given solid is a function of the total (as opposed to any other proposed parameters of) liquid surface tension. Lack of fit detected in the model did add to the ± 6.4 confidence interval but discussion of this aspect of the data will be deferred until section 4.2.7.2 where the most dominant correlation is discussed.

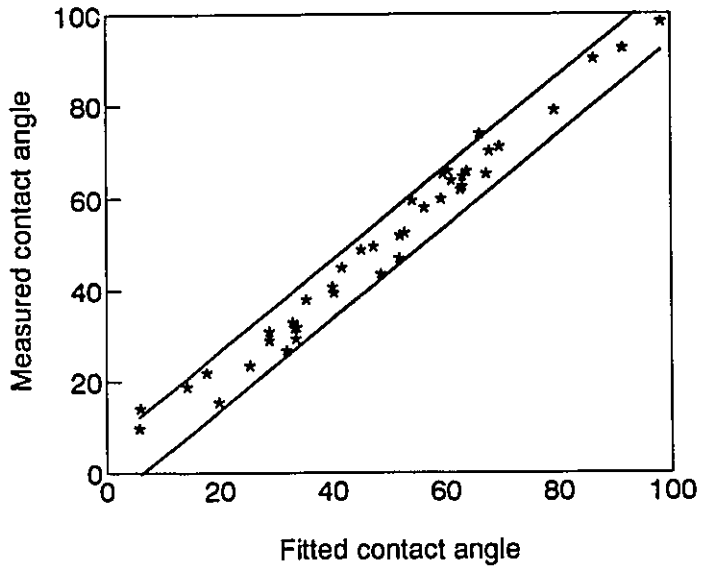

Figure 4.2.15: Measured versus modeled contact angle data for new empirical model. 95% confidence interval is included to show the precision of fit for the extended set of 14 surfaces and three liquids.

One method for analyzing contact angle data is to plot the work of adhesion for glycerol and DMSO versus the work of adhesion for water (see Figure 4.2.5). Using the simple model outlined in equations 4.2.21-23 it was possible to calculate the work of adhesion for various liquids and plot them against the work of adhesion for water (see Figure 4.2.16).

The model predicts that the work of adhesion for glycerol, water, and DMSO converge near a value of 65 mN/m and this compares quite closely with the real data for the same liquids presented earlier in Figure 4.2.5.

The value of $\Delta\theta_{wL}$ for toluene ($\Delta\theta_{wT}$) was estimated to be 70° based on only one data point, i.e. a 28° contact angle on teflon measured in our laboratory. Based on this value of $\Delta\theta_{wL}$ the model predictions for toluene are also depicted in Figure 4.2.16.

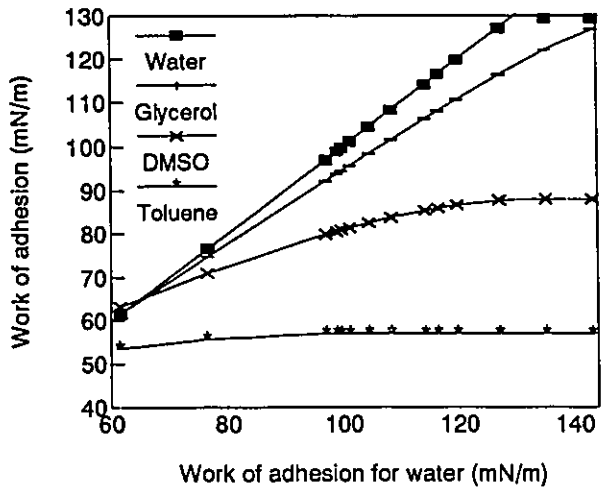

Figure 4.2.16: Modeled relationship (among four liquids) for work of adhesion. See Figure 4.2.5 for a direct comparison with real data. The model fit to data was very close.

$\Delta\theta_{wL}$ for each liquid was plotted against various transformations of the liquid surface tension in order to find some kind of simple relationship which might allow the prediction of $\Delta\theta_{wL}$ for other liquids. The $\Delta\theta_{wL}$ values for water, DMSO, and glycerol produced a straight line when plotted against the inverse of liquid surface tension. When the relationship was extrapolated to γ_{LV} = 484 mN/m, the surface tension of liquid mercury, a contact angle on teflon of 145° was predicted. This compares favorably to the value of 152° reported by Wu (1982).

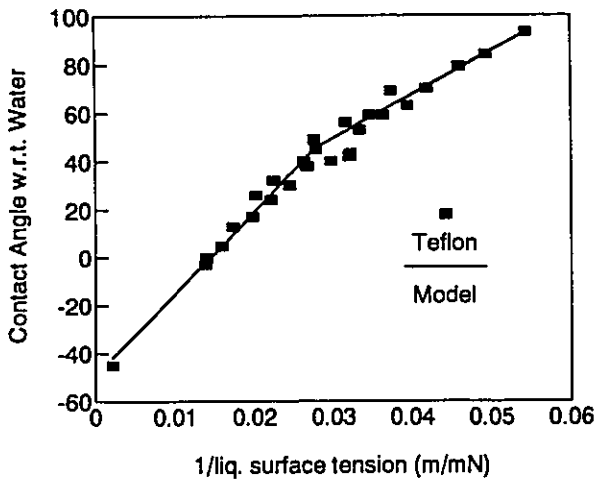

Figure 4.2.17: A two regime model fit to teflon data for estimating the contact angle relative to water ($\Delta\theta_{WL}$) for all liquids. This model may be useful as a first approximation for determining $\Delta\theta_{WL}$ in the absence of better data.

The observation regarding mercury on teflon and the form of the model led to the investigation of teflon as a model surface on which to base a relationship between $\Delta\theta_{wL}$ and γ_{LV}. Wu's data for a wide range of liquids on teflon are given in Figure 4.2.17. The data in Figure 4.2.17 were fit to straight lines over two regimes above and below 36 mN/m. The fitted equations were:

$$\Delta\theta_{wL} = 1800/\gamma_{LV} - 2.90 \qquad \gamma_{LV} < 36mN/m \quad [4.2.24]$$

$$\Delta\theta_{wL} = 3409/\gamma_{LV} - 47.4 \qquad \gamma_{LV} > 36mN/m \quad [4.2.25]$$

The 36 mN/m transition corresponds with the upper limit of validity for many traditional theories for interactions between nonpolar solids and nonpolar liquids (see Figures 4.2.7-9). Equations 4.2.24 and 4.2.25 are based on data not obtained in this laboratory, but predict values of $\Delta\theta_{wg}$ of 6.38 ± 7.5 mN/m and $\Delta\theta_{wd}$ of 30.1 ± 7.5 mN/m (glycerol and DMSO respectively). These 95% confidence intervals contain the experimentally determined values obtained in this study on silanes. Thus, preliminary comparisons between our data and those found in the literature suggest that the value of $\Delta\theta_{wL}$ may be predicted for any liquid given

only its total surface tension γ_{LV} and equations similar to [4.2.24] and [4.2.25]. Further studies will be required using a variety of liquids and solids to determine if Equations 4.2.24 and 4.2.25 can be justified statistically under a wide range of conditions.

For the time being, Equations 4.2.24 and 4.2.25 were used to model the relationship between the work of adhesion and liquid surface tension on individual solids. Figure 4.2.18 shows the model predictions for surfaces similar to pure silica, NH2, C18, and teflon. The trends match very closely those for the real data depicted earlier in Figures 4.2.3 and 4.2.4. Curves for three of the solids appear to converge near a $W_{SL/V}$ value of 70 mN/m, i.e. near the transition surface tension value of 36 mN/m. The separate $W_{SL/V}$ versus γ_{LV} plot for teflon in the same figure follows precisely the two regime behavior seen earlier in Figures 4.2.7-9, for the regimes above and below 36 mN/m.

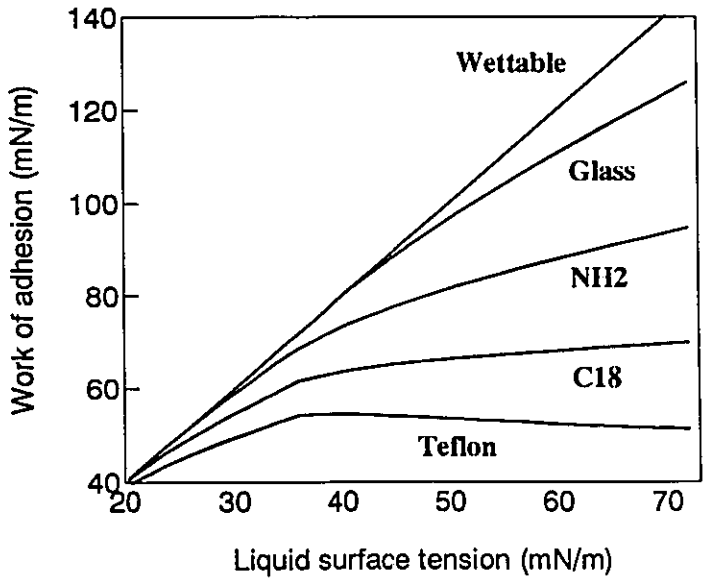

Figure 4.2.18: New empirical model for work of adhesion as a function of liquid surface tension for five imagined surfaces. The wettable surface has 0° water contact angle, as one might expect for glass: 40°, NH2: 70°, C18: 90°, and teflon: 105°.

4.2.7.1 An Empirical Macroscopic Model

The preceding model embodies a simple empirical approach to the interpretation of contact angles. Its ability to fit the data with a precision only slightly less than experimental error suggests that contact angles are due largely to a macroscopic interaction between the work of adhesion and the work of cohesion in a liquid. The method can only be valid for systems of solids and liquids which do not significantly interact by means of swelling and or dissolution. Systems in which these effects occur cannot be compared since the physicochemical properties of the surface are different in each case. These conclusions correspond with the hypotheses of Neumann (Ward and Neumann, 1974) who has proposed the existence of an equation of state linking solid surface tension to a single contact angle measurement. His equation of state is, however, only valid for surfaces which produce a water contact angle greater than 90°. With the empirical model presented here we do not claim to determine solid surface tensions but, using the empirical model, a wide range of surfaces, including wettable ones, can be characterized in a simple, consistent manner.

Microscopic theorists have hypothesized that two or three contact angles need to be measured in order to characterize a surface uniquely in terms of its surface tension components. The results of this study would initially tend to refute this hypothesis, but a further analysis of the residual error of the proposed model suggests that microscopic effects do play a small but significant role. The results of this analysis will be discussed separately in the following section. Despite this acknowledgement of the possible importance of microscopic interactions, the use of surface tension components in the classical sense of Fowkes, is not supported by the model presented here. The accepted values of surface tension components may in fact be "predicted" using the empirical model described herein, both for liquid and solid surfaces. The values of liquid surface tension components currently accepted, greatly overstate the importance of microscopic interactions for contact angles because they are based on the hypothesis that only microscopic interactions are involved.

4.2.7.2 The Influence of Microscopic Surface Chemical Effects on Contact Angles

In section 4.2.7, a new model describing the relationships between contact angles and liquid surface tension on different surfaces was presented. The model is based on the observation that, on average, the contact angles for two given liquids differ by a constant

amount regardless of the solid being tested. This difference was defined for each liquid (L) relative to water (w) by a parameter $\Delta\theta_{wL}$ unique to liquid L. $\Delta\theta_{ww}$ is by definition equal to zero. A series of silanized silica plates were investigated and $\Delta\theta_{wg}$ for glycerol was estimated to be 6.84 ± 2.80° assuming a constant $\Delta\theta_{wg}$ for 14 degrees of freedom. $\Delta\theta_{wd}$ for dimethyl sulfoxide was estimated to be 34.34 ± 3.87° for 9 degrees of freedom.

The hypothesis that $\Delta\theta_{wL}$ is in fact independent of the solid required verification by checking for correlations in the model's residuals for different liquids. A residual was defined to be the difference of the model prediction for contact angle and the corresponding experimentally determined value. Model predictions were considered to be valid only for surfaces with all three contact angles greater than 10°. Contact angle measurement was less precise and subject to additional physical limitations for smaller contact angles (see Section 4.2.2).

Residuals plotted against contact angle data, model predictions and liquid surface tension demonstrated no significant correlation. By these criteria the model had no obvious lack of fit.

More interesting results arose from the comparisons among the data for the individual liquids. No correlation was found between residuals for water and glycerol, or DMSO and glycerol. For water and DMSO, however, a significant linear relationship was found (see Figure 4.2.19). The observed trend suggests that when the contact angle of water is 8° or so, higher than average on a given surface, the complementary DMSO angle is 6° or so lower. The residuals for water and DMSO were pooled (by subtraction due to their inverse relationship) and are ranked in Table 4.2.4. The surfaces fall into a rank order that is highly correlated with their expected surface charge. The negative surfaces, SO3 and Qz, were found at one end of the spectrum, the positive NH2 surfaces were at the opposite end and teflon and C18, both nonpolar surfaces, were intermediate.

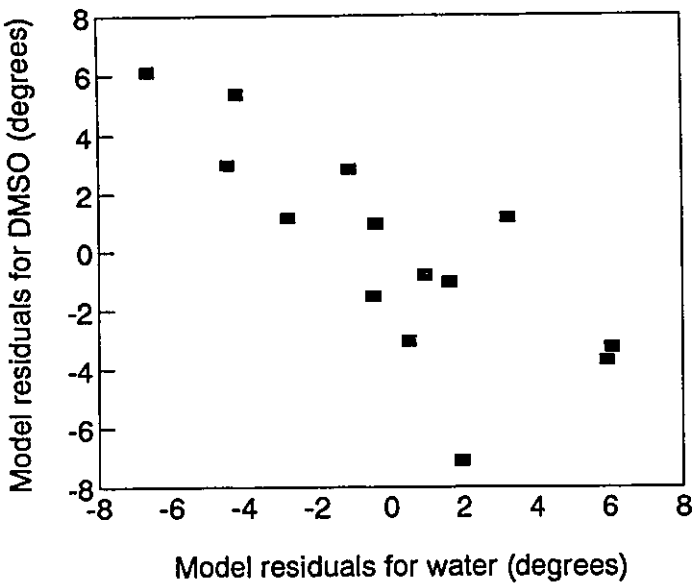

Figure 4.2.19: Relationship between model residuals for water and DMSO. Correlation appears to be due to polar interactions between water, DMSO, and the surfaces.

Table 4.2.4: Ranking of surface charge from negative to positive based on correlation between residuals for water and DMSO

Surface	Abbreviation	Combined water & DMSO lack of fit to standard model lack of fit
sulfonated silane	SO3	9.6
pure silica	Qz	9.3
pure silica	Qzb	9.0
lysine attached to SO3	lys	3.5
Ureido silane	Ur	2.6
Amino silane	NH2	2.0
Teflon	PTFE	1.7
Hexamethyl disilazane	CH3	1.0
Epoxy silane	Ep	-1.4
Octadecyl silane	C18	-4.0
Mercapto silane	SH	-4.0
sulfonate & amino mixture	SO3 > NH2	-7.5
sulfonate & amino mixture	SO3 + NH2	-9.6
Aminosilane	NH2b	-12.8

Water was found to have a lower contact angle, i.e. or greater interaction with negatively charged surfaces, suggesting that its dominant behavior with solid surfaces is as a positive monopole, as defined by van Oss et al, 1987.

DMSO apparently has a greater interaction with positively charged surfaces containing NH2 than with negative surfaces. This would suggest that DMSO has a dominantly negative monopole interaction with surfaces. DMSO does have a S=O dipole, but the partially positive-charged sulfur atom may be shielded due to the proximity of the two methyl groups. This would leave the negatively charged oxygen as the dominant mode for interaction with surfaces. The negative character of DMSO hypothesized here agrees with the proposal of Good, Van Oss, and Chaudhury who described DMSO as a negatively monopolar liquid in the development of their acid-base interfacial tension model (van Oss, et al, 1987).

4.2.7.3 An Extended Contact Angle Data Base for Model Testing

In order to test the hypothesis that microscopic interactions, in addition to macroscopic interactions, do in fact influence the contact angle, an extended survey of contact angles was undertaken. The survey was designed to include silanized surfaces, polymers, ceramics, and metals. The precise chemical composition of the surfaces was not known and only moderate care was taken to ensure cleanliness of the surfaces. Samples were cleaned with a nondamaging solvent (usually water, soap solution (Liquinox), and/or acetone) and dried briefly in a 60°C oven. The presence of oxide layers, adsorbed organics, and other possible contaminants were accepted as inevitable and no extraordinary precautions were taken to eliminate them. These surfaces were occasionally less smooth than the silanized silica substrates and this too was expected to be an additional source of error. The most troubling potential source of error was the possibility of interaction between liquid and solid. For example, it was not known *a priori* if the polymeric materials would resist swelling or dissolution by the various solvents and thus change their properties over time. Surface dissolution or liquid interaction with organic and oxide layers were also potential sources of error for the individual measured contact angles.

The liquids employed for the extended contact angle survey included aniline (γ_w = 42.9 mN/m), ethylene glycol (γ_{LA} = 47.5 mN/m), dimethyl sulfoxide, glycerol, and water. Of the twenty surfaces tested, only 14 had contact angles large enough for all liquids to be

useful in the determination of $\Delta\theta_{wL}$, the average contact angle relative to water. A list of the $\Delta\theta_{wL}$ values found for each liquid along with the associated 95% confidence interval (13 degrees of freedom) is given in Table 4.2.5.

Table 4.2.5: $\Delta\theta_{wL}$ values determined experimentally with 95% confidence intervals for 13 degrees of freedom

water	$\Delta\theta_{ww} = 0$ by definition
glycerol	$\Delta\theta_{wg} = 10.16 \pm 3.36$
DMSO	$\Delta\theta_{wd} = 37.81 \pm 5.00$
ethylene glycol	$\Delta\theta_{we} = 24.04 \pm 4.73$
aniline	$\Delta\theta_{wa} = 42.63 \pm 5.41$

A pooled average water contact angle θ_{w^*} was determined for each solid using the following equation:

$$\theta_{w^*} = \frac{\sum^{Nliquids} (\theta_{L/S/V} + \Delta\theta_{wL})}{N}, \qquad N = 5 \quad [4.2.26]$$

The corresponding model values for other liquids θ_{L^*}, were determined using equation 4.2.27 for each solid/liquid pair.

$$\theta_{L^*} = \theta_{w^*} - \Delta\theta_{wL} \qquad L = G, D, E, A \quad [4.2.27]$$

The resulting correlation between θ_{L^*} and $\theta_{L/S/V}$ is shown in Figure 4.2.20. The variance was found to be constant over the range of contact angles measured. As expected, the estimated 95% confidence interval for the extended survey data was ± 11° greater than (approximately twice) that for the smooth, stable silanized surfaces. Such a large error could be explained in part by the additional effects of surface roughness and liquid-solid interactions in the expanded set of test materials. For comparison, the average error for each set of ten measurements used to obtain a single water contact angle was about ± 4° on clean, smooth silanized silica.

The residual errors for each liquid were compared in the same way as before for the silanized surfaces. As was found on the silanes, the only liquid-liquid pair to have a significant residual correlation was DMSO-water. The water residuals were related inversely

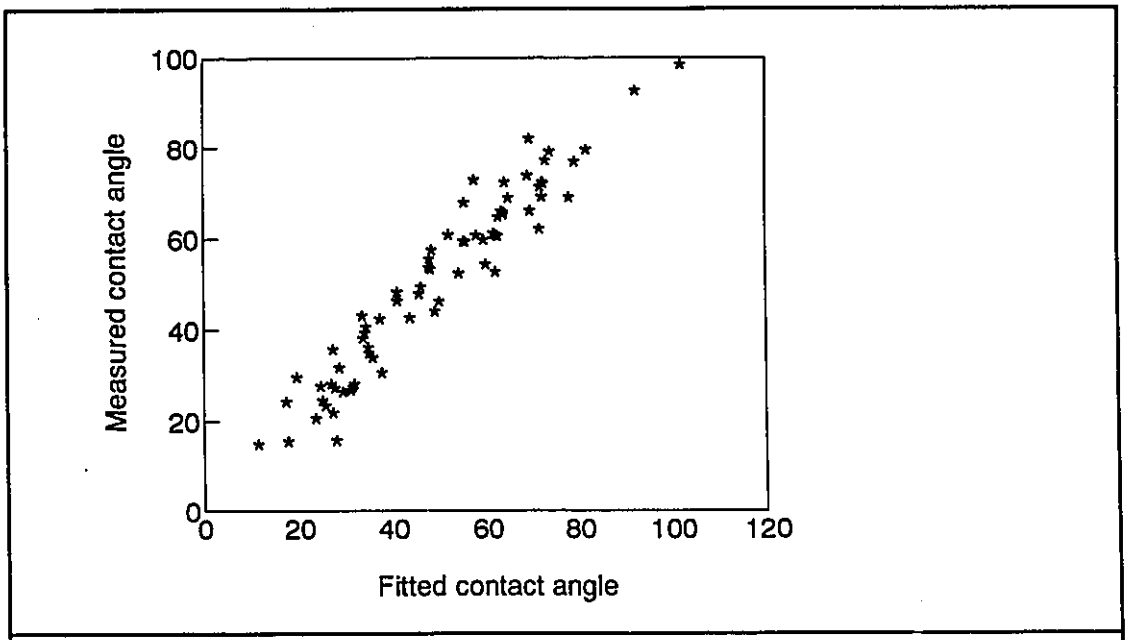

Figure 4.2.20: Measured versus modeled contact angle data for an extended study of surfaces and liquids. The solids included silanes, polymers, metals, and ceramics. The two additional liquids were aniline and ethylene glycol. The residuals are significantly more scattered than for the data in Figure 4.2.15 due mainly to the increased roughness and heterogeneity of the samples.

to the DMSO residuals as for the correlation of the silanized surfaces. The surfaces were ranked in order of the difference between water and DMSO residuals as shown in Table 4.2.6.

Extrapolating the observations drawn from Table 4.2.4 to Table 4.2.6, it is apparent that in both sets of data the trends, with respect to surface chemistry, are identical despite the variety of materials tested.

A brief description of the surfaces listed in Table 4.2.6 is now given to accompany discussion of their ranking. PZT, Al2O3, and YSZ are ceramic materials with relatively smooth surfaces. PZT is a solid solution of lead zirconate and lead titanate (52% $PbZrO_3$, 48% $PbTiO_3$ and 0.1% Nb_2O_5) with piezoelectric properties. Al2O3 is a typical structural aluminate ceramic. YSZ is an yttrium stabilized zirconia consisting of about 8 mol% Y_2O_3 in ZrO_2 and is typically used as a structural material. While all the ceramics have oxygen present in large quantities near the surface, they are not as likely to have surface hydroxyl groups as pure silica. The surfaces are more hydrophobic than silica as a result. The high

Table 4.2.6: A ranking of surfaces with respect to their relative affinity for water from hydrophilic to "DMSO-philic"

Material	Combined water & DMSO lack of fit to standard model
PZT	18.7
Al2O3	7.9
YSZ	7.3
Cu	6.5
PTFE	5.2
Al	4.5
PE	0.9
Act	-2.7
SO3 > NH2	-4.9
Fipetri	-4.7
SO3 + NH2	-6.1
Fapetri	-7.4
NH2 st	-9.3

oxygen content in the ceramics may give them the negative character that is apparent in the residual ranking in Table 4.2.6. Al2O3 and YSZ are less electronegative than SO3, Qz, and Qzb in Table 4.2.4. PZT, the piezoelectric ceramic, is the material most strongly associated with a negative character of all those tested. The individual ranking of PZT is less important, however, than is the overall observed relationship between residuals and surface chemistry for all the tested surfaces.

The metals copper (Cu) and aluminum (Al) do not appear to have significant surface polarity based on available data.

Some of the polymeric materials employed, PTFE, PE, Act, Fipetri, and Fapetri, have lower DMSO contact angles than predicted by the simple empirical model. This may have been due to solvent interactions such as swelling or dissolution in addition to electrostatic effects. However, no surface was visibly altered by contact with the test solvents used in this study. Toluene did affect some test materials. The Fapetri surface, which showed the highest relative affinity for DMSO, is a plastic "Tissue Culture" petri dish manufactured by Falcon (catalogue no. 3003). The material is a polystyrene with a surface treatment to enhance cell adhesion and growth. Fipetri is a standard polystyrene petri dish from Fischer. PE is a sample of high density polyethylene and Act is a clear cellulose acetate overhead

projector transparency. Except for the tissue culture dish, all polymers were ranked in the midrange of Table 4.2.6. The tissue culture dish appeared to interact more strongly with DMSO than the other polymers.

4.2.7.4 Summary of Macroscopic and Microscopic Effects on Contact Angles

The contact angles measured by different liquids on the same solid surface are highly correlated. Experimental data supports the hypothesis that for surfaces which are not fully wetted, the difference between contact angles for liquid pairs is the same on all surfaces. The difference between contact angles for water and other individual liquids is highly correlated with their total surface tension. This relationship suggests that the measured macroscopic contact angle is largely a function of the total liquid surface tension and not necessarily a function of liquid or solid surface chemistry. Using a simple empirical model based on these observations, it was shown that each surface and liquid may be characterized by a single parameter to define contact angle phenomena associated with them. A solid surface may be characterized by its standardized water contact angle θ_{w}. based on data for a variety of liquid drops. A liquid may be associated with its contact angle relative to water, $\Delta\theta_{wL}$. High quality experimental data requires smooth surfaces that are not altered by the different liquids with which it comes into contact.

Microscopic chemical effects appear to have a significant effect on the measured contact angle. These effects were detected in the residual error between model and experimental contact angles for each solid-liquid pair. None of these residuals was correlated with the measured or modeled angles. There was, however, some correlation between the residuals for different liquids, especially water and dimethyl sulfoxide. The correlation was consistent with trends in the chemical composition of the test surfaces. DMSO showed a higher affinity for positively charged surfaces while water spread more on negatively charged ones. These conclusions are based solely on an *a priori* knowledge of the chemical composition of the surfaces and were not confirmed by an independent investigation of surface charge or polarity.

Contact angles on stable surfaces should continue to be investigated over a wider range of solids and liquids in order to verify the observations made in this study. If the hypothesized

relationships hold up, then a database of parameters for standard materials may be established to allow the characterization of adhesion properties and polarity by the measurement of as few as two contact angles.

For the purposes of surface characterization as required by the present work, no parameter was found to be any better than the raw data for advancing water contact angles. This is the parameter most often used in section 4.4 when so-called "surface energetic" data is compared with surface chemistry, protein adsorption and blood coagulation.

4.3 Protein Adsorption

4.3.1 Simulation of Protein Adsorption

4.3.1.1 Numerical Simulation Algorithm

In section 1.1.5 the problems associated with modeling protein adsorption using steady-state or equilibrium isotherms was addressed. It was concluded that for all practical purposes, protein adsorption is kinetically limited. Not only are kinetic models more complicated than isotherms but the transport processes which bring the molecules to the adsorbing surface must be taken into account. The following section describes the algorithm developed to allow the study of proposed mechanistic, mathematical models on the kinetics of adsorption in the experimental geometry (cylindrical) described in section 2.4.2 (Wojciechowski and Brash, 1990). The same algorithm was also adapted to study adsorption in different geometries (Cornelius et al, 1991) and to fit kinetic rate parameters to experimental data (section 4.3.2).

The continuity equation (Bird et al, 1960) for a single dilute component in a nonflowing system in cylindrical geometry is given by,

$$\frac{\partial C(r,t)}{\partial t} = \frac{D}{r}\frac{\partial}{\partial r} r \frac{\partial C(r,t)}{\partial r} \qquad [4.3.1]$$

where C is the concentration of the dilute component (protein);

t is the time since adsorption began;

r is radial position relative to the central axis; and

D is the diffusivity of a dilute component in a continuous medium (assumed to be constant for the purposes of this study but not a requirement of the method).

The three boundary conditions that must be specified before equation 4.3.1 may be solved are defined below.

1) The concentration profile across the tube and the adsorbed amount on the wall must be known at t=0 (initial condition).

$$C(r,0) = C_0(r) \qquad [4.3.2]$$

2) The concentration profile is assumed to be symmetrical about the center of the tube at all times.

$$\frac{dC(0,t)}{dr} = 0 \qquad [4.3.3]$$

3) The concentration gradient at the tubing wall may be related to the rate of adsorption using differential equations based on a proposed mechanistic model.

$$\frac{dC(R,t)}{dr} = \text{adsorption model} \qquad [4.3.4]$$

where R is the overall inner diameter of the tube.

A simple example of an "adsorption model" for equation 4.3.4 could be a first order irreversible adsorption :

$$\frac{d\Gamma}{dt} = k_{ads}C(R,t) \qquad [4.3.5]$$

where Γ is the surface concentration of adsorbed protein and

k_{ads} is the rate constant for adsorption.

More complex models may consist of several ordinary differential equations (o.d.e.'s) incorporating the possibility of multiple adsorbed states, reversibility, surface transitions, time-dependent parameters, and explicit expressions defining other constraints on the adsorption process. A brief review of frequently hypothesized mechanisms of protein adsorption is presented later in this report.

Analytical solutions for equation 4.3.1 are possible for simple cases including the well known diffusion limited case involving rapid, irreversible adsorption onto a sparsely covered, flat surface from a semi-infinite medium with an initial concentration of C_{bulk} (Andrade, 1985b; MacRitchie, 1978).

$$\Gamma = 2\left(\frac{Dt}{\pi}\right)^{1/2} C_{bulk} \qquad [4.3.6]$$

Protein adsorption models encompassing high surface coverage do not lend themselves to many simplifications and require a more fundamental approach beginning with equation 4.3.1. In order to obtain the solution for equation 4.3.1 given a complex protein adsorption model at the wall, it is necessary to employ numerical methods. The partial differential equation (p.d.e.) described by [4.3.1] can be converted into a system of ordinary differential equations (o.d.e.'s). First, [4.3.1] may be expanded to the form:

$$\frac{\partial C(r,t)}{\partial t} = D\left(\frac{\partial^2 C(r,t)}{\partial r^2} + \frac{1}{r}\frac{\partial C(r,t)}{\partial r}\right) \qquad [4.3.7]$$

and subsequently expressed in the form of a forward first order difference equation at specific radial positions, r_i where i is an index defining the position relative to the center of the tube (i=0).

$$\frac{dC_i}{dt} = D\left(\frac{2}{h_i + h_{i+1}}\left(\frac{C_{i+1} - C_i}{h_{i+1}} - \frac{C_i - C_{i-1}}{h_i}\right) + \frac{1}{r_i}\left(\frac{C_{i+1} - C_{i-1}}{h_{i+1} + h_i}\right)\right) \qquad [4.3.8]$$

By choosing a first order method one has the option to solve the system for non-equispaced intervals, h_i, which is in this case the most computationally efficient choice. If the intervals, h_i, were the same size equation 4.3.8 would approach the accuracy of a typical second order method. The determination of values for h_i depends on the nature of the system and for this reason is explained more fully later in this section. An algorithm employing an equation similar to 4.3.8 was employed by Sincovec and Madsen (1975) but most modern undergraduate texts concerning numerical methods outline similar approaches (Gerald and Wheatley, 1989).

The technique of solving a partial differential equation as a system of o.d.e.'s is known as the "method of lines" (Byrne and Hindmarsh, 1987), because the conditions on a two dimensional surface are solved by simultaneously solving the conditions on a series of lines parallel to one variable axis. The advantage of the method of lines is that the system of p.d.e.'s may be solved by any of a number of readily available o.d.e. solvers.

Equation 4.3.8 may be solved for i ranging from 0 to the number of radial intervals, N, given the three boundary conditions defined earlier. The initial protein concentration profile (equation 4.3.2) across the tube must be defined. For example, a uniform profile across the tube is specified by:

$$C_i = C_{bulk} \qquad for\, i = 0,N \qquad [4.3.9]$$

The symmetry boundary condition (equation 4.3.3) requires that the first derivative of concentration with respect to radial position be zero at the center of the tube. Thus a special case for equation 4.3.8 must be specified at this location (i=0):

$$\frac{dC_0}{dt} = D\frac{1}{h_1}\left(\frac{2C_1 - 2C_0}{h_1}\right) \qquad [4.3.10]$$

The final boundary condition describes the adsorption of protein from the solution immediately adjacent to the wall (equation 4.3.4). In order to accomplish this in the framework of equation 4.3.8 the rate of adsorption must be converted to an equivalent rate of diffusion across an imaginary boundary layer immediately behind the wall using Fick's rate law:

$$D\left(C_N - \frac{C_{imaginary}}{h_N}\right) = f(C_N, k_i, \Gamma_j) \qquad [4.3.11]$$

The left hand side of equation 4.3.11 is the diffusion rate across a layer of thickness h_N to a point behind the wall where the unknown imaginary concentration is $C_{imaginary}$. The right hand side of the equation is the actual rate of adsorption based on a user supplied function of the concentration at the wall C_N, the adsorption model parameters k_i, and the surface coverage of protein in j possible states, Γ_j. Equation 4.3.11 may be rearranged to solve for the imaginary concentration $C_{imaginary}$.

$$C_{imaginary} = C_N - \frac{h_N}{D} f(C_N, k_i, \Gamma_j) \qquad [4.3.12]$$

Equation 4.3.12 may be used in to complete the description of the left hand side of equation 4.3.11 which is in turn used to complete the definition of equation [4.3.8] for the condition i=N, (i.e. at the adsorbing wall).

At this point the simulation has N+1 o.d.e.'s and an explicit expression describing $C_{imaginary}$. A further j o.d.e.'s are required to describe the kinetic behavior of the j surface states of bound protein. Equation 4.3.5 is one of the simplest possibilities but much more complex models may also be employed. It is important to ensure that the mass units for Γ and C_i are compatible, otherwise a conversion factor must be incorporated.

To solve this simultaneous set of N+j+1 o.d.e.'s a software package capable of handling stiff sets of differential equations must be used. Due to the nature of the process, concentrations at the wall are changing at rates orders of magnitude higher than those in the middle of tube. This makes the problem "stiff" because accurate solutions will require the o.d.e. solver to take very small time steps for some o.d.e.'s (especially for points near the wall), while others could be more efficiently solved using much larger ones. The adaptive step-size algorithm available in stiff o.d.e. software is able to solve stiff systems much more quickly and efficiently than traditional methods (Byrne and Hindmarsh, 1987).

A computer simulation was written to describe the experimental system typically employed in this laboratory (Brash and ten Hove, 1984) The procedure involves the adsorption of ^{125}I labeled protein from a nonflowing solution to the walls of tubing of known surface composition. The adsorption data collected using this protocol are quantitative, reproducible and protein conformation independent; however, the effects of rinsing, flow during injection, and labeling on measured adsorption are difficult to determine and potentially important. The qualitative trends observed in the data are useful and revealing but the quantitative requirements of modeling demand increasingly the careful attention to the effects of the experimental protocol on the measured adsorption that is provided by the simulation.

The simulation of the system described above was based on equation 4.3.1 for the radial diffusion of a single component in a nonflowing cylindrical geometry.

The first boundary condition for equation 4.3.1 was satisfied by defining the concentration profile of protein across the tube and setting the adsorbed amount equal to zero at zero time. The initial profile was not necessarily assumed to be uniform. The displacement of an equilibrating buffer by a protein solution in laminar flow may result in the development of a significant concentration boundary layer (or zone of protein depletion) near the tubing wall (Bird et al, 1960). Rapid adsorption during injection may also result in a similar effect. The presence of a depleted layer can cause a slower than expected initial rate of adsorption as well as an axial dependence of total adsorption. The initial concentration profile adopted in this simulation incorporates a linear gradient ranging from zero at the wall to the bulk concentration across a boundary layer whose thickness is specified by the user.

The simulation is written in FORTRAN 77 using the Microsoft FORTRAN version 4.1 compiler. The stiff o.d.e solver used is the Livermore Solver for Ordinary Differential Equations (LSODE) (Hindmarsh, 1983). The user may choose stiff or nonstiff routines by specifying a "method flag". In the present work, nonstiff methods were unable to converge to an accurate solution given a typical adsorption system. Stiff methods were found to converge to a solution under most conditions. However, the accuracy faltered as the specified boundary layer thickness became smaller. The same problem, resulting from a discontinuity at the wall, has been reported by others attempting similar simulations using a uniformly spaced grid (Schaaf and Dejardin, 1987; Aizenbud et al, 1985). In a sense the system is "stiff" in the radial dimension as well as in time. The most rapid changes occur in a small region close to the wall. It is therefore necessary to compress the grid to have narrow divisions near the wall while providing more widely spaced points near the center of the system where concentration changes are less dramatic. Thus the r_i and h_i values for Equation 4.3.8 were defined by:

$$r_i = r_N\left(1 - 10^{-MC\left(\frac{i}{N}\right)} + 10^{-MC}\right) \qquad for\, i = 0, N \quad [4.3.13]$$

and

$$h_i = r_i - r_{i-1} \qquad [4.3.14]$$

MC is a "mesh compression" factor specified by the user. A larger value of MC causes more grid compression near the wall at the expense of reducing the number of points near the center of the tube. To balance an increase in MC a larger number of radial points, N, may be specified.

Table 4.3.1: A listing of inputs required to run the protein adsorption simulation including example values.

Variable	Description	Typical Value
B	boundary layer thickness	0.0 cm
RADIUS	radius of the tube	0.15 cm
MESHCOMP	mesh compression near the wall	1.8
D	diffusion coefficient	$2x10^{-7}$ cm^2/s (fibrinogen)
N	number of positions at which the concentration of protein is estimated	20
MODEQ	number of differential equations in the adsorption model	1
J	number of rate parameters in adsorption model	2
THET(J)	an array of parameters for the adsorption model	an array of J parameters
MAXADS	maximum adsorption to be displayed on the graph	1.0 $\mu g/cm^2$
TOUT	final time	50 min.
CIN	initial concentration of protein	.003 mg/mL
MONITOR	1=linear variable, 2=sqrt variable	2
VARYWHAT	the quantity to be varied 1=CIN, 2=B, 3=D, 4=TOUT, 4+I=THET(I)	4
NVARY	number of conditions at which to evaluate the variable	21
VARYMIN	minimum value of the varied quantity.	0 minutes
VARYMAX	maximum value of the varied quantity	60 minutes

The output of the simulation is presented graphically using FORTRAN callable subroutines. Two graphs are plotted side by side. One is adsorption versus either time or concentration (chosen by the user) depicted by a single curve. The second graph depicts

the concentration profile across the tube for each time or concentration at which the system is evaluated. The concentration profiles are instructive in depicting the interplay between diffusion and reaction limitations near the adsorbing surface.

To obtain the desired output, the user must specify a number of input conditions (see Table 4.3.1). Since considerable variation in adsorption may occur at short times and low concentrations the user may also evaluate the adsorption at nonequispaced intervals for the independent variables, in order to obtain smoother curves (see the "MONITOR" specification in Table 4.3.1).

The simulation, like protein adsorption itself, is "history dependent". Kinetic data may be obtained quite rapidly as the o.d.e. solver steps forward in time. However, adsorption versus concentration data are simulated much more slowly since the o.d.e.'s must be reset to their zero time conditions for each new concentration.

4.3.1.2 Applications of the Simulation to the Testing of Hypothesized Mechanisms

In order to use the simulation to mimic protein adsorption experiments, a mathematical model for the adsorption process must be proposed. Equation 4.3.5 is a simple example of an irreversible adsorption in its early stages. A model valid for monolayer adsorption must also include a surface coverage limit. If we assume molecules adsorbing to a limit of Γ_{max} then equation 4.3.5 for adsorption at the wall may be modified:

$$\frac{d\Gamma}{dt} = k_1 C_N \left(1 - \frac{\Gamma}{\Gamma_{max}} \right) \qquad [4.3.15]$$

Equation 4.3.15 is analogous to the "Langmuir excluded surface effect" employed by Dejardin to limit surface coverage to a monolayer in his analytical solution for a well-stirred particle system (Dejardin, 1989). Despite being valid for a complete monolayer, equation 4.3.15 is still most useful for the investigation of the effect of k_1, the rate constant, on the initial stages of adsorption. Figure 4.3.1 depicts the adsorption kinetics predicted by the simulation when the process is entirely diffusion limited for a protein with a diffusion coefficient of 2×10^{-7} cm^2/s (Andrade and Hlady, 1988) at an initial concentration of 0.005

mg/mL and a relatively fast surface binding rate, k_1, of 0.1 cm/s. Γ_{max} was chosen to be large enough (1.0 $\mu g/cm^2$) that it did not limit the rate of adsorption for the conditions in Figure 4.3.1. The curve exactly fits the model for diffusion limited adsorption given by equation 4.3.6.

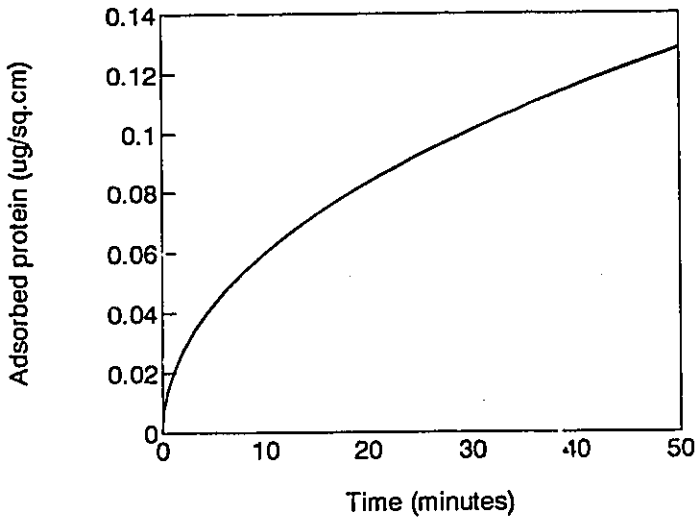

Figure 4.3.1: A simulation of irreversible fibrinogen adsorption kinetics in tubing governed solely by diffusion limitations for the conditions specified in Table 4.3.1. k_1 (see equation 4.3.12) for this system has been set to the relatively high value of 0.1 cm/s to ensure that it does not limit the overall adsorption process.

While Figure 4.3.1 may be expected to predict the behavior of fibrinogen which has a known diffusion coefficient of $2x10^{-7}$ cm^2/s, experience has shown that experimental adsorption levels are frequently lower than expected (Young et al, 1988a,b; Wojciechowski et al, 1986; Van Dulm and Norde, 1983). Data indicate that the actual rate of diffusion is "depressed" to an extent which appears to be surface dependent. It remains a challenge to determine which surface properties may be responsible for this effect that one would not normally attribute solely to surface properties. Rather it would be expected that important surface characteristics would manifest themselves in the rate parameters describing the binding kinetics between the protein and the solid surface. There are also several possible explanations for the observed depression of D, based on systematic effects. The simulation is used here to investigate the effect of several hypothesized influences on adsorption kinetics.

If k_1 (the first order rate constant for adsorption) is decreased it is possible to see how it can become a limitation. For k_1 greater than 0.1 cm/s as is the case in Figure 4.3.1, there is no additional adsorption of protein because the system is completely diffusion limited. The reason for this limitation is more apparent in the concentration profiles as shown in Figure 4.3.2. The profiles in this figure occur after 50 minutes in a 0.30 cm ID tube for conditions similar to those in Figure 4.3.1 except that different values of the surface binding rate were used in the simulation. At high values of k_1 the local concentration of protein at the wall is essentially zero since the protein is adsorbed as rapidly as it arrives. Even at a rate of 0.0001 cm/s (cf. the relatively fast 0.1 cm/s used in Figure 4.3.1) the adsorption process is virtually diffusion limited. But as k_1 decreases to 0.000004 cm/s, the rate of surface binding limits the adsorption enough to allow an accumulation of protein near the wall. A low value of k_1 could be a manifestation of the potential energy barrier to adsorption proposed by Norde (Van Dulm and Norde, 1983; Norde, 1986). If the rate of binding is precisely zero, the profile remains flat since the protein is not being taken from the solution layer adjacent to the wall. For a protein concentration at the wall significantly greater than zero, the adsorption process is at least partially rate limited. Diffusion limitations also contribute as long as there is a significant concentration gradient near the wall. Thus, there is a range of conditions over which both rate of binding and rate of diffusion control adsorption kinetics. A simplification of this coupled process can often lead to an erroneous prediction of the kinetics.

Figure 4.3.3 illustrates the coupled effect of diffusion and binding rates on the kinetics of adsorption. A completely diffusion limited case (k_1 = 0.1 cm/s) results in a linear plot of adsorption versus square root time with an intercept at the origin, assuming surface coverage or solution depletion do not come into play. As the binding rate is reduced, a "lag time" between the beginning of adsorption and the approach to a diffusion limited slope becomes evident. The reason for this lag time is a slower development of the protein depleted layer near the wall. At high binding rates the time needed to bring the concentration at the wall to zero is brief in comparison to the time over which adsorption occurs. At a k_1 of 0.00003 cm/s, about 10 min is required for diffusion limitations to completely dominate (slope becomes constant) and at 0.0001 cm/s the lag time is about one minute.

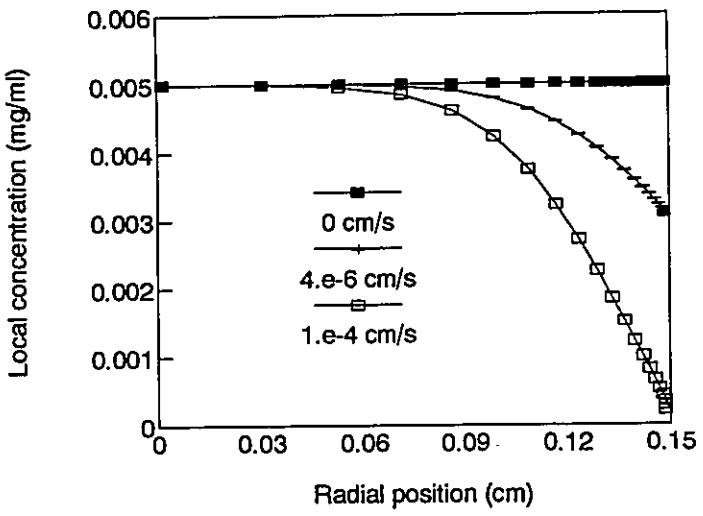

Figure 4.3.2: The effect of irreversible surface binding rate constant on the diffusion limited protein concentration profile. The system is the same as that depicted in Figure 4.3.1 except that a "snapshot" of the concentration profile is shown at 50 min for different values of the surface binding rate, k_1, identified in the legend. Only when k_1 becomes less than .0001 cm/s is the concentration at the wall significantly increased and thus the rate of uptake reduced.

The development of a concentration boundary layer caused by rapid adsorption during injection could also lower the apparent diffusion coefficient significantly. It is also possible that surface roughness could enhance the development of a boundary layer, but even smooth surfaces like glass appear to demonstrate an apparent depression of the diffusion coefficient (Wojciechowski et al, 1986). Figure 4.3.4 depicts the irreversible adsorption of protein at low surface coverage onto a rapidly binding (k_1 =0.1 cm/s) surface for three different concentration boundary layer thicknesses. The presence of a boundary layer decreases the diffusion limited rate in a manner very similar to the effect of low surface binding rates shown in Figure 4.3.3. Given kinetic adsorption data for one surface it may be difficult to determine which mechanism (if either) is responsible for the observed effects. Data for a number of surfaces and proteins may be required to show if the effect is systematic or surface-dependent.

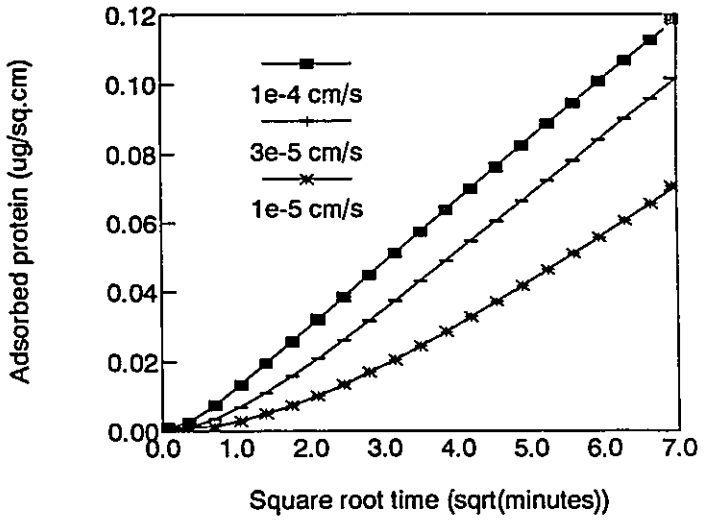

Figure 4.3.3: The effect of irreversible binding rate on the kinetics of adsorption. The simulated data are plotted versus the square root of time for various surface binding rates, k_1 (see the legend), in order to illustrate the deviation from diffusion limited behavior (see equation 4.3.6). The system is the same as those employed in previous figures, i.e. involving fibrinogen adsorption from a 0.003mg/mL solution onto a sparsely covered surface. The data for a surface binding rate of 0.0001 cm/s deviate only slightly from purely diffusion limited kinetics.

One aspect of the protein adsorption mechanism which is a continuing source of speculation and controversy is the question of "reversibility". Some observers have detected two types of protein on the surface: one reversibly and the other irreversibly bound (Chan and Brash, 1981; Beissinger and Leonard, 1981 and 1982). It is generally accepted that at short residence times adsorbed protein is bound more loosely (and presumably more reversibly) than protein that has resided on the surface for some time (Slack and Horbett, 1989; Soderquist and Walton, 1980). It has been hypothesized that when protein first adsorbs, it does so by only one reversibly bound segment (MacRitchie, 1978). Equation 4.3.15 can be modified to allow for desorption with rate constant, k_{-1}.

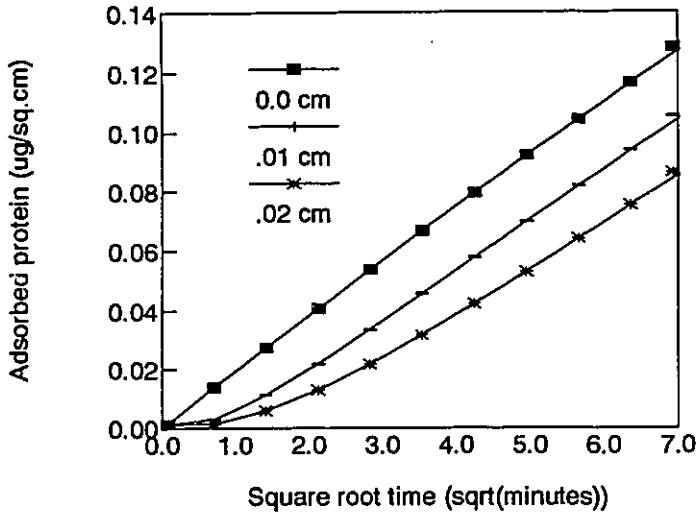

Figure 4.3.4: The effect of a zone of protein depletion near the tube wall before adsorption begins. This simulation is for irreversible fibrinogen adsorption (k_1 =0.1 cm/s) onto a sparsely covered surface from a 0.003 mg/mL solution for different initial concentration boundary layer thicknesses (identified in the legend). This kinetic behavior can be confused with the effect of slow surface binding shown in Figure 4.3.3.

$$\frac{d\Gamma}{dt} = k_1 C_N \left(1 - \frac{\Gamma}{\Gamma_{max}}\right) - k_{-1}\Gamma \qquad [4.3.16]$$

If this adsorption model is incorporated into the simulation, it is possible to show that diffusion limited adsorption can occur more slowly and in a way quite different from that for the purely irreversible case. Figure 4.3.5 shows simulated adsorption from a 0.1 mg/mL protein solution onto a surface with a binding rate of 0.01 cm/s for two different rates of desorption, k_{-1}. In both cases the initial stages of adsorption are purely diffusion limited, but as the adsorption progresses in the reversible case, a dynamic equilibrium is established which maintains a stable interfacial concentration. This has the effect of reducing the concentration gradient, and correspondingly the rate of adsorption, by a factor proportional to the concentration at the wall.

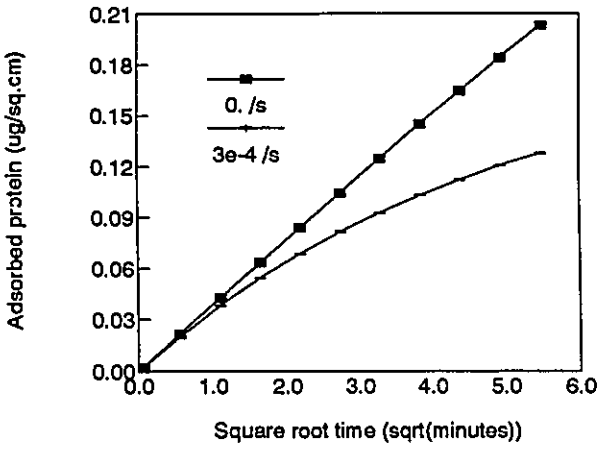

Figure 4.3.5: The effect of reversibility on the kinetics of adsorption. This simulation was run for fibrinogen adsorption onto a sparsely covered surface from a 0.006 mg/mL solution and k_1 of 0.01 cm/s. Two values for the rate constant for desorption, k_{-1} are shown in the legend. The limiting effect of a reversible mechanism on overall adsorption contrasts with the irreversible rate limitations depicted in Figure 4.3.3.

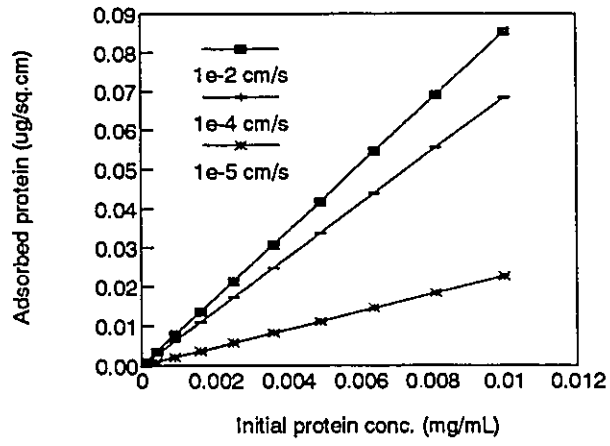

Figure 4.3.6: The effect of irreversible binding rates on simulated fibrinogen adsorption after five minutes. If data are collected in this "isotherm" fashion one may be falsely led to believe that the slope is a direct indication of diffusion limitations alone. k_1 (indicated in the legend) is able in this case to "depress" the apparent diffusion coefficient.

Whether the adsorption is limited by reversible or irreversible rate effects, the deviation from purely diffusion limited kinetics can be distinguished using appropriate experimental data versus time. If, on the other hand, data are collected as a function of concentration for a fixed time (often called "isotherms), it is impossible to determine the source of rate limitations based on the initial slope. Five minute "isotherms" are shown for adsorption simulations limited by irreversible (Figure 4.3.6) and reversible (Figure 4.3.7) effects. In either case the behavior is linear and the initial slope is "depressed" (relative to that expected for diffusion limitation) to an extent determined by the limiting rate parameter. Clearly, there is considerable potential for error if initial slopes of this type are used to determine the diffusion coefficient of an adsorbing protein.

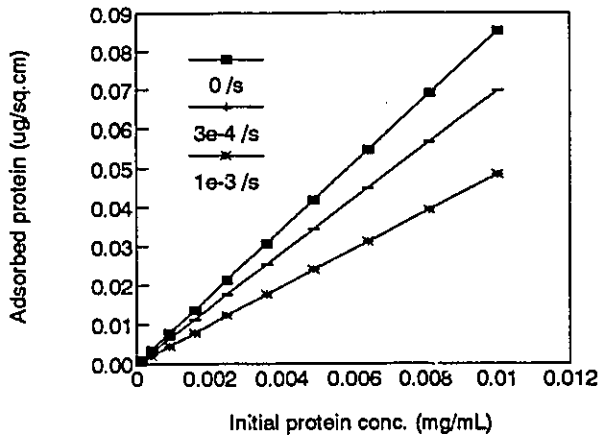

Figure 4.3.7: The effect of a reversible adsorption mechanism on simulated fibrinogen adsorption as a function of protein concentration after five minutes. k_1 is constant at 0.01 cm/s in this simulation while k_{-1} varies as indicated in the legend. Behavior is indistinguishable from that in Figure 4.3.6 and can similarly lead to erroneous estimates of the protein's diffusion coefficient.

The use of "isotherms" for "equilibrium" data collected after long times to determine protein "affinities" for different surfaces is equally open to question. Even if protein adsorption achieves equilibrium at high concentration, the behavior at low concentration is strongly influenced by solution depletion and diffusion limitations. The initial slope is more likely to be an indication of these influences than of affinity even after times as long as 24 hours.

If the mechanism in equation 4.3.16 is feasible it is difficult to understand why more or even all of the protein would not desorb during any rinsing step used in the protocol. There are two possible explanations. First, the actual rate of desorption may be very low and under these conditions a brief rinse would result in negligible desorption. Second, the adsorbed protein may undergo a conformational change on the surface rendering it irreversibly or much less reversibly adsorbed. Both mechanisms have been observed and both are probably involved to a certain extent. Using the simulation developed here it is possible to allow for such multiple adsorbed states on the surface. For the purposes of illustration we assume that state 1 is a loosely bound, relatively compact molecule which may undergo "spreading" with a rate constant k_2 on the surface to an irreversible "flat" conformation referred to as state 2. This mechanism may be described by equations 4.3.17 to 4.3.19:

$$\frac{d\Gamma_1}{dt} = k_1 C_N(1-\theta) - k_{-1}\Gamma_1 - k_2\Gamma_1(1-\theta) \qquad [4.3.17]$$

$$\frac{d\Gamma_2}{dt} = k_2\Gamma_1(1-\theta) \qquad [4.3.18]$$

where

$$\theta = \frac{\Gamma_1}{\Gamma_{1\max}} + \frac{\Gamma_2}{\Gamma_{2\max}} \qquad [4.3.19]$$

A typical adsorption kinetics simulation using equations 4.3.17 to 4.3.19 results in the adsorption behavior in Figure 4.3.8. The loosely bound state 1 is gradually replaced by irreversibly bound state 2. The behavior of state 1 is reminiscent of the Vroman effect for fibrinogen adsorbing to glass from plasma (Wojciechowski et al, 1986). Perhaps the same kind of surface rearrangements are involved. The number and type of surface states that can be proposed, some of which were presented before, are virtually limitless. Nygren (1988b) has reported on co-operatively interacting states of albumin. The theory of random sequential adsorption (RSA) predicts that only 54.7% of a surface may be covered by randomly adsorbing spheres or disks based on stochastic and topological considerations (Giaever and Keese, 1987; Schaaf and Talbot, 1989; Schaaf et al, 1988). Surface diffusion (Burghardt and Axelrod, 1981) may subsequently allow a higher surface coverage of these randomly adsorbed molecules through co-operative interactions. There may in fact be an enormous number of surface states for a given protein ranging from those bound by a single reversibly attached segment to those with large numbers of bound segments. The goal of

modeling is to develop a simplified depiction of this reality capable of predicting adsorption behavior over a wide range of conditions. The simulation presented here is a tool which allows one to focus on the mechanism at the wall i.e. the adsorption itself. The physical process of transport and diffusion which often tend to confound the issue are systematically taken into account.

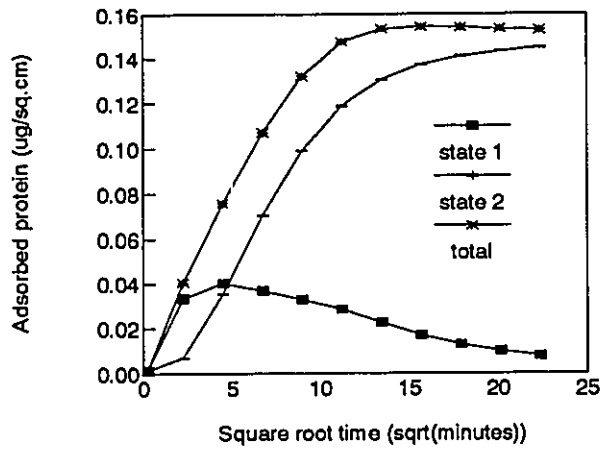

Figure 4.3.8: The kinetics of adsorption involving two states (see the legend) for fibrinogen adsorbing from a 0.005 mg/mL solution. The first reversible state is adsorbed at a rate of 0.01 cm/s with a desorption rate of 0.0001 /s. This state has a maximum monolayer coverage of 1.0μg/cm^2 and is converted to an irreversible second state (with a 0.15μg/cm^2 monolayer capacity) at a rate of 0.001 /s. This relatively simple example is intended to demonstrate the ability of the simulation to handle more complex adsorption models that may be hypothesized.

4.3.1.3 Limitations and Further Applications of the Simulation

There are clearly many combinations of events that can occur when a protein arrives at a solid-liquid interface depending on the protein, its environment in solution and the nature of the surface. Only a small number of simple mechanisms have been considered here. Many more complex mechanisms may be investigated individually or in combination using the technique of simulation.

The classical method for discriminating between proposed mechanisms involves the fitting of experimental data to their respective mathematical models. This can be accomplished in the present context by coupling the simulation with a nonlinear least squares parameter estimation routine (Meeter and Wolfe, 1965). Any parameters including monolayer coverage, diffusion coefficient and rate constants may be estimated assuming the data and the model are well-conditioned. Unfortunately the program runs slowly due to the iterative nature of nonlinear parameter estimation and the complexity of the simulation. Nonetheless, estimating parameters may be useful when a model can be found to adequately explain a wide range of adsorption behavior. Rate constants and monolayer coverages may be useful as quantitative surface characteristics to be correlated with blood compatibility data or may be used to predict competitive adsorption from multicomponent systems including plasma.

The simulation developed here may be adapted to more complex protocols such as desorption and exchange experiments. Different experimental systems including particles and flow channels of variable geometry can also be accommodated. Modeling of adsorption from more complex protein mixtures is possible but in a binary system for example the number of o.d.e.'s would approximately double since the diffusion of each component must be treated separately. To model a system as complex as plasma would require simplifications which may or may not render the simulation unable to describe real adsorption behavior. The major limitation in the application of simulations to the study of protein adsorption is the availability of computational power. The technique of simulation however, seems indispensable to the study of adsorptive processes which are in many instances, limited by kinetic rather than equilibrium phenomena.

4.3.2 Mathematical Modeling of Protein Adsorption

Given the simulation of protein adsorption described in Section 4.3.1, one may fit real data to hypothetical models using a nonlinear least squares estimation algorithm. UWHAUS (Meeter and Wolfe, 1965) is a FORTRAN subroutine designed for this purpose. Inputs to UWHAUS include experimental data, a mathematical model, and initial parameter estimates. The outputs include updated parameter estimates and statistics useful for evaluating the adequacy of the model fit to the data. Because the model was based on a numerical solution of a stiff set of ordinary differential equations, the parameter estimation routine

was very slow. Complete parameter estimation required up to eight hours on an IBM AT compatible computer with a math coprocessor. The number of models tested was necessarily limited and much more computational power will be required to fit more complicated models to larger data sets.

Some of the conceptual hypotheses concerning protein adsorption mechanisms were described in section 1.1.5. Many of these mechanisms may be modeled mathematically in the form of a series of ordinary differential equations describing the rate of accumulation of adsorbed species. In single component protein adsorption, the different "species" are actually model "states" of adsorbed protein distinguished by their conformation, orientation, or the strength of binding. Real proteins can undoubtedly attain an infinite variety of adsorbed "states", but in order to model the system mathematically, an arbitrary and finite set of adsorption states must be specified. The rate of accumulation of each state may be influenced by direct adsorption, desorption, state transitions, and exchange with the proteins in bulk solution. The simplest and most commonly employed model for adsorption is the Langmuir model as described in Section 4.3.1. It is a one state model based on reversible adsorption up to a monolayer limit (see equation 4.3.16). Of course the assumptions upon which this model was developed are all violated by the known behavior of protein adsorption but it provides a useful starting point for the development of more complicated models.

Before discussing model fitting, it is important to recall the observations made in section 3.3.1 regarding the error associated with protein adsorption measurements. The magnitude of the error was found to be proportional to the measured adsorption, whereas the parameter estimation routine (UWHAUS) assumed a constant variance for the dependent variable. In order to satisfy this assumption, UWHAUS was given as input the logarithm of model parameter estimates and adsorption data since the logarithm of adsorption data had essentially constant variance. The effect of this transformation was to put greater emphasis on the fitting of low surface coverage data.

Figure 4.3.9 is a 45° plot showing the correspondence between the Langmuir adsorption model and data for fibrinogen adsorption on the C18 surface. It is apparent that the Langmuir model describes low surface coverage quite well, but cannot explain the higher

"plateau" adsorption that was observed on all surfaces. The trends were similar for fibrinogen and albumin adsorption on C18 and SO3. Table 4.3.2 lists the four parameters that were estimated in all four systems.

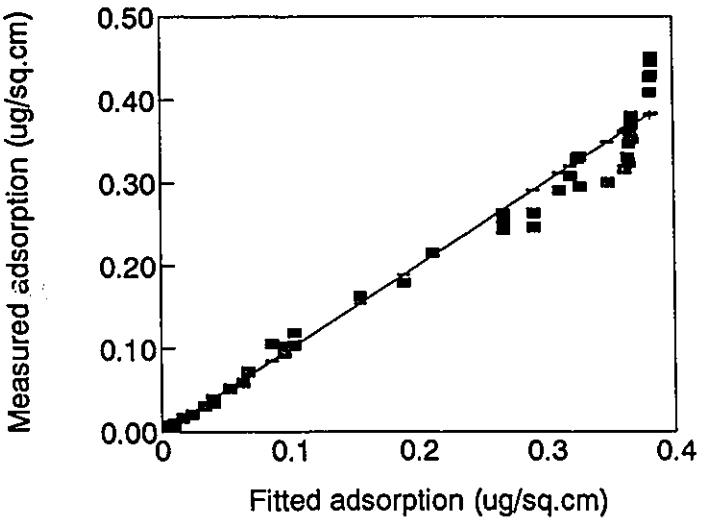

Figure 4.3.9: Langmuir model (equation 4.3.16) fit to fibrinogen adsorption data on the C18 surface. Note the inability of the model to fit the data at high surface coverage.

Table 4.3.2: List of parameters resulting from a fit of the Langmuir adsorption model to experimental data. n defined = 60 for each system. The confidence interval is not explicitly stated for the parameters of this simple model but a question mark (?) is used instead to indicate that the 95% confidence interval for the parameter estimate contains zero.

		Albumin C18	Albumin SO3	Fibrinogen C18	Fibrinogen SO3
k_1	cm/s	3.07×10^{-4}?	1.59×10^{-4}	1.12×10^{-4}	1.04×10^{-4}
K_{-1}	cm^{-1}	8.10×10^{-3}	1.38×10^{-2}	1.18×10^{-2}	8.69×10^{-3}
Γ_{max}	$\mu g/cm^2$	9.61×10^{-3}	8.58×10^{-2}	0.385	0.523
D	cm^2/s	2.80×10^{-7}	9.70×10^{-8}?	1.23×10^{-7}	1.20×10^{-7}
$s^2_{residuals}$	$\mu g^2/cm^4$	0.0235	0.132	0.0081	0.0258

The parameter K_{-1} in Table 4.3.2 is the inverse affinity constant equal to k_{-1}/k_1 and is therefore proportional to the desorption rate constant. The forward and reverse rate constants were found to be highly correlated and reliable separate estimates could not be obtained. By using the inverse affinity constant instead of k_{-1} better parameter estimates with narrower confidence intervals were possible. This parameter transformation was found to be helpful in all adsorption models which contained desorption rates.

As one might expect, the parameters D and k_1 were found to be strongly correlated and this influenced their estimated values. In the two albumin systems where the initial rates of adsorption differed greatly, the estimates of diffusivity were very different. Even the higher diffusivity of 2.8×10^{-7} cm^2/s estimated from the C18 data was significantly lower than the value of 6×10^{-7} cm^2/s quoted by Hlady and Andrade (1987). The estimates for fibrinogen diffusivity were in closer agreement with each other but were significantly lower than the commonly accepted value of 2×10^{-7} cm^2/s. The simulation was designed to account for the effect of adsorption rate limitations on the apparent diffusion coefficient but there are other possible experimental and mechanistic explanations for the "depressed" diffusion coefficients. Experimentally, rinsing may remove a fraction of loosely adsorbed protein while a mechanistic hypothesis might be that the initial adsorption of protein may be more complicated than a first order binding reaction. Since proteins are surfactants, they may accumulate in high concentration at the solid-liquid interface before actually binding. The question of diffusivity estimates based on adsorption data has been recently addressed by Wojciechowski and Brash (1991).

It can be concluded that the Langmuir model fits low coverage data fairly well and thus the emphasis in this study is to test other models for their ability to fit higher surface coverage data.

One model proposed specifically to explain protein adsorption over a wider range of surface coverage was that of Cuypers et al (1987). The Cuypers model is a modification of the Langmuirian model in which the parameters k_1 and K_{-1} are assumed to be exponential functions of the surface coverage. The modifications are empirical rather than mechanistic, and are based on general observations made in real systems. One of these general observations suggested that protein adsorption is progressively slower at higher surface coverage. This behavior is typical of macromolecular adsorption in general and is often attributed to rearrangements on the surface which allow additional adsorption while remaining in the

monolayer coverage regime. There was evidence of such a slow adsorption at high surface coverage in the raw protein adsorption data for fibrinogen (see Figures 3.3.11 to 14). This effect was modeled by Cuypers by making the adsorption rate constant k_1 a decreasing exponential function of the total surface coverage:

$$k_1 = k_{1c} e^{-\alpha \Gamma} \qquad 4.3.20$$

where k_{1c} is the adsorption rate constant at zero surface coverage and α is an empirical positive parameter related to the decrease in adsorption rate caused by adsorbed protein.

The rate of desorption, k_{-1} was redefined by Cuypers in a similar manner to take into account experimental evidence that desorption of some adsorbed protein is rapid at high surface coverage and slow at low surface coverage:

$$k_{-1} = k_{-1c} e^{B\Gamma} \qquad 4.3.21$$

where B is an empirical constant which causes k_{-1} to increase as Γ increases, and k_{-1c} is the lowest possible desorption rate at low surface coverage. The model does not take into account the observed tendency for proteins to adsorb more strongly to a surface over time.

The Cuypers model was fit to the data to determine if it is in fact better than the Langmuir model. Parameter estimates are listed in Table 4.3.3.

For each of the four protein/surface systems in Table 4.3.3, the variance of residuals is less for the six parameter Cuypers model than for the four parameter Langmuir model. The improvement to overall fit was, however, only slight. Figure 4.3.10 depicts the 45° plot analogous to that in Figure 4.3.9. By comparing these two figures, one can see that the Cuypers model is a slight improvement over the Langmuir but still does not adequately represent the adsorption data at higher surface coverage. There are a number of observable phenomena which are not included directly in the Cuypers model that may contribute to its inadequacy. One important mechanism contributing to protein adsorption is that of multiple adsorbed states in which proteins may undergo transitions from compact to spread, or side-on to end-on which are equivalent to a reversible to irreversible transition. It can be argued that the Cuypers model attempts to account for these transitions in an empirical manner as a function of surface coverage. There are other models which have been proposed to describe multistate adsorption in a mechanistic fashion as a function of time.

Table 4.3.3: List of parameters resulting from a fit of the Cuypers adsorption model to experimental data. n = 60 for each system. A question mark (?) indicates that the 95% confidence interval for the parameter estimate contains zero.

		Albumin C18	Albumin SO3	Fibrinogen C18	Fibrinogen SO3
k_{1c}	cm/s	0.902?	2.5×10^{-5}	1.88×10^{-4}	2.76×10^{-3}
α	$cm^2/\mu g$	165	70.3?	4.70	18.6
K_{-1c}	cm^{-1}	4.41×10^{-4}?	5.1×10^{-3}?	7.36×10^{-3}	4.19×10^{-3}
B	$cm^2/\mu g$	108?	31.9	0.822?	14.5
Γ_{max}	$\mu g/cm^2$	0.130?	2.04×10^{4}?	0.425	0.834
D	cm^2/s	1.94×10^{-7}	1.37×10^{-7}	1.05×10^{-7}	0.801×10^{-7}
s^2		0.0171	0.0418	0.0063	0.0201

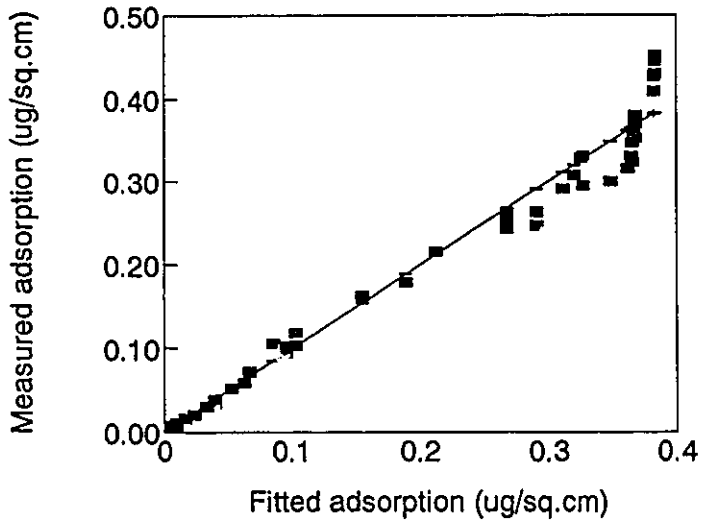

Figure 4.3.10: Cuypers' model (Equations 4.3.16, 4.3.20, 4.3.21) fit to fibrinogen adsorption data on the C18 surface. Note the inability of the model to fit the data at high surface coverage.

Many two state models have been proposed previously and all are based on essentially the same principle. A protein is first reversibly adsorbed from solution in state 1. The state 1 protein may then desorb or progress to state 2, usually a more spread, less reversibly attached protein. Studies showing that proteins strengthen their attachment to surfaces as a function of residence time helped to justify this hypothesis. Models of this type have been proposed by Beissinger and Leonard (1982), and Lundstrom (1985). Their models, which are similar, were adapted to give two o.d.e.'s describing the rate of accumulation of states 1 and 2.

$$\frac{d\Gamma_1}{dt} = k_1 C_N(1-\theta) - k_2 \frac{\Gamma_1}{\Gamma_{1\max}}(1-\theta) \qquad 4.3.22$$

$$\frac{d\Gamma_2}{dt} = k_2 \frac{\Gamma_1}{\Gamma_{1\max}}(1-\theta) \qquad 4.3.23$$

$$\theta = \frac{\Gamma_1}{\Gamma_{1\max}} + \frac{\Gamma_2}{\Gamma_{2\max}} \qquad 4.3.24$$

The rate constant for the transition from state 1 to 2 is named k_2 as it was in section 4.3.1.2.

Equations 4.3.22 to 4.3.24 do not contain any desorption terms from either state 1 or 2. The model was tested with desorption parameters but no improvement in fit was observed, nor could these parameters be shown to be significantly greater than zero. The two state model as represented by equation 4.3.22 to 4.3.24 was fit only to fibrinogen adsorption data. Table 4.3.4 contains the estimated parameters for adsorption to C18 and SO3.

The parameters in Table 4.3.4 provide quantitative evidence that the standard two state model with a transition from compact to spread states cannot explain the kinetics of protein adsorption. The parameters associated with state 2 (k_2 and Γ_{2max}) are not significantly greater than zero and show that protein "spreading" on the surface cannot explain the slowly increasing adsorption that is observed kinetically for experiments at high surface coverage (see Figure 4.3.11). The model fit was in fact worse for the irreversible two state model than for the Langmuir model. Many other multistate models were tested but showed no improvement in fit. One interesting observation, however, was that experimental data fit better to a two state model in which a transition from side-on to end-on (or spread to compact) occurred. Even for this model there was significant lack of fit. Other models incorporating

Table 4.3.4: List of estimated parameters for two state adsorption model: fibrinogen/SO3 and fibrinogen/C18. A question mark (?) indicates that the 95% confidence interval of the parameter estimate contains zero.

Parameter	units	C18	SO3
k_1	m/s	1.73×10^{-4}	1.99×10^{-4}
k_2	cm/s	3.48×10^{-5}	1.97×10^{-5}
Γ_{1max}	$\mu g/cm^2$	0.393	0.469
Γ_{2max}	$\mu g/cm^2$	0.0905?	0.0144?
D	cm^2/s	0.864×10^{-7}	0.740×10^{-7}
variance, s^2	$\mu g^2/cm^4$	0.015	0.014
# of data, n		60	39

three adsorbed states, exchange with bulk protein, and up to 10 parameters were tested but could not adequately fit the data. The failure of the multistate class of models was surprising given the fact that their development is based on observed phenomena and the hypothesis that protein adsorption does not exceed a monolayer. The monolayer limitation is widely accepted in the protein adsorption field as a "rule of thumb" and slow increases in adsorbed protein on covered surfaces have been attributed to molecular rearrangement and in most cases, total surface coverage does not exceed the theoretical maximum estimated from molecular dimensions.

Recently Young and coworkers (1988) have suggested based on kinetic adsorption data for proteins on polymers that multilayer formation may occur. This suggestion is based partly on the observation that total adsorption exceeded estimated maximum monolayer coverage. For fibrinogen, monolayer capacity was estimated to be as high as 0.67 $\mu g/cm^2$ using dimensions obtained from electron micrographs of fibrinogen in the dry state. Other researchers have speculated that monolayer coverage of fibrinogen may be as high as 1.8 $\mu g/cm^2$ for end-on adsorption (Brynda et al, 1987). This value is rarely exceeded experimentally. Young et al also showed that there were two distinct affinity regimes for albumin, fibrinogen and IgG adsorption, but these data could also be interpreted to be a result of surface rearrangement. They did not compare the ability of different models to fit the same

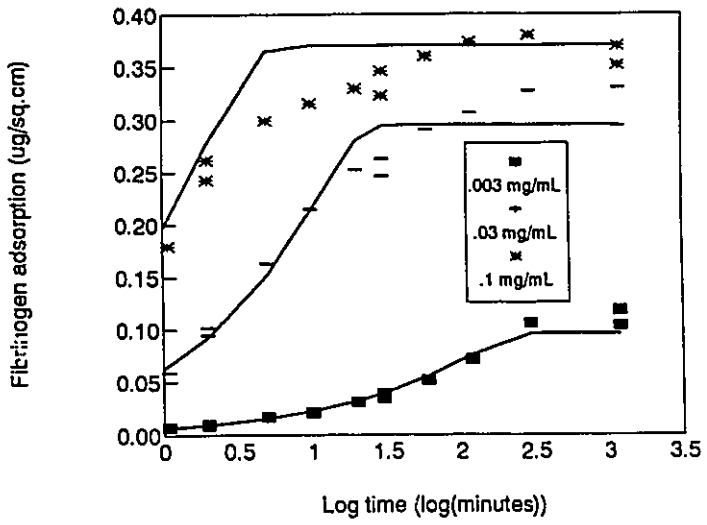

Figure 4.3.11: Two state model (Equations 4.3.22 to 24) fit to the kinetic data for fibrinogen adsorption on the C18 surface. The model reaches a plateau much more rapidly than the experimental data.

data. Despite the fact that the model of Young et al was not proven to be better than existing monolayer models, the proposal of a bilayer mechanism was significant in a field where such a mechanism had not previously been seriously considered.

In the present investigation, there was evidence of multilayer adsorption in the data for fibrinogen adsorption to the model silanized surfaces (see Figures 3.3.15 and 3.3.16). A two regime mechanism was evident on virtually all the materials tested and there was little evidence that a plateau was reached in any of the fibrinogen/surface systems. Data for albumin and fibrinogen adsorption to C18 and SO3 were fit to a kinetic bilayer model as described by Equations 4.3.25 and 4.3.26.

$$\frac{d\Gamma_1}{dt} = k_1 C(1-\theta_1) - K_{-1}k_1(\theta_1 - \theta_2) \qquad 4.3.25$$

$$\frac{d\Gamma_2}{dt} = k_2 C(\theta_1 - \theta_2) - K_{-2}k_2\theta_2 \qquad 4.3.26$$

$$\theta_1 = \frac{\Gamma_1}{\Gamma_{1\max}} \qquad 4.3.27$$

$$\theta_2 = \frac{\Gamma_2}{\Gamma_{2\max}} \qquad 4.3.28$$

Table 4.3.5: Estimated parameters for bilayer model based on experimental data for fibrinogen and albumin adsorption to C18 and SO3. A question mark (?) indicates that the 95% confidence interval of the parameter estimate contains zero. The units are similar to those used in Table 4.3.2.

Protein> Surface>	Albumin C18	Albumin SO3	Fibrinogen C18	Fibrinogen SO3
k_1	$(8.5\pm25)\times10^{-4}$?	$(1.9\pm0.8)\times10^{-5}$	$(1.4\pm0.5)\times10^{-4}$	$(1.2\pm0.6)\times10^{-4}$
K_{-1}	$(4.3\pm3.6)\times10^{-8}$	$(8.03\pm6.14)\times10^{-8}$	$(4.9\pm6.9)\times10^{-6}$	$(6.3\pm7.4)\times10^{-8}$
k_2	$(5.0\pm2.0)\times10^{-4}$	$(3.9\pm4.7)\times10^{-4}$	$(2.8\pm0.9)\times10^{-3}$	$(3.2\pm1.0)\times10^{-3}$
K_{-2}	5.6±5.3	0.82±0.80	0.74±0.95	0.47±0.48
$\Gamma_{1\max}$	0.086±.004	0.057±0.009	0.30±.05	0.44±0.03
$\Gamma_{2\max}$	0.104±.101	0.16±.10	0.16±0.05	0.54±0.32
D	$(2.3\pm0.8)\times10^{-7}$	$(0.87\pm.90)\times10^{-7}$	$(1.13\pm0.18)\times10^{-7}$	$(1.13\pm0.24)\times10^{-7}$
s^2	0.0114	0.0633	0.00545	0.0114

This reversible bilayer model involves seven parameters including k_1 and k_2, the adsorption rate constants for the first and second layer. K_{-1} and K_{-2} are inverse affinity constants for the two layers. It was assumed that desorption of molecules from the first monolayer could take place only if they were not covered by the second layer (see equations 4.3.25-28). The estimated parameters are listed in Table 4.3.5.

The bilayer model fit the experimental data significantly better than previous models especially in the troublesome high surface coverage regime (see Figure 4.3.12). A lack of fit is apparent for albumin adsorption on SO3 but the other three systems are well fit. Some general observations can be made about the parameter estimates. The parameter k_2 was the same size or larger than k_1 which would suggest that the driving force for bilayer adsorption is quite strong. In the case of fibrinogen, the second layer was adsorbed more quickly than

the first layer. The second layer was apparently much more reversibly adsorbed than the first. This is consistent with the observations that have shown proteins exist in reversibly and irreversibly bound states. Of all the models tested, the bilayer model was best able to fit a wide range of experimental data.

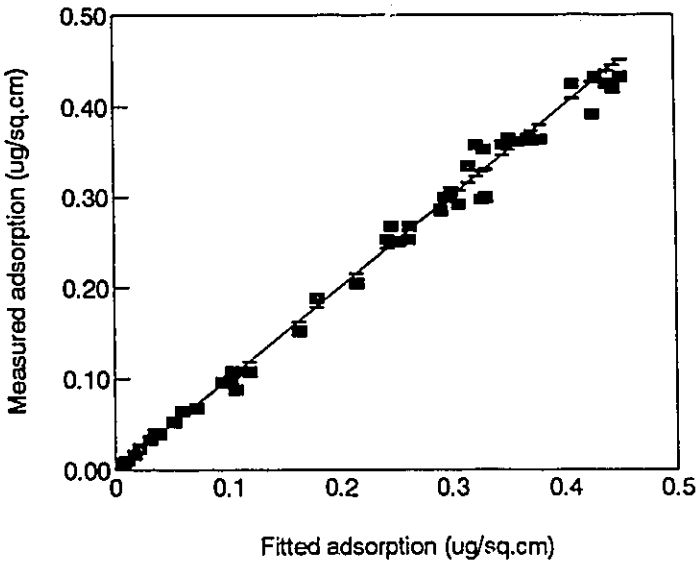

Figure 4.3.12: Bilayer model (Equations 4.3.25 to 28) fit to fibrinogen adsorption data on the C18 surface. The fit is good, even at high surface coverage. (Compare with Figures 4.3.9 and 4.3.10.)

In the case of albumin adsorption to SO3, the bilayer model did not fit as well as the model of Cuypers. The lack of fit for this surface may be due to the presence of a true multilayer mechanism. There is no reason why multilayer adsorption must be limited to bilayers, but rapid desorption may hinder its detection. No attempt was made to fit a trilayer model to the albumin/SO3 data to test this hypothesis, in part because the ±21% error associated with the measurements was too large to ensure well conditioned parameter estimates.

Figure 4.3.13 demonstrates the ability of the bilayer model for adsorption to fit kinetic data for fibrinogen on C18 over a wide range of conditions. The relatively poor lack of fit

at high adsorption was not considered to be significant by the fitting routine which uses the logarithm of adsorption. Residual error was amplified at high surface coverage by converting the 'log' data back to its original form.

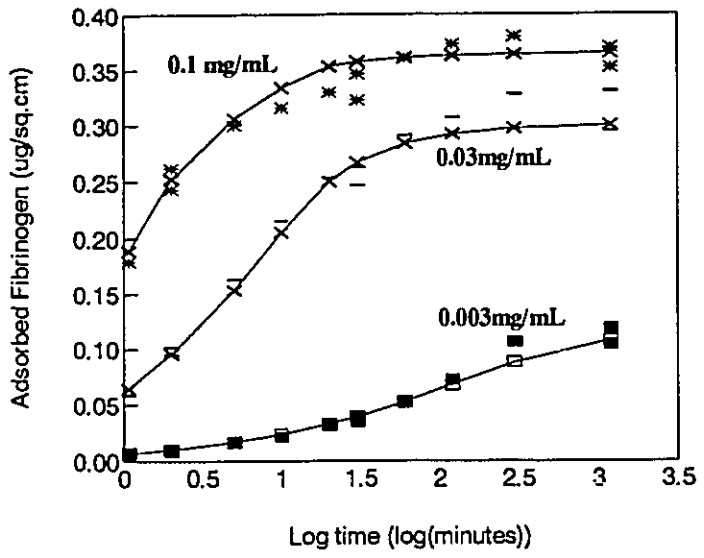

Figure 4.3.13: Comparison of fitted bilayer model with fibrinogen adsorption kinetics on C18.

Figure 4.3.14 demonstrates the ability of the model to explain the effect of adsorption kinetics on the apparent diffusivity calculated using equation 4.3.6. An estimate of diffusivity would obviously be affected by any significant adsorption rate limitations. The highest possible estimate for D given the experimental data is about 0.85×10^{-7} cm^2/s. This value is less than the parameter estimate (see Table 4.3.5) and much less than the literature value of 2×10^{-7} cm^2/s. In general, estimates of D using adsorption data are strongly influenced by surface binding kinetics and thus will tend to be significantly lower than the true value in static systems.

The fit of the bilayer model to fibrinogen adsorption isotherms on C18 is depicted in Figure 4.3.15. Again, the model fits reasonably well but there is some indication that surface coverage could continue to increase at protein concentrations greater than 1.0 mg/mL. This

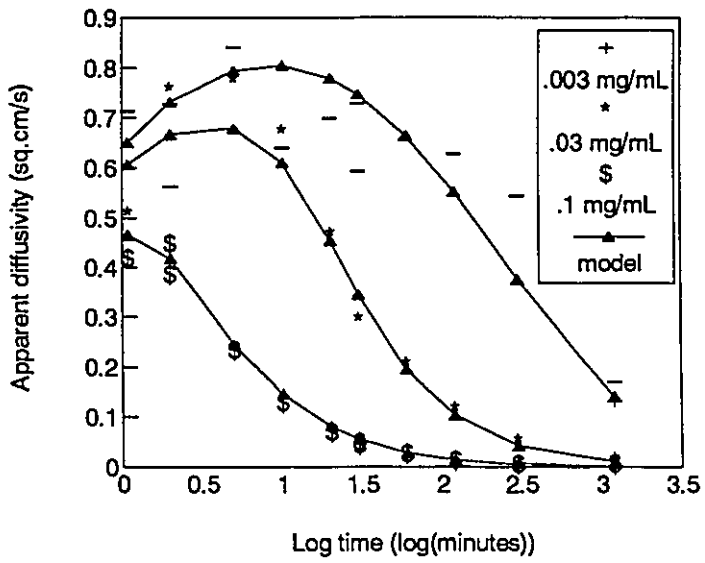

Figure 4.3.14: A demonstration of how the simulated model for adsorption (the solid line was calculated based on the bilayer model) explains the effect of kinetics on the apparent diffusion coefficient of fibrinogen. The effect is a strong one and thus suggests that estimates of diffusivity should not be based on raw adsorption data in static systems.

may indicate that adsorption is capable of multilayer formation beyond the bilayer modeled here, or simply that the second layer has a capacity greater than could be estimated using the available data.

It is important to point out that the bilayer model developed here is ultimately an empirical one despite its being based on in proposed adsorption mechanisms. The relevance of the estimated model parameters is limited to similar *ex situ* systems which undergo a rinsing step prior to the determination of adsorbed quantities. A more recent study in this laboratory has demonstrated quantitatively that rinsing has a significant effect on fibrinogen adsorption to glass beads (Cornelius, Wojciechowski, and Brash, 1991). The effects of rinsing, bulk-surface exchange, and complex protocols have not been incorporated into either the simulation or the protein adsorption model. The usefulness of the model is limited to the fitting of data from experimental systems similar to that described here. The model parameters may be useful for the characterization of proteins and surfaces but may only be compared with other parameters estimated in similar experimental systems.

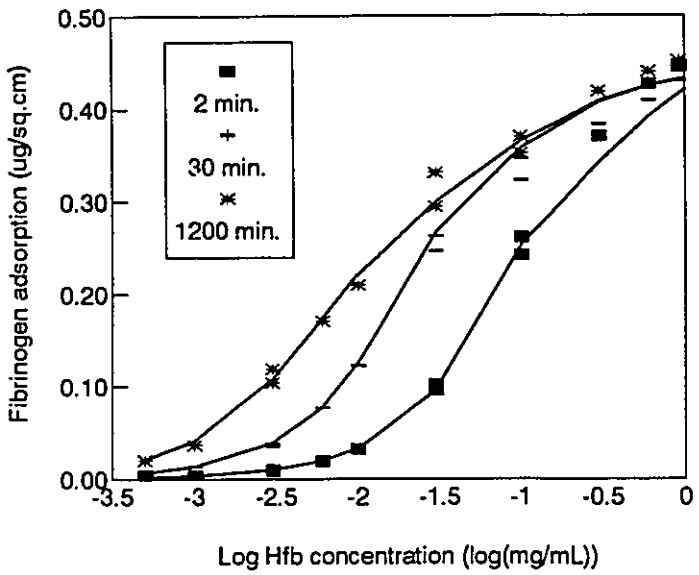

Figure 4.3.15: Comparison of fitted bilayer model with fibrinogen adsorption isotherms on C18.

The major conclusion from the modeling work described in this thesis is that the bilayer model quantitatively explains experimental data better than monolayer models.

Recently Yan and Déjardin have fitted a two regime model to data for fibrinogen adsorption under flow conditions on polyacrylonitrile fibers (Yan and Déjardin, 1991) and estimated the rate constant, k_1, to be 2.35×10^{-4} cm/s. They also recognized what they believed to be multilayers of protein on polyacryonitrile as well as on Pyrex glass (Boumaza et al, 1991) but could not rule out the influence of surface roughness on their observations.

A study of fibronectin adsorption on polystyrene by Giroux and Cooper (1989), based on experimental data using an *in situ* Fourier transform infrared (FTIR) technique at 37°C, led to similar conclusions. A bilayer model fit the kinetic data better than either the Langmuir or Cuypers models. These authors found that less fibronectin was adsorbed to a more hydrophilic ammonia plasma treated polystyrene and attributed the effect to wettability. This conclusion does not agree with the findings of this study which show that fibrinogen apparently has a higher affinity for the more hydrophilic SO3 surface than for C18. The

commonly accepted 'rule of thumb' which states that protein adsorption increases as a function of hydrophobicity must be considered to be a generalization which does not always explain observed behavior.

In order that further progress may be made in the modeling of protein adsorption, increasingly sophisticated methods will have to be employed. It is no longer possible to justify the use of isotherms in systems which display significant hysteresis if not actual thermodynamic irreversibility. Even kinetic modeling, which appears to be a more valid approach, will require models more sophisticated than the Langmuirian mechanism in order to describe real behavior. If the goal of modeling is to allow the prediction of protein adsorption in different experimental systems including *in situ*, *ex situ*, flow, static and in a variety of geometries, then simulations must attempt to incorporate all effects of the protocol on adsorption. Some interesting and informative experiments involve the multiple steps of adsorption, rinsing, desorption, displacement, and exchange. Simulations should be designed in the future to allow for such discrete stages and could be especially useful for the estimation of certain parameters, in particular desorption, displacement and exchange rates. Algorithms capable of describing sequential processes will be more complex than the one stage adsorption simulation presented here, but in the end will be necessary to model accurately the processes that occur in real, experimental protocols.

4.4 Relationships among Surface Properties, Protein Adsorption and Blood Compatibility

4.4.1 An Introduction to the Data and Parameters Used in the Comparative Study

This project was designed to allow characterizations of surface properties, protein adsorption, and blood compatibility to be compared. One way to empirically determine the relationships among correlated variables is by multivariate regression. Linear least squares regression works on the assumption that the independent variables are free from error and that the dependent variables have a constant variance. The data collected in this study did not fit the traditional assumptions of least squares regression since all the variables were associated with error which was in several cases nonconstant. In addition, there was no way to categorize variables as dependent or independent. Nonetheless simple regression methods serve a useful purpose in the screening of relationships among correlated variables (Geladi and Kowalski, 1986) even if their application is not strictly rigorous. If one wishes to build models for the prediction of blood compatibility based on a highly correlated set of error containing variables, a more rigorous and powerful method known as partial least squares or PLS (Wold et al, 1986) is available. PLS frees the researcher from the need to study a response as a function of only one or two variables at a time. Such methods will become increasingly useful in the biomaterials field as researchers learn to trust them and become proficient in their application. However, for the present work only linear regression was employed to screen the correlations and no attempt was made to build predictive models that would require a larger database of surface properties for a wider variety of surfaces.

The successful application of a multivariate regression to the screening of relationships among variables depends strongly on the experimental design used to obtain the data. Traditional experimental design divides variables into independent and dependent categories in which the independent variables are inputs controlled by the experimenter and dependent variables are the measured responses and contain random, experimental, and systematic error. In the present study, the variables involved could not be fairly categorized as independent or dependent and could not be controlled in the manner of an input. A good experimental design depended entirely on the preparation of a suitably varied selection of

model surfaces which would simultaneously provide a wide variation in all manner of measured responses. The considerations given to surface design are described more fully in sections 1.5 and 1.6. Multivariate correlations necessitate that each variable cover a broad range (at least several times greater than the standard error) of values in order that relationships can be determined to be significant at a reasonable level of confidence.

A total of 19 parameters (9 surface chemistry parameters, 5 contact angle parameters, 3 fibrinogen adsorption parameters, and 2 clotting time parameters) were collected to characterize the 15 surfaces prepared for this study. The values of these parameters were found to vary widely on the fifteen model materials tested. Advancing water contact angles varied from 7° to 90°. Maximum and minimum plateau fibrinogen adsorption levels from buffer varied by six-fold, and peak fibrinogen adsorption from plasma covered a twelve-fold range (see Tables 3.3.2 and 3.3.3). Clotting time ranged from 3 to 11 minutes but was the least well suited to multivariate analysis since the experimental error associated with it was large (see section 3.4).

The nomenclature for the nine surface characterization parameters is described first. N30 and N90 are the nitrogen content (atom percent) of the surface as determined by XPS at 30° and 90° detector angles, respectively. S30 and S90 are elemental surface content of sulfur (atom percent) and Si/C30 and Si/C90 describe the atomic ratio of silicon to carbon at the surface. The surface content of silicon (Si90), carbon (C90), and oxygen (O90) based on 90° XPS detector angles were used to characterize the three elements common to all surfaces. The values for the surface chemical parameters are listed in Table 3.4.1.

Five parameters were used to characterize the "surface energetics" of the model surfaces. These are the advancing contact angles for water (CONTANG), glycerol (GLYCDROP) and dimethyl sulfoxide (DMSODROP), the standardized angle (STDANG) (combining information from all three liquids; see section 4.2.1), and the surface polarity (POLAR) as defined in section 4.2.7.2.

Fibrinogen adsorption was described by experimental data as defined in Tables 3.3.2 and 3.3.3. These data were deemed to be indicative of the initial slope of the isotherm (Fibslop), the plateau of the isotherm (Fibplat), and the Vroman effect peak height (Fibpeak) for 30 minute plasma experiments.

The thrombin generation assay expressed as a clotting time (Thromb) was used to describe intrinsic coagulation. Due to the nature of the error associated with Thromb (see section 3.4), its logarithm (Thromblog) was considered to be better suited to multivariate linear regression since the variance of Thromblog was more nearly constant.

The correlation of clotting time data with other data was subject to additional uncertainty since the substrate for the model surfaces was disposable borosilicate glass and not pure silica. The reactivity of silica and glass to silanes was not expected to be very different since the same reactive groups (hydroxyls) dominate both surfaces. It was therefore assumed that the chemistry of both substrates after silanization was sufficiently similar to allow comparisons to be drawn between clotting times and other parameters.

4.4.2 An Overall Comparison of Surface Properties

A number of statistical parameters and transformations were looked at in order to elucidate relationships among the various surface characterizations. These included Pearson correlation matrices, principal components analysis and cluster diagrams. Figure 4.4.1 was adapted from a hierarchical cluster diagram (created using the "Join" command in Systat, a statistical software package (Systat, Evanston, IL)) and represents the covariance between the properties of the surfaces used in this study based on the results of XPS, contact angle, protein adsorption, and blood coagulation studies. Those surfaces that are directly connected were the most similar from test to test. As the connections are made further to the right, the materials show less similarity. The PEG surface appears to be essentially unique while C18, SH, CH3, Ep and NH2, NH2b, Ur are the groups among which there is the greatest similarity.

The fact that C18, SH, CH3, and Ep are all so similar may be explained by the silane chemistry used to make them. SH and Ep were both made using slowly reacting ethoxysilanes. Unreacted silanol groups were blocked with the same silane used to make the CH3 surface. As a result, all four surfaces tended to behave as hydrocarbon surfaces. The surfaces containing amino groups, i.e. NH2, NH2b and Ur, were also made using ethoxysilanes but reacted faster with silica due to their autocatalytic behavior (Plueddemann, 1986).

The Qz and Qzb surfaces were found to resemble more closely the hydrocarbon surfaces than the other hydrophilic surfaces. The relatively thick adsorbed organic carbon

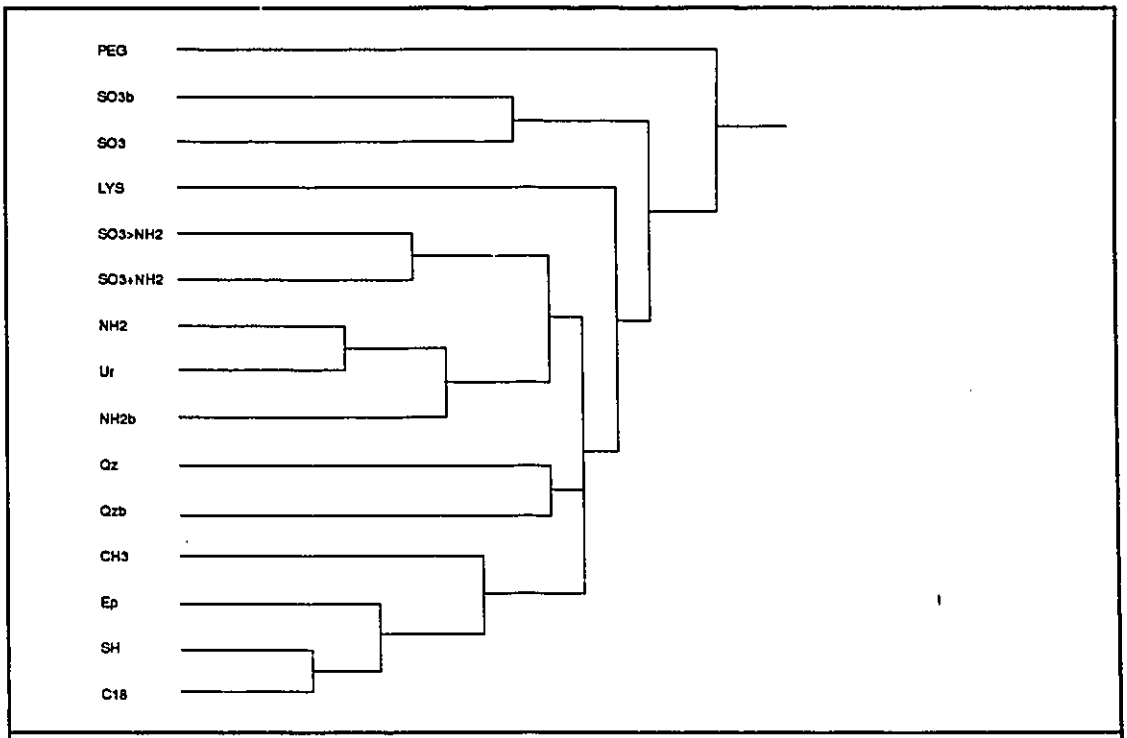

Figure 4.4.1: Cluster diagram showing (qualitatively) the correlations among the different surfaces prepared for use in this study.

overlayer (detected by XPS) was most likely responsible for this behavior. This observation reinforces the contention that surface chemical analyses are important in biomaterial characterization.

The two independently prepared sulfonated surfaces SO3 and SO3b were similar to each other but quite distinct from the other materials, even those containing sulfonate groups (LYS, PEG, SO3>NH2, SO3+NH2). The length of the bridge connecting SO3 and SO3b suggests (qualitatively) that their behavior is by no means identical and that the differences in their preparation had an impact on ultimate properties. Even the two silica standards show large differences perhaps due to the variation in storage times before testing. The two surfaces containing mixtures of sulfonate and amino silane show similar behavior despite the different protocols used to prepare them. The properties of the SO3/NH2 surfaces are quite different from those for the pure sulfonate or pure amino silane surfaces.

Perhaps the most important observations that can be made regarding Figure 4.4.1 are that it contains no unexpected correlations, and shows that the surfaces examined covered a wide range of properties. None of the groups of materials were "excessively" correlated meaning that the relationships among them could be determined using a fairly well-conditioned matrix of measured properties. The results would have been less satisfactory if a series of hydrophobic polymers alone had been used. The goal of designing a series of surfaces with a wide range of properties appears to have been successful.

4.4.3 Fibrinogen Adsorption Correlations

Fibrinogen adsorption was found to be best correlated with other surface properties, especially surface chemistry and contact angle data (but not with clotting time). Many relationships were investigated but only the most robust ones will be discussed here. The relationships described here can only be considered to be empirical and as such are in search of more fundamental, mechanistic explanations. The relationships are expressed throughout this section as functions of the variables in their original units. This is done to allow a more intuitive interpretation of their meaning and implications in real physical systems. Proper statistical procedure requires that the data be normalized first before such analyses are performed but the resulting equations are more difficult to interpret since the variables are "scaled". For the data collected in this study the use of normalized and raw data yielded relationships which were practically identical.

Protein adsorption is believed to be most extensive on hydrophobic surfaces (Absolom et al, 1987), or those surfaces with large water contact angles (greater than about 70°). Based on the data obtained in the present study, this was not found to be a good "rule of thumb". Fibrinogen adsorption was found to be a much stronger function of surface chemistry in general, and sulfur and nitrogen content in particular.

Equation 4.4.1 is the general relationship that was found based on the results for all 15 model surfaces and equation 4.4.2 is the relationship obtained for data on the initial eight surfaces. It must be emphasized that this empirical model is based on a linear hypothesis and while it fits the available data quite well, its interpretation should not be extrapolated to conditions of chemical content outside of those available in this study. For example, one would expect an upper limit of fibrinogen coverage which could not be exceeded by a continual increase in the surface sulfur (sulfonate) content.

$$(Fibplat \pm 0.089) = (0.42 \pm 0.04) + (0.29 \pm 0.04)S90 - (0.12 \pm 0.03)N90 \qquad [4.4.1]$$

$$(Fibplat \pm 0.089) = (0.43 \pm 0.04) + (0.25 \pm 0.06)S90 - (0.07 \pm 0.03)N90 \qquad [4.4.2]$$

The parameters in each equation are the same within experimental error and suggest that the relationship is the same whether the initial eight or the entire fifteen materials are considered. The similarity in the parameters is in fact surprising considering the small number of model surfaces with sulfur and/or nitrogen that were available in the original set of eight. All of the seven supplemental surfaces contained sulfur and/or nitrogen and this greatly enhanced the information available for parameter estimation.

Equations 4.4.1 and 4.4.2 tell us that the average plateau adsorption on surfaces containing only Si, O, and C (i.e. CH3, C18, SH, Ep) was 0.419 ± 0.041 $\mu g/cm^2$. Less adsorption was observed on "pure" silica, but this may have been correlated with the surface nitrogen detected by XPS (about 1%). Of those surfaces which contained neither nitrogen nor sulfur, fibrinogen adsorption was correlated with the contact angle but not at the same level of significance as Fibplat was correlated with N and S. Equation 4.4.1 shows that the fibrinogen "plateau" was increased by an average of 0.29 ± 0.04 $\mu g/cm^2$ for an increase of 1% sulfur content measured at a 90° XPS detector angle, and decreased by 0.12 ± 0.03 $\mu g/cm^2$ for an increase of 1% nitrogen content detected at 90°. All of these parameters were justifiable at a level of confidence of greater than 99%, which confirms the statistical significance of this relationship. Any attempt to justify the relationship mechanistically, however, will clearly require consideration of the functionality of the surfaces i.e. the importance of the chemical groups in which the elements exist. For example, the presence of sulfonate groups is undoubtedly of greater significance than the presence of sulfur atoms. A similar argument could be made for amino groups and nitrogen.

Equation 4.4.1 presents an interesting possibility for further study of protein adsorption. One may be able to design surfaces with a range of affinities for fibrinogen by controlling the surface content of sulfonate and amine groups. Such model surfaces may be useful in the design of experiments for platelet retention. blood interactions, or mathematical modeling of protein adsorption. Perhaps surfaces prepared to have a hydrophobicity or chemical "gradient" could be prepared to qualitatively evaluate the effect of fibrinogen adsorption on some other aspect of blood compatibility.

The initial rate of adsorption as quantified by Fibslop was found to be a linear function of two variables as shown in equations 4.4.3 and 4.4.4.

$$(Fibslop \pm 0.030) = (0.38 \pm 0.02)Fibplat + (0.00095 \pm 0.00020)Contang \quad [4.4.3]$$

$$(Fibslop \pm 0.025) = (0.41 \pm 0.05)Fibplat + (0.00081 \pm 0.00033)Contang \quad [4.4.4]$$

Equation 4.4.3 was the relationship found for all 15 surfaces while equation 4.4.4 was found for the original eight surfaces. It was expected that Fibslop and Fibplat would be highly correlated judging by the shape of the 30 minute adsorption curves (see Figures 3.3.15 and 3.3.16) and by the fact that the two values were gleaned from the same experimental data sets. The residuals from the Fibslop versus Fibplat relationship were found to be strongly correlated with the advancing water contact angle, Contang. This finding was interesting because it relates to a "rule of thumb" which states that the more hydrophobic the surface, the "stronger" the adsorption. Equation 4.4.3 suggests that fibrinogen may in fact be adsorbed more "rapidly" on hydrophobic surfaces. Such an hypothesis would be consistent with an adsorption process governed by an interfacial free energy driving force. It is generally accepted that hydrophobic surfaces have a higher interfacial tension with water than hydrophilic surfaces.

In section 4.3.2 it was concluded that fibrinogen adsorption on the model surfaces follows a bilayer mechanism. Equations 4.4.3 and 4.4.4 may also be interpreted in light of this hypothesis such that the first layer, represented by Fibslop, is influenced by surface chemistry and energetics while the capacity of the second layer (Fibplat) is related mainly to the chemistry of the underlying surface.

The "Vroman effect" was described previously (section 1.1.6) as the sequential adsorption and displacement of proteins adsorbed from plasma, ending in a disproportionate accumulation of trace clotting factors on the surface. Fibrinogen is one of the proteins adsorbed and displaced whose behavior may be correlated with blood compatibility. This hypothesis is entirely speculative and was tested for the first time in this study. Previously it has been reported that the Vroman peak height (Fibpeak) is not directly correlated with any single parameter such as water contact angle (Wojciechowski et al, 1986). The data for the first eight model surfaces suggested the following simple relation with fibrinogen adsorption from buffer.

$$(Fibpeak \pm 0.026) = (0.23 \pm 0.02)Fibplat \quad [4.4.5]$$

The effect appeared to be nonspecific with respect to the underlying surface chemistry but the data for the surfaces in the extended study produced some apparently anomalous results. Three of the surfaces (SO3+NH2, SO3>NH2, and Lys) deviate significantly from the relationship described by equation 4.4.5. In fact, the Vroman effect virtually disappeared on these three surfaces (i.e. a plateau rather than a peak was achieved). A characteristic these three surfaces have in common (which none of the others has) is that they contain both amino and sulfonate groups. Santerre (1990) also found that the Vroman effect was eliminated on sulfonated polyurethanes but attributed this behavior solely to the sulfonate groups. The present study indicates that the presence of nitrogen-containing groups in the polyurethane ureas may contribute to, and be necessary for the suppression of the Vroman effect.

When the model given by equation 4.4.5 was fit to the model surfaces that did not contain both amino and sulfonate groups, equation 4.4.6 was obtained:

$$(Fibpeak \pm 0.025) = (0.22 \pm 0.02)Fibplat \quad [4.4.6]$$

The importance of equations 4.4.5 and 4.4.6 is that they suggest a simple relationship between the single component adsorption of fibrinogen and its adsorption from the vastly more complicated plasma system. A similar relationship was found by Slack and Horbett (1988) who demonstrated a correlation between the fibrinogen displacement rate by plasma components, and fibrinogen elutability by a surfactant, SDS (sodium dodecylsulfate).

4.4.4 Correlations Involving Coagulation Data

It was hoped at the outset of this study, that some direct relationship could be found to help predict the rate of surface activated coagulation based on "Vroman effect" data. Thrombin generation data for the fifteen surfaces in this study do not reveal such a relationship with the "Vroman effect" or any other parameter related to protein adsorption. Only the surface chemistry of the model surfaces was found to correlate significantly with the clotting times. The validity of these conclusions may be questioned since the surface chemistry of the clotting tubes was not proven to be identical to that of the pure silica XPS samples. It can be assumed, however, that the surface chemistry of these materials is similar and the relationships that were found are worthy of further investigation. In future studies,

fragments of the glass culture tubes should be included in the silanization process to provide a means of directly comparing the chemistry of similarly treated quartz and borosilicate glass. In fact it may be possible to employ regular glass instead of pure silica as substrates for future model surfaces as long as their chemistry can still be easily characterized using XPS.

The clotting time ("Clot", see table 3.4.1 for data) was found to be most strongly related to a combination of oxygen (or silicon) and nitrogen content measured at a 90° detector angle ("O90" and "N90"). The polarity of the surfaces ("Polar") as defined in the "lack of fit" column in Table 4.2.4 was also found to be fairly strongly correlated with clotting time. The physical meaning of this variable is still unclear but the discovery of its involvement in the correlation served to increase interest in it. It may be hypothesized that positive values of "Polar" reflect the strength of the negative charge on a surface and vice versa. Equation 4.4.7 shows the empirical relationship found between the four variables described above, where "Clot" is in minutes, "O90" and "N90" are in atom%, and "Polar" is in degrees (° angle).

$$Clot \pm 1.5 = (0.09 \pm 0.01)O90 + (1.9 \pm 0.5)N90 - (0.20 \pm 0.06)Polar \qquad [4.4.7]$$

All parameter estimates in equation 4.4.7 are significant at a level greater than 99.5%. The F-ratio for the model was 89, with a level of significance greater than 99.9%. The fact that the model contains no constant term is probably coincidental and a result of the relatively large variation in the clotting time data. The full model, including a constant is shown in equation 4.4.8.

$$(Clot \pm 1.5) = (-3.9 \pm 5.2) + (0.15 \pm 0.09)O90 + (2.4 \pm 0.8)N90 - (0.19 \pm 0.06)Polar \qquad [4.4.8]$$

The constant parameter in equation 4.4.8 was not significantly greater than zero and its inclusion did not lower the residual sum of squares.

Equation 4.4.7 is useful for an intuitive interpretation of the empirical relationship found between clotting times and surface chemistry. The model suggests that the rate of contact activation is strongly reduced by the presence of nitrogen and slightly reduced by the presence of oxygen (or silicon since Si and O content are so strongly linked in these materials). The influence of carbon or sulfur content was not found to be important. A positively charged surface (assuming that a negative value of "Polar" represents a positive

charge) has the effect of increasing clotting times. This agrees with the hypothesis that negatively charged surfaces catalyze the activation of factor XII, but disagrees with the view that a net negative charge like that found on the vascular endothelium improves compatibility (Bouma and Griffin, 1986).

Equation 4.4.7 is not the best mathematical form for the fitting of clotting time data due to the error associated with the parameter "Clot". A more appropriate logarithmic form in which the response has a more nearly constant variance is given in equation 4.4.9.

$$(\log(Clot) \pm 0.1) = (0.012 \pm 0.001)O90 + (0.17 \pm 0.03)N90 - (0.014 \pm 0.004)Polar \qquad [4.4.9]$$

In this model also, the constant term (0.028±0.341) was found to be insignificant and was therefore left out. The estimated parameters are better conditioned than those in 4.4.7, but it is more difficult to see the effects of surface properties on the clotting time in terms of minutes. The trends in all of equations 4.4.7 to 4.4.9 give the same qualitative information about the effects of surface properties on blood coagulation. It is possible that the empirical relationship found was the result of random chance, but the analysis of variance estimates the probability of this to be less than 1%. Despite this fact, hypotheses made on the basis of equation 4.4.7 will still require further experimentation on a wide range of additional model surfaces that have been fully characterized.

Of the "independent" variables in equation 4.4.9, "Polar" has the strongest pairwise correlation with clotting time ($r^2 = 0.65$). Clotting time is less correlated with N90($r^2 = 0.51$) and uncorrelated with O90 ($r^2 = 0.05$). O90 plays two roles in equation 4.4.9: 1) as a constant of about 50 since it varies between 40 and 60 atom%, and 2) as a variable between those extremes. Therefore, its importance is probably overstated here. A more appropriate test of the importance of O90 was made using normalized data having a mean value of zero. O90 was still found to be significant but only at a level of 90% confidence.

The importance of "Polar" as a parameter to help predict *in vitro* surface activated coagulation appears to be supported by the empirical relationships described here, but its true physical meaning is not established. More needs to be learned about it before recommendations can be made regarding the design of more compatible surfaces. The nitrogen content on silica is a more "tangible" parameter which is correlated to the rate of surface activated coagulation.

In conclusion it should be cautioned that there is not enough information in this study upon which to build a model for the effect of surface properties on surface activated coagulation. A number of factors including precision of the clotting time measurements, difference between substrates, and the limited variety of surface chemistry makes the observations relatively inconclusive. The data do suggest an influence of surface chemistry and charge on clotting but more surfaces need to be tested using more and better coagulation assays in order to verify these hypotheses. All of these observations highlight the enormity of the task which faces those involved in the systematic study of biomaterials and blood compatibility. Clearly some sort of cooperative program will have to be established in order to provide a large enough body of data and to take advantage of the broad range of expertise in surface preparation and characterization available to biomaterials researchers. Only a very large survey of surfaces and their properties will begin to yield enough data to allow the development of a general model for the prediction of blood compatibility and the rational design of more compatible surfaces. It is hard to imagine that one group would have the resources to pursue such a program alone.

5 Conclusions and Recommendations for Future Studies

5.1 Conclusions

1) Silica surfaces were modified by the covalent attachment of monolayers of various silanes to produce a series of model surfaces with a variety of physicochemical properties. The chemical composition of these surfaces was verified and quantified by x-ray photo-electron spectroscopy.

2) Interfacial tension models based on microscopic and macroscopic theory were unable to estimate consistently the solid surface energy (as defined by the Young equation) of the model surfaces using contact angle data. It appears that the assumptions associated with these models are not internaliy consistent. Based on these findings and the rigid nature of solid surfaces, the utility of the Young equation to determine solid surface tension is questioned.

3) An empirical model, not based on any theory of surface energy, was developed and was able to fit advancing contact angle data well, not only on silane monolayers but on other surfaces including metals, ceramics, and polymers. There was some indication that dimethyl sulfoxide behaves as a negative monopole (as suggested by van Oss et al, 1987) and water as a positive monopole based on the correlated variation in contact angles on the model surfaces. These properties may make water and DMSO useful for determining the polarity of a solid surface using contact angles.

4) A simulation was written to couple the reactive and transport processes involved in protein adsorption in static systems. The effects of adsorption rate constants, diffusivity, and adsorption mechanisms were illustrated. The simulation may easily be adapted to describe adsorption kinetics in a variety of simple geometries.

5) Kinetic fibrinogen and albumin adsorption data were fit to a number of models including Langmuir's and Cuypers' one state monolayer models, Beissinger and Leonard's two-state monolayer model, and a bilayer model. All monolayer models demonstrated a significant lack of fit. The bilayer mechanism showed the best fit of all the models studied.

6) A thrombin generation assay interpreted in terms of a plasma coagulation time was found to be a more reproducible method for quantifying surface activated coagulation than recalcification time or partial thromboplastin time. Clotting times ranging from 2 to 11 minutes were measured on the model surfaces.

7) Contrary to prior speculation, clotting times were not found to be correlated with the Vroman effect for fibrinogen. However, significant correlations were found between clotting time and surface polarity as defined by the empirical model in section 4.2.7 and between clotting time and nitrogen content.

8) Fibrinogen adsorption from plasma was found to be linearly related to fibrinogen adsorption from buffer on most surfaces. This suggests that the Vroman effect reflects in general a competition between proteins influenced very little by surface chemistry. Surfaces which contained both sulfonate and amino groups were found to reduce the ability of plasma proteins such as high molecular weight kininogen and high density lipoproteins to displace initially adsorbed fibrinogen.

9) Fibrinogen adsorption to surfaces from buffer was not found to be a strong function of hydrophobicity, as has been frequently hypothesized. The dominant correlation found was between adsorption and the chemical composition of the surface. The presence of sulfonate groups tended to increase fibrinogen adsorption while amine groups reduced it. The only apparent effect of hydrophobicity was to increase slightly the rate of adsorption.

5.2 Recommendations

1) The multivariate approach to studying complicated biomaterial/tissue interactions presented here can be expanded in terms of a number of new materials and/or new characterizations. The large amount of data that can be collected is well suited for evaluation by statistical tools such as principal components analysis or partial least squares. These methods should find increasing utility in the biomaterials field for the creation of multivariate models capable of predicting blood compatibilty and aiding in the design of more compatible surfaces.

2) It may be feasible to use less expensive glass substrates (rather than pure silica) for the model surfaces as long as XPS analyses can provide good data to quantify the surface

chemistry. It will be important to ensure that all forms of a given model surface have the same chemical and physical composition to allow comparison between the different characterizations. Better methods for cleaning the model surfaces must be investigated.

3) A large scale study of the empirical contact angle model developed here should be carried out to help elucidate its strengths and limitations. Special emphasis should be placed on testing the hypothesis that water and DMSO contact angles may be used to estimate surface charge or polarity.

4) The testing of surfaces should be expanded to include a wide variety of practical ("non-model") biomaterials to see if their behavior tends to follow the same trends found in this study. New protocols may be required to test different substrate forms (e.g. sheets instead of tubing).

5) Only a limited array of model surface chemistries was employed in this study. Future studies should endeavor to expand the variety of surface chemistries to include many more chemical groups. Additional studies could include testing of all the amino acids, hydrocarbon chains ranging from C_1 to C_{100} or higher, and poly(ethylene oxide) of varying chain length. Such studies should be able to show whether improvements in blood compatibility arise as a direct result of surface chemistry, wettability, protein adsorption, or some other effect.

6) The protein adsorption simulation should be adapted to describe protein adsorption in a variety of experimental systems especially those involving rinsing, flow, and sequential steps. The simulation has already been adapted to describe single protein adsorption onto glass beads in a well-stirred, continuous flow reactor (Cornelius et al, 1991).

7) The single component adsorption model for fibrinogen should be extended to explain its adsorption from blood plasma, including the Vroman effect. The current bilayer model fits the data well and comparative studies suggest that the Vroman effect is closely correlated to adsorption from buffer. Perhaps the fibrinogen-displacing components of plasma are capable of exerting their influence in the second layer of adsorbed protein where fibrinogen is adsorbed relatively loosely and slowly.

8) Protein modeling studies should be done for more complicated systems and protocols. The sophistication of the mathematical form should be increased to allow the prediction of desorption, exchange, and displacement as well as simple adsorption.

6 References

Absolom D.R., Neumann A.W., Zingg W., van Oss C.J., Trans. Am. Soc. Artif. Intern. Organs, **25**, 152 (1979).

Absolom D.R., Zingg W., Neumann A.W., J. Biomed. Mater. Res., **21**, 161 (1987).

Adamson A., **Physical Chemistry of Surfaces**, 5th edition, Wiley Interscience, New York (1990).

Aizenbud B., Volterra V., Priel Z., J. Colloid Interface Sci., **103**, 133 (1985).

Andrade J.D., Ma S.M., King R.N., Gregonis D.E., J. Colloid Interface Sci., **72**, 488 (1979).

Andrade J.D., ed., **Surface and Interfacial Aspects of Biomedical Polymers, Volume 1: Surface Chemistry and Physics**, Plenum Press, New York (1985a).

Andrade J.D., ed., **Surface and Interfacial Aspects of Biomedical Polymers, Volume 2: Protein Adsorption**, Plenum Press, New York (1985b).

Andrade J.D., in **Polymers in Medicine II**, Chiellini E., Giusti P., Migliaresi C., Nicolais L., eds., Plenum, New York, pp 29-40 (1985c).

Andrade J.D., Hlady V., Adv. Polymer Sci., **79**, 1 (1986).

Andrade J.D., Hlady V., in **Blood in Contact with Natural and Artificial Surfaces**, Leonard E.F., Turitto V.T., Vroman L., eds., Ann. N.Y. Acad. Sci., **516**, pp 158-172 (1987).

Andrade J.D., Lea A.S., Pungor A., Hlady V., Herron J.N., Voss E.W.Jr., Proc. 7th International Conference of Surface and Colloid Science, Volume I - Part 2, Abstract #A2/P34, p. 132 (1991).

Arnebrant T., Nylander T., J. Colloid Interface Sci., **111**, 529 (1986).

Bagnall R.D., Arundel P.A., J. Biomed. Mater. Res., **17**, 459 (1982).

Barenberg S.A., Brozoski-Varnell B., English A.D., Hassel R.L., Johnson R.E. Jr., Kelley M.J., Starkweather H.W. Jr., in **Blood Compatibility**, Vol. II, Williams D.F., ed., pp 1-47, CRC Series in Biocompatibility, CRC Press, Boca Raton, FL (1987).

Beissinger R.L., Leonard E.F., Trans. Am. Soc. Artif. Intern. Organs, **27**, 225 (1981).

Beissinger R.L., Leonard E.F., J. Colloid Interface Sci., **85**, 521 (1982).

Berrettini M., Lammle B., Griffin J.H., in **Thrombosis and Haemostasis 1987**, M. Verstrate et al, eds., Leuven University Press, Leuven, Belgium, pp 473-495 (1987).

Bikerman J.J., **Physical Surface**. Academic Press, New York (1970).

Bird R.B., Stewart W.E., Lightfoot E.N., **Transport Phenomena**, Wiley, New York (1960).

Bohnert J. L., Horbett T.A., J. Colloid Interface Sci., **111**, 363 (1986).

Bots J.G.F., van der Does L., Bantjes A., in **Polymers in Medicine II**, E. Chiellini et al, eds., pp 223-234, Plenum Press, New York (1986).

Bouma B.N., Griffin J.H., in **Blood Coagulation**, Zwaal R.F.A. and Hemker H.C. eds., Elsevier, Amsterdam, pp 103-128 (1986).

Boumaza F., Déjardin Ph., Yan F., Bauduin F., Holl Y., submitted (1991).

Box G.E.P., Hunter W.G., Hunter J.S., **Statistics for Experimenters**, John Wiley & Sons, New York (1978).

Brash J.L., Samak Q.M., J. Colloid Interface Sci., **65**, 495 (1978).

Brash J.L., ten Hove P., Thromb. Haemostas., **51**, 326 (1984).

Brash J.L., Chan B.M.C., Szota P., Thibodeau J.A., J. Biomed. Mater. Res., **19**, 1017 (1985).

Brash J.L., Thibodeau J.A., J. Biomed. Mater. Res., **20**, 1263 (1986).

Brash J.L., Horbett T.A., eds., **Proteins at Interfaces: Physicochemical and Biochemical Studies**, ACS Symposium Series, **343**, (1987).

Brash J.L., in **Blood in Contact with Natural and Artificial Surfaces**, Leonard E.F., Turitto V.T., Vroman L., eds., Ann. N.Y. Acad. Sci., **516**, pp 206-222 (1987).

Brash J.L., Scott C.F., ten Hove P., Wojciechowski P., Colman R.W., Blood, **71**, 932 (1988).

Breemhaar W., Brinkman E., Ellens D.J., Beugeling T., Bantjes A., Biomaterials, **5**, 269 (1984).

Brinkhous K.M., Langdell R.D., Penick A.D., Graham J.S., Wagner R.H., JAMA, **154**, 481 (1954).

Bruck S.D., **Properties of Biomaterials in the Physiological Environment**, CRC Press, Boca Raton FL (1980).

Brynda E., Houska M., Lednicky F., J. Colloid Interface Sci., **113**, 164 (1987).

Burghardt T.P., Axelrod D., Biophys. J., **33**, 455 (1981).

Burkel W.E., Graham L.M., Stanley J.C., in **Blood in Contact with Natural and Artificial Surfaces**, Leonard E.F., Turitto V.T., Vroman L., eds., Ann. N.Y. Acad. Sci., **516**, pp 131-144 (1987).

Byrne G.D., Hindmarsh A.C., J. Computational Phys., **70**, 1 (1987).

Cazabat A.M., Heslot F., Colloids and Surfaces, **51**, 309 (1990).

Chan B.M.C., Brash J.L., J. Colloid Interface Sci., **82**, 217 (1981).

Chandler A.B., Lab. Invest., **7**, 110 (1958).

Chang T.M.S., Can. J. Physiol. Pharmacol., **52**, 275 (1974).

Chiu T-H., Nyilas E., Turcotte L.R., Trans. Am. Soc. Artif. Intern. Organs, **29**, 389 (1978).

Chuang H.Y.K., J. Biomed. Mater. Res., **18**, 547 (1984).

Clark H.G., ikenberry L.D., Mason R.G., in **Clean Surfaces: Their Preparation and Characterization for Interfacial Studies**, Goldfinger G., ed., Marcel Dekker, New York, pp. 45-63 (1970).

Coleman D.L., Gregonis D.E., Andrade J.D., J. Biomed. Mater. Res., **16**, 381 (1982).

Collen D., Lijnen H.R., in **Blood Coagulation**, Zwaal R.F.A., Hemker H.C., eds., Elsevier, Amsterdam, pp. 243-258 (1986).

Colman R.W., Scott C.F., Schmaier A.H., Wachtfogel Y.T., Pixley R.A., Edmunds L.H., in **Blood in Contact with Natural and Artificial Surfaces**, Leonard E.F., Turitto V.T., Vroman L., eds., Ann. N.Y. Acad. Sci., **516**, pp 253-267 (1987).

Cornelius R., Masters Thesis, McMaster University, Hamilton, Canada (1988).

Cornelius R., Wojciechowski P., Brash J.L., J. Colloid Interface Sci., in press (1991).

Cottonaro C.N., Roohk H.V., Bartlett R.H., Servas F.M., Sperling D.R., Trans. Am. Soc. Artif. Intern. Organs, **28**, 478 (1982).

Creighton T.E., **Proteins: Structures and Molecular Properties**, Freeman, New York (1984).

Cuypers P.A., Willems G.M., Hemker H.C., Hermens W.T., Ann. N.Y. Acad. Sci., **516**, pp 244-252 (1987).

Dalal E.N., Langmuir, **3**, 1009 (1987).

Dardik H. ed., **Graft Materials in Vascular Surgery**, Symposia Specialists, Miami (1978).

de Feijter J.A., in **Thin Liquid Films**, I.B. Ivanov, ed., Marcel Dekker, New York, pp 1-47 (1988).

de Gennes P.G., Rev. Mod. Phys., **57**, 827 (1985).

Dejardin P., J. Colloid Interface Sci., **133**, 418 (1989).

Didisheim P., Dewanjee M.K., Kaye M.P., Frisk C.S., Fass D.N., Wahner H.W., Tirrell M.V., Zollman P.E., Trans. Am. Soc. Artif. Intern. Organs, **30**, 370 (1984).

Dong D.E., Andrade J.D., Coleman D.L., J. Biomed. Mater. Res., **21**, 683 (1987).

Doolittle R.F., Sci. Am., **245**, 129 (Dec. 1981)

Douzon C., Kanmangne F.M., Serne H., Labarre D., Jozefowicz M., Biomaterials, **8**, 190 (1987).

Eirich F.R., J. Colloid Interface Sci., **58**, 423 (1977).

Elwing H., Askendal A., Lundstrom I., J. Biomed. Mater. Res., **21**, 1023 (1987a).

Elwing H., Welin S., Askendal A., Nilsson U. and Lundstrom I., J.Colloid Interface Sci., **119**, 203 (1987b).

Fersht A., **Enzyme Structure and Mechanism**, Second Edition, W.H. Freeman and Company, New York (1985).

Fowkes F.M., Ind. Eng. Chem., **56**, 40 (1964).

Fox H.W., Zisman W.A., J. Colloid Sci., **5**, 514 (1950).

Galletti P.M., in **Polymers in Medicine II**, Chiellini E., Giusti P., Migliaresi C., Nicolais L., eds., Plenum, New York, pp 175-185 (1986).

Geladi P., Kowalski B.R., Analytica Chimica Acta, **185**, 1 (1986).

Gendreau R.M., Leininger R.I., Winters S., Jakobsen R.J., in **Biomaterials: Interfacial Phenomena and Applications**, Cooper S.L., Peppas N.A., eds., ACS Adv. Chem. Series, **199**, pp 371-394 (1982).

Gerald C.F., Wheatley P.O., **Applied Numerical Analysis**, 4th edition, Addison-Wesley, New York (1989).

Giaever I., Keese C.R., in **Proteins at Interfaces: Physicochemical and Biochemical Studies**, Brash J.L., Horbett T.A., eds., ACS Symposium Series, **343**, pp 582-602 (1987).

Girifalco L.A., Good R.J., J. Colloid Sci., **61**, 904 (1957).

Giroux T., Cooper S.L., submitted.

Goldsmith H.L., Turitto V.T., Thromb. Haemostas., **55**, 415 (1986).

Good W.R., J. Colloid Interface Sci., **44**, 63 (1973).

Gott V.I., Koepke D.E., Dagget R.L., Zarnstorff W., Young W.P., Surgery, **50**, 382 (1961).

Grasel T.G., Cooper S.L., J. Biomed. Mater. Res., **23**, 311 (1989).

Guiseppi-Elie A., Wnek G.E., Langmuir, **2**, 508 (1986).

Gulliver G., **The Works of William Hewson.**, London, Sydenham Society (1846).

Haycox C.L., Ratner B.D., Horbett T.A., Proc. Soc. Biomater., **14**, 40 (1991a).

Haycox C.L., Ratner B.D., Horbett T.A., J. Biomed. Mater. Res., 25, 1317 (1991b).

Heslot F., Fraysse N., Cazabat A.M., Levinson P., Carles P., in **Wetting Phenomena**, DeConinck J., Dunlop F., eds., Lecture Notes in Physics, **354**, 41 (1990).

Heyman P.W., Cho C.S., McRea J.C., Olsen D.B., Kim S.W., J. Biomed. Mater. Res., **19**, 419 (1985).

Hindmarsh A.C., Scientific Computing, **1**, 55 (1983).

Hirsh J., Brain E.A., **Hemostasis and Thrombosis: A Conceptual Approach**, Churchill Livingstone, New York (1983).

Hoffman A.S., in **Polymeric Biomaterials**, Piskin E., Hoffman A.S., eds., Martinus Nijhoff Publ., Dordrecht, FRG, pp. 1-14 (1986).

Hoffman A.S., Ann. N.Y. Acad. Sci., **516**, pp 96-101 (1987).

Holly F.J., Colloids and Surfaces, **10**, 343 (1984).

Horbett T.A., Weathersby P.K., J. Biomed. Mater. Res., **15**, 403 (1981).

Horbett T.A., J. Biomed. Mater. Res., **15**, 673 (1981).

Horbett T.A., Thromb. Haemostas., **51**, 174 (1984).

Horbett T.A., Cheng C.M., Ratner B.D., Hoffman A.S., J. Biomed. Mater. Res., **20**, 739 (1986).

Horbett T.A., Brash J.L., in **Proteins at Interfaces: Physicochemical and Biochemical Studies**, Brash J.L., Horbett T.A., eds., ACS Symposium Series, **343**, pp 1-33 (1987).

Horbett T.A., Techniques for protein adsorption studies, in **Blood Compatibility,** Vol. II, Williams D.F., ed., CRC Series in Biocompatibility, CRC Press, Boca Raton, pp. 183-214, FL (1987).

Ikada Y., Adv. Polym. Sci., **57**, 103 (1984).

Iordanski A.L., Polischuk A.Ja., Zaikov G.E., J. Macromol. Sci.; Rev. Macromol. Chem. Phys. **C23**, 33 (1983).

Ivarsson B., Lundstrom I., CRC Critical Reviews in Biocompatibility, **2**, pp 1-95 (1986).

Jennissen H.P., in **Surface and Interfacial Aspects of Biomedical Polymers; Volume 2, Protein Adsorption**, Andrade J.D., ed., Plenum Press, New York, pp 295-320 (1985).

Johnson R.E. Jr., Dettre R.H., Langmuir, **5**, 293 (1989).

Joist J.H., Pennington D.G., Trans. Am. Soc. Artif. Intern. Organs, **33**, 341 (1987).

Jozefowicz M., Jozefonvicz J., in **Polymers in Medicine II**, Chiellini et al, eds., pp 41-65, Plenum Press, New York (1986).

Kambic H., Murabayashi S., Nose Y., C&EN, 31 (Apr. 1986).

Kloubek J., Langmuir, **5**, 1127 (1989).

Ku C.S.L., Bornstein I., Breillatt J., Ung-Chhun S.N., Johnson R., Lindon J., Pokropinski S., Rimer D., Trans. Soc. Biomater., **14**, 44 (1991).

Laki K., **Fibrinogen**, Marcel Dekker, New York (1968).

Lavielle L., Lischetti G., Sanfeld A., Schultz J., J. Colloid Interface Sci., **138**, 134 (1990).

Leach-Scampavia D.K., Castner D.G., Ratner B.D., ESCA Characterization of Quartz Surfaces. Report prepared for J.L.Brash and P.W.Wojciechowski, National ESCA and Surface Analysis Center for Biomedical Problems, Seattle WA, August 21 (1990).

Lelah M.D., Cooper S.L., **Polyurethanes in Medicine**, CRC Press, Inc., Boca Raton, Florida (1986).

Lemm W., J. Biomater. Sci. Polymer Edn, **2**, 15 (1991).

Leonard E.F., Turitto V.T., Vroman L., eds., **Blood in Contact with Natural and Artificial Surfaces**, Ann. N.Y. Acad. Sci., **516** (1987).

Leyden D.E., **Silanes, Surfaces, and Interfaces**, Gordon and Breach Science Publishers, New York (1986).

Lindon J.N., McManama G., Kushner L., Kloczewiak M., Hawiger J., Merrill E.W., Salzman E.W., in **Proteins at Interfaces: Physicochemical and Biochemical Studies**, Brash J.L., Horbett T.A., eds., ACS Symposium Series, **343**, pp 507-526 (1987).

Lindon J.N., Kushner L., Salzman E.W., Methods in Enzymology, **169**, 104 (1989).

Lister J., Proc. Roy. Soc. London, **12**, 580 (1863).

Lok B.K., Cheng Y.L., Robertson C.R., J. Colloid Interface Sci., **91**, 104 (1983).

Lottenberg R., Christensen U., Jackson C.M., Coleman P.L., Meth. Enz., **80**, 341 (1981).

Lundstrom I., Progr. Colloid & Polymer Sci., **70**, 76 (1985).

Lyklema J., Colloids and Surfaces, **10**, 33 (1984).

Lyman D.J., Muir W.M., Lee I.J., Trans. Am. Soc. Artif. Intern. Organs, **11**, 301 (1965).

Lyman D.J., Brash J.L., Klein K.G., in **Proceeding of the Artificial Heart Program Conference**, Washington D.C. (1969).

Lyman D.J., Knutson K., McNeill B., Shibatani K., Trans. Am. Soc. Artif. Intern. Organs, **21**, 49 (1975).

MacRitchie F., Adv. Protein Chem., **32**, 283 (1978).

MacRitchie F., in **Proteins at Interfaces: Physicochemical and Biochemical Studies**, Brash J.L., Horbett T.A., eds., ACS Symposium Series, **343**, pp 165-179 (1987).

Marchalonis J.J., Biochem. J., **113**, 299 (1969).

Marchant R.E., Lea A.S., Andrade J.D., Brockenstedt P., Ginsberg D., Proc. Soc. Biomater., **14**, 125 (1991).

Marmur A., Adv. Colloid Interface Sci., **19**, 75 (1983).

Mason R.G., Mohammad S.F., Chuang H.Y.K.,in **Hemostasis and Thrombosis: Basic Principles and Clinical Practice**, Colman R.W., Hirsh J., Marder V.J., eds., J.B. Lippincott Company, Philadelphia PA (1982).

Mason R.G., ed., **Guidelines for Blood-Material Interactions**: Report of the National Heart, Lung and Blood Institute, NIH Publication No. 85-2185, September (1985).

Massia S.P., Hubbell J.A., Trans. Soc. Biomater., **14**, 238 (1991).

McFarlane A.S., J. Clin. Invest., **42**, 346 (1963).

McGuire J., Lee E., Sproull R.D., Surface Interface Anal., **15**, 603 (1990).

McMillin C.P., Walton A.G., J. Colloid Interface Sci., **48**, 345 (1974).

Meeter D.A., Wolfe P.J., "Nonlinear Least Squares", University of Wisconsin Computing Center UWCC ID Code C0017-00/S0017-00 (Dec. 1965).

Meltzer H., Silberberg A., J. Colloid Interface Sci., **126**, 292 (1988).

Merrill E.W., Salzman E.W., Lipps B.J., Gilliland E.R., Austen W.G., Joison J., Trans. Am. Soc. Artif. Intern. Organs, **12**, 139 (1966).

Merritt K., Edwards C.R., Brown S.A., J. Biomed. Mater. Res., **22**, 99 (1988).

Migonney V., Fougnot C., Jozefowicz M., Biomaterials, **9**, 145 (1988).

Moreno E.C., Kresak M., Kane J.J., Hay D.I., Langmuir, **3**, 511 (1987).

Morita T., Kato H., Iwanaga S., Takada K., Kimura T., Sakakibara S., J. Biochem., **82**, 1495 (1977).

Morra M., Occhiello E., Garbassi F., Adv. Colloid Interface Sci., **32**, 79 (1990).

Moy E., Neumann A.W., J. Colloid Interface Sci., **119**, 296 (1987).

Munro M.S., Eberhart R.C., Maki N.J., Brink B.E., Fry W.J., Am. Soc. Artif. Intern. Organs J., **6**, 65 (1983).

Mysels K.J., Frisch H.J., J. Colloid Interface Sci., **99**, 136 (1984).

Naito K., Fujikawa K., J. Biol. Chem., **266**, 7353 (1991).

Nakao A., Okhura K., Nonami T., Harada A., Takagi H., Mori Y., Trans. Am. Soc. Artif. Intern. Organs, **32**, 319 (1986).

Neumann A.W., Good R.J., Hope C.J., Sejpal M., J. Colloid Interface Sci., **49**, 291 (1974).

Norde W., Lyklema J., J. Colloid Interface Sci., **66**, 257 (1978).

Norde W., Lyklema J., J. Colloid Interface Sci., **71**, 350 (1979).

Norde W., Adv. Colloid Interface Sci., **25**, 267 (1986).

Nye A.W., Graham J.B., Brinkhous K.M., Am. J. Med. Sci., **243**, 279 (1962).

Nygren H., J. Biomed. Mater. Res., **22**, 1 (1988a).

Nygren H., J. Immun. Meth., **114**, 107 (1988b).

Nygren H., Stenberg M., J. Biomed. Ma:. Res., **22**, 1 (1988).

Ogston D., Bennett B., British Medical Bulletin, **34**, 107-112 (1978).

Okkema A.Z., Grasel T.G., Zdrahala R.J., Solomon D.D., Cooper S.L., J. Biomater. Sci. Polymer Edn. **1**, 43 (1989).

Owens D.K., Wendt R.C., J. Appl. Polymer Sci., **13**, 1741 (1969).

Park K., Mao F.W., Park H., Biomaterials, **11**, 24 (1990).

Park K., Mao F.W., Park H., J. Biomed. Mater. Res., **25**, 407 (1991).

Pefferkorn E., Carroy A., Varoqui R., Macromolecules, **18**, 2252 (1985).

Pelzer H., in **Polyurethanes in Biomedical Engineering**, Planck H., Egbers G., Syré I., eds., Elsevier, Amsterdam, pp 69-81 (1984).

Phillips L.V., Hercules D.M., in **Silanes, Surfaces, and Interfaces**, D.E. Leyden, ed., Gordon and Breach Science Publishers, New York, pp 235-265 (1986).

Pitt W.G., Park K., Cooper S.L., J. Colloid Interface Sci., **111**, 2, 343 (1986).

Pitt W.G., Cooper S.L., J. Biomed. Mater. Res., **22**, 359 (1988).

Pitt W.G., J.Colloid Interface Sci., **133**(1) 223 (1989).

Platé N.A., Valuev L.I., Adv. Polymer Sci., **79**, 95 (1986).

Plueddemann E.P., in **Silanes, Surfaces, and Interfaces**, D.E. Leyden, ed., Gordon and Breach Science Publishers, New York, pp 1-24 (1986).

Price T.M., Rudee M.L., in **Proteins at Interfaces: Physicochemical and Biochemical Studies**, Brash J.L., Horbett T.A., eds., ACS Symposium Series, **343**, pp 48-62 (1987).

Privalov P.L., Adv. Protein Chem., **33**, 167 (1979).

Radke C.J., Prausnitz J.M., AIChE Journal, **18**, 761 (1972).

Ratner B.D., in **Polymers in Medicine II**, Chiellini et al, eds., Plenum, New York, pp 13-28 (1986).

Rollason G., Sefton M.V., submitted.

Ross J., Greenfield L.J., Bowman R.L., Morrow A.G., in **Prosthetic Valves for Cardiac Surgery**, Merendino K.A., ed., Thomas, Springfield, IL, 212 (1961).

Ruckenstein E., Gourisankar S.V., J. Colloid Interface Sci., **101**, 436 (1984).

Ryan U.S., in **Blood in Contact with Natural and Artificial Surfaces**, Leonard E.F., Turitto V.T., Vroman L., eds., Ann. N.Y. Acad. Sci., **516**, 22 (1987).

Salzman E.W., Lindon J., McManama G., Ware J.A., in **Blood in Contact with Natural and Artificial Surfaces**, Leonard E.F., Turitto V.T., Vroman L., eds., Ann. N.Y. Acad. Sci., **516**, 184 (1987).

Salzman E.W., Merrill E.W., in **Hemostasis and Thrombosis: Basic Principles and Clinical Practice**, Colman R.W., Hirsh J., Marder V.J., eds., J.B. Lippincott Company, Philadelphia PA. (1982).

Santerre J.P., Ph.D Thesis, McMaster University, Hamilton, Ontario, Canada (1990).

Santerre J.P., Ph.D Research Proposal, McMaster University, Hamilton, Ont., March (1987).

Santerre J.P., Vanderkamp N., Brash J.L., Trans. Soc. Biomat., **12**, 113 (1989).

Saunders J.H., Frisch K.C., **Polyurethanes. Chemistry and Technology. Part 1. Chemistry**, Interscience Publishers, New York (1967).

Sawyer P.N., ed., **Biophysical Mechanisms in Vascular Homeostasis and Intravascular Thrombosis.**, Appleton Century Crofts, New York (1965).

Schaaf P., Dejardin Ph., Colloids and Surfaces, **24**, 239 (1987).

Schaaf P., Dejardin Ph., Colloids and Surfaces, **31**, 89 (1988).

Schaaf P., Talbot J., Rabeony H.M., Reiss H., J. Phys. Chem., **92**, 4826 (1988).

Schaaf P., Talbot J., Phys. Rev. Lett., **62**, 175 (1989).

Schmaier A.H., Silver L., Adams A.L., Fischer G.C., Munoz P.C., Vroman L., Colman R.W., Thromb. Res., **33**, 51 (1983).

Schultz J., Tsutsumi K., Donnet J.B., J. Colloid Interface Sci., **59**, 277 (1977).

Schulz G.E., Schirmer R.H., **Principles of Protein Structure**, Springer-Verlag, New York (1979).

Scott C.F., Silver L.D., Purdon A.D., Colman R.W., J. Biol. Chem., **260**, 10856 (1985).

Sefton M.V., Cholakis C.H., Llanos G., in **Blood Compatibility**, Williams D.F., ed., CRC Series in Biocompatibility, CRC Press, Boca Raton, FL (1987).

Silverberg M., Diehl S.V., in **Blood in Contact with Natural and Artificial Surfaces**, Leonard E.F., Turitto V.T., Vroman L., eds., Ann. N.Y. Acad. Sci., **516**, 268 (1987).

Sinkovec R.F., Madsen N.K., ACM Transactions on Mathematical Software, **1**, 232 (1975).

Slack S.M., Horbett T.A., J. Colloid Interface Sci., **124**, 535 (1988).

Slack S.M., Horbett T.A., J. Colloid Interface Sci., **133**, 148 (1989).

Soderquist M.E., Walton A.G., J. Colloid Interface Sci., **75**, 386 (1980).

Spaet T.H., in Blood in Contact with Natural and Artificial Surfaces, Leonard E.F., Turitto V.T., Vroman L., eds., Ann. N.Y. Acad. Sci., **516**, 1 (1987).

Spelt J.K., Neumann A.W., Langmuir, **3**, 588 (1987).

Sugitachi A., Takagi K., Imaoka S., Kosaki G., Thrombos. Haemostas., **39**, 426 (1978).

Takahara A., Jo N.J., Kajiyama T., J. Biomater. Sci. Polymer Edn. **1**, 17 (1989).

Tsutsumi K., Abe Y., Colloid Polym. Sci., **267**, 637 (1989).

Van Dam-Mieras M.C.E., Muller A., in **Blood Coagulation**, Zwaal R.F.A. and Hemker H.C. eds., Elsevier, Amsterdam, pp.1-13 (1986).

Van Dulm P., Norde W., J. Colloid Interface Sci., **91**, 248 (1983).

van Oss C.J., Chaudhury M.K., Good R.J., Adv. Colloid Interface Sci., **28**, 35 (1987).

van Oss C.J., Ju L., Chaudhury M.K., Good R.J., J. Colloid Interface Sci., **128**, 313 (1988).

van Oss C.J., Giese R.F. Jr., Good R.J., Langmuir, **6**, 1711 (1990).

Voegel J.C., DeBaillou N., Sturm J., Schmitt A., Colloids and Surfaces, **10**, 9 (1984).

Vroman L., in **Biophysical Mechanisms in Vascular Homeostasis and Intravascular Thrombosis.**, Sawyer P.N., ed., Appleton Century Crofts, New York, pp 81-95 (1965).

Vroman L., Adams A.L., J. Biomed. Mater. Res., **3**, 43 (1969).

Vroman L., in **Blood in Contact with Natural and Artificial Surfaces**, Leonard E.F., Turitto V.T., Vroman L., eds., Ann. N.Y. Acad. Sci., **516**, 300-305 (1987a).

Vroman L., Seminars in Thrombosis and Hemostasis, **13**, 79 (1987b).

Vroman L., Adams A.L., in **Proteins at Interfaces: Physicochemical and Biochemical Studies**, Brash J.L., Horbett T.A., eds., ACS Symposium Series, **343**, pp 154-164 (1987).

Walton A.G., Koltisko B., ACS Adv. Chem., **199**, 245 (1982).

Ward C.A., Neumann A.W., J. Colloid Interface Sci., **49**, 286 (1974).

Ward R.A., Wellhausen S.R., Dobbins J.J., Johnson G.S., DeVries W.C., in **Blood in Contact with Natural and Artificial Surfaces**, Leonard E.F., Turitto V.T., Vroman L., eds., Ann. N.Y. Acad. Sci., **516**, 638 (1987).

Wenzel E., Scheffler P., Kiehl R., Doeneke P., Volkmer I., Bambauer R., Simonis G., Ehrich W., Harbauer G., Miyashita C., in **Polyurethanes in Biomedical Engineering**, Planck H., Egbers G., Syré I., eds., Elsevier, Amsterdam, pp. 17-39 (1984).

Williams D.F., in **Blood Compatibility**: Volume 1, Williams D.F., ed., CRC Series in Biocompatibility, CRC Press, Boca Raton, FL, pp.5-35 (1987).

Williams S.K., Jarrell B.E., in Leonard E.F., Turitto V.T., Vroman L., eds., **Blood in Contact with Natural and Artificial Surfaces**, Ann. N.Y. Acad. Sci., **516**, 145 (1987).

Wilson R.S., Cooper S.L., in **Polymeric Biomaterials**, Piskin E., Hoffman A.S., eds., Martinus Nijhoff Publ., Dordrecht, FRG, pp. 15-28 (1986).

Wilson R.S., Lelah M.D., Cooper S.L., in **Blood Compatibility, Vol. II**, Williams D.F., ed., pp. 151-181, CRC Series in Biocompatibility, CRC Press, Boca Raton FL (1987).

Wojciechowski P., Masters Thesis, McMaster University (1986).

Wojciechowski P., ten Hove P., Brash J.L., J. Colloid Interface Sci., **111**, 2, 455 (1986).

Wojciechowski P., Brash J.L., J. Colloid Interface Sci., **140**, 239 (1990).

Wojciechowski P., Brash J.L., J. Biomater. Sci. Polymer Edn., **2**, 203 (1991).

Wold S., Sjöström M., Carlson R., Lundstedt T., Hellberg S., Skagerberg B., Wikström C., Öhman J., Analytica Chimica Acta, **191**, 17 (1986).

Woodhouse K.A., Santerre J.P., Brash J.L., Trans. Soc. Biomater., **14**, 94 (1991).

Wu S., **Polymer Interface and Adhesion**, Marcel Dekker, New York (1982).

Yan F., Déjardin P., submitted.

Yoon S.C., Ratner B.D., Macromolecules, **19**, 1068 (1986).

Young B.R., Pitt W.G., Cooper S.L., J. Colloid Interface Sci., **124**, 28 (1988a).

Young B.R., Pitt W.G., Cooper S.L., J. Colloid Interface Sci., **125**, 246 (1988b)

Yu X.J., Brash J.L. in **Test Procedures for Blood Compatibility of Biomaterials**, Davids S., ed., Kluwer Academic Publishers, Dordrecht, The Netherlands, in press.

Zangwill A., **Physics at Surfaces**, Cambridge, New York (1988).